RECLAMATION
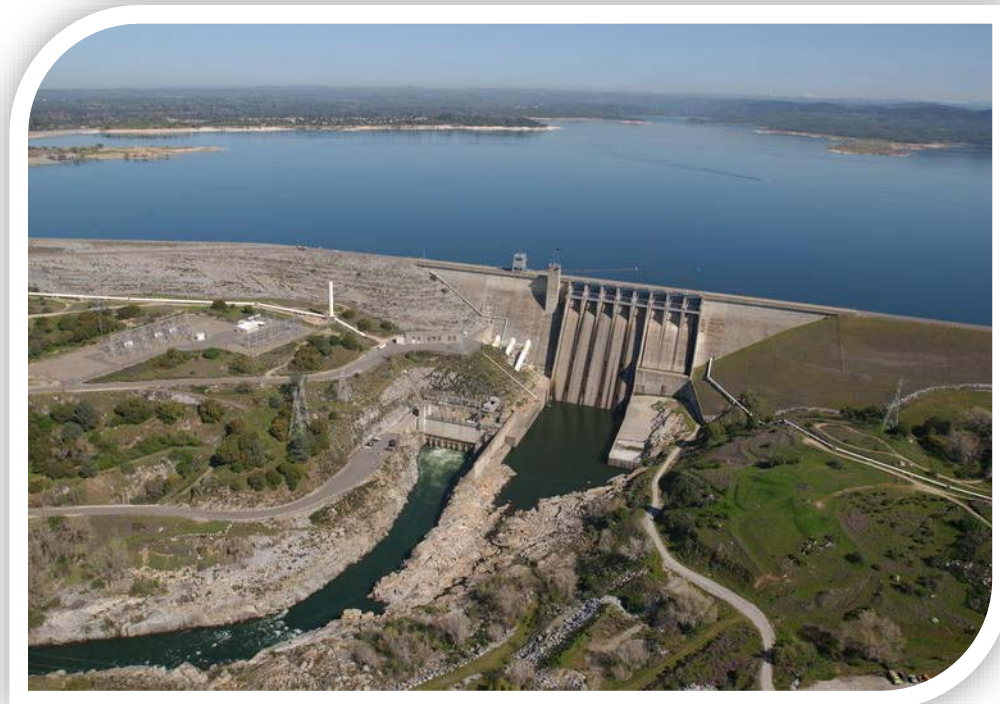## *Managing Water in the West*

An Integrated Mercury Model: Literature, Methodology and Data

Research and Development Office
Science and Technology Program
Final Report ST-2017-3425-01

Mission Statements

Protecting America's Great Outdoors and Powering Our Future

The Department of the Interior protects and manages the Nation's natural resources and cultural heritage; provides scientific and other information about those resources; and honors its trust responsibilities or special commitments to American Indians, Alaska Natives, and affiliated island communities.

Disclaimer:

REPORT DOCUMENTATION PAGE		*Form Approved* *OMB No. 0704-0188*
T1. REPORT DATE: SEPTEMBER 2017	**T2. REPORT TYPE:** RESEARCH	**T3. DATES COVERED** 10/01/2014 – 10/01/2017
T4. TITLE AND SUBTITLE An Integrated Mercury Model: Literature, Methodology and Data		**5a. CONTRACT NUMBER** **RY1541EN201523425**
		5b. GRANT NUMBER 3425
		5c. PROGRAM ELEMENT NUMBER 1541 (S&T)
6. AUTHOR(S) Yong G. Lai, Ph.D., Hydraulic Engineer Sedimentation and River Hydraulics Technical Service Center U.S. Bureau of Reclamation Denver, Colorado 80225		**5d. PROJECT NUMBER** 3425
		5e. TASK NUMBER
		5f. WORK UNIT NUMBER P.O. Box 25007
7. PERFORMING ORGANIZATION NAME(S) AND ADDRESS(ES) Yong G. Lai, Sedimentation and River Hydraulics, Technical Service Center, Denver, Colorado 80225		**8. PERFORMING ORGANIZATION REPORT NUMBER** SRH-2017-35
9. SPONSORING / MONITORING AGENCY NAME(S) AND ADDRESS(ES) Research and Development Office U.S. Department of the Interior, Bureau of Reclamation, PO Box 25007, Denver CO 80225-0007		**10. SPONSOR/MONITOR'S ACRONYM(S)** **R&D:** Research and Development Office **BOR/USBR:** Bureau of Reclamation DOI: Department of the Interior
		11. SPONSOR/MONITOR'S REPORT NUMBER(S) ST-2017-3425-01
12. DISTRIBUTION / AVAILABILITY STATEMENT **Final report can be downloaded from Reclamation's website: https://www.usbr.gov/research/**		
13. SUPPLEMENTARY NOTES		

14. ABSTRACT *(Maximum 200 words)*

Mercury is a toxic metal that is found both naturally and as an introduced contaminant in an aquatic environment. Even very low concentrations of Methylmercury (MeHg) in water lead to bioaccumulation through food web and may cause high levels of mercury contamination in fish in aquatic systems. So, MeHg is the form of the greatest concern for both human health and ecosystems. In this research a two-dimensional (2D) depth-averaged mercury and water quality model is developed by integrating SRH-2D model and mercury modules (MMs). SRH-2D is a 2D depth-averaged flow and sediment transport model developed at the U.S. Bureau of Reclamation and widely used for engineering projects. MMs are developed at the US Army Corps of Engineer (USACE) which has been incorporated into HEC-RAS 1Dand AdH. This report provides the literature review, model methodology design and discussion, theoretical background of the model, data inputs, and data collection and sites identifications for future model validation and applications.

15. SUBJECT TERMS
Mercury Modeling, Water Quality Model, 2D Model

16. SECURITY CLASSIFICATION OF:			17. LIMITATION OF ABSTRACT U	18. NUMBER OF PAGES 112	19a. NAME OF RESPONSIBLE PERSON Yong G. Lai
a. REPORT U	b. ABSTRACT U	c. THIS PAGE U			19b. TELEPHONE NUMBER 303-445-3560

BUREAU OF RECLAMATION

Research and Development Office
Science and Technology Program

Sedimentation and River Hydraulics Group, Technical Service Center, 86-68240

Final Report ST-2017-3425-01

An Integrated Mercury Model: Literature, Methodology and Data

Prepared by:

Yong G. Lai, Ph.D., Hydraulic Engineer
Sedimentation and River Hydraulics Group, Technical Service Center, 86-68240
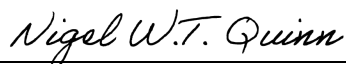
Nigel Quinn, Ph.D., P.E.
Berkeley National Laboratory, Berkeley, CA

Michael Mosley, P.E., Water Quality Coordinator
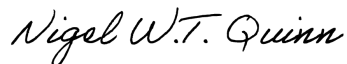Mid-Pacific Region, Bureau of Reclamation, Sacramento CA

Zhonglong Zhang, Ph.D.
LimoTech, Environmental Laboratory, US Army Corp of Engineers
Environmental Research and Development Center, Vicksburg, MS

Joel Sh~
_____
Checked by: Joel Sholtes, Ph.D., Hydraulic Engineer
Sedimentation and River Hydraulics Group, Technical Service Center, 86-68240

Nigel W.T. Quinn
_____
Technical Approval: Nigel W.T. Quinn, Berkeley National Laboratory, Berkeley, California

Nigel W.T. Quinn
_____
Peer Review: Nigel W.T. Quinn, Berkeley National Laboratory, Berkeley, California

Acknowledgements

Executive Summary

This document reports the literature study, the proposed methodology of an integrated mercury transport model, data needs and potential data for model validation. It serves as a companion report to the other report by Lai (2017) titled, "SRH-WQ: A Water Quality and Mercury Transport Model for Streams and Reservoirs." Both reports are the results of a 3-year research project, "An Integrated Modeling Tool to Assess Mercury Transport and Transformation Processes at Reservoirs." The project is funded by Reclamation Science and Technology Program, with additional funding support by the Reclamation Mid-pacific Region and cost-share and in-kind participation of Environmental Laboratory, US Army Corp of Engineers (USACE) at the Research and Development Center (ERDC), Berkeley National Laboratory and other California State Agencies.

This report documents primarily the research activities as summarized below:

- A literature study: The review extended to include new literature relevant to the mercury modeling research and ascertain the current status of mercury research and numerical modeling. Existing mercury cycling models were reviewed and updated in this report.

- The proposed methodology of developing a mercury model: The new integrated mercury model, named SRH-WQ), is for mercury transport and transformation and initially intended for stream and reservoir modeling. SRH-WQ will be based on the aquatic mercury simulation module HgSM developed by ERDC along with other water quality modules, the two-dimensional (2D) flow and sediment transport model SRH-2D developed at Reclamation, and development of a 2D transport module for water quality and mercury constituent movement through streams and reservoirs. The theory and governing equations of HgSM, SRH-2D and SRH-WQ are fully documented in a separate companioning report entitled "SRH-WQ: A Water Quality and Mercury Transport Model for Streams and Reservoirs - Technical Report No. SRH-2017-32".

- Data needs and data for model verification: The initial plan of the study was to focus on Folsom dam/reservoir as a future site for model verification and model application. Data gathering initiated during year 1 provided very little usable data and very little information to assist with mercury speciation or environmental conditions at the time of data collection. Since the project integrates streams and reservoirs in the simulation of mercury fate and transport – well designed data gathering campaigns are needed to collect data simultaneously in both systems. An alternative data collection and synthesis approach is described in this document that promotes the development of proxy relationships based on monitoring in adjacent Cache and Putah Creek watersheds

Contents

Tables

Figures

1. Introduction

1.1 About Mercury Research

Mercury is a toxic metal that is found both naturally and as an introduced contaminant in an aquatic environment. Mercury exists in several different chemical species with highly differing behaviors and toxicities. The most important species of environmental concern are elementary mercury (Hg0), inorganic mercury (HgII) and organic mercury, particularly methylmercury (MeHg). Hg0 is the most common form of mercury found in the atmosphere (USEPA 1997). HgII and MeHg can exist in the dissolved phase as well as in the colloidal and suspended phases in aquatic systems. Inorganic mercury is bound to chloride, sulfide, or organic acids and is lumped together by most mercury-cycling models into a single species which is identified by reactive mercury (HgII). During the biogeochemical cycling of mercury, organic mercury species can be produced. MeHg accounts for the majority of the organic mercury species in freshwater systems. Even very low concentrations of MeHg in water lead to bioaccumulation through food web and may cause high levels of mercury contamination in fish in aquatic systems (Wang et al., 2004). So, MeHg is the form of the greatest concern for both human health and ecosystems (USEPA, 1997; Carroll et al., 2000).

Presence of methylmercury (MeHg) in many western reservoirs has led to the identification of state-level water quality standards and control programs, e.g., in California, Oregon, Washington, Colorado and other states. Reservoir owners will be required to comply with these new standards as they need to develop and implement various reservoir mercury management practices. A number of current research projects have demonstrated that some management practices can lead to MeHg reduction, but that there is no standard for the reservoir environment. Research has also indicated that each aquatic environment should be evaluated individually; similar conditions in separate reservoirs have been shown to produce different rates of mercury bioaccumulation. The reasons for these mercury bioaccumulation differences are often specific to the particular water body. Therefore, management practices should be evaluated at an individual reservoir basis. Untested management practices may be ineffective at providing the appropriate level of mitigation and can be cost prohibitive for large reservoir operators at Reclamation.

1.2 Research Needs and benefits

Methylmercury in reservoirs is becoming an urgent water quality issue for many agencies since state water quality regulatory agencies have established water quality standards for mercury in many states such as California, Oregon, Washington, and Colorado. Enforcement of the mercury water quality standard varies by state but reservoir owners will be required to comply with the new standards. Some states choose to mandate management practices while others choose collaborative approaches. The State of California, for example, has performed research and is using the research to develop and encourage mercury management practices as a part of a TMDL development process. These practices may be cost prohibitive for large reservoir operators within the state. Even if they are implemented, the success of providing the appropriate level of mitigation in Reclamation facilities is uncertain since these practices have not been tested and researched. There is an urgent

need to have access to a reliable mercury model that may be used to assess the feasibility of mercury management measures at reservoirs. Without a means to evaluate reservoir mercury processes agencies may be forced to implement unreasonable mercury control practices. In the Mid-Pacific Region of Reclamation, for example, the need has been identified to develop a framework for decision making related to mercury management in reservoirs. This research will assist in finding the most efficient and cost effective solutions. At the present, a reliable modeling tool to assess methyl-mercury processes is the best alternative. A modeling tool may benefit the reservoir managers and operators to answer the question of whether reservoir operational changes can be developed to reduce mercury methylation. In the San Joaquin River Basin the concept of real-time salinity management has been incorporated into the current Basin water Quality Control Plan as an alternative to typical TMDL load-based salinity management. Real-time salinity management allows greater mass loading of salt to the San Joaquin River while maintaining compliance with River salinity objectives. The modeling tool might be used for real-time decision support in a similar manner – reducing the cost of mercury management activities while maintaining compliance with River methyl- mercury objectives.

The State Water Resources Control Board in California initiated a mercury control program for reservoirs in 2007 to begin to address mercury contamination above the water quality standard in 74 reservoirs. At the time of the initial meeting, little was known by the regulatory agency about the mercury cycle and how reservoir conditions affect mercury methylation. The timeline below (Figure 1) depicts the regulatory milestones related to the California Mercury Control Program.
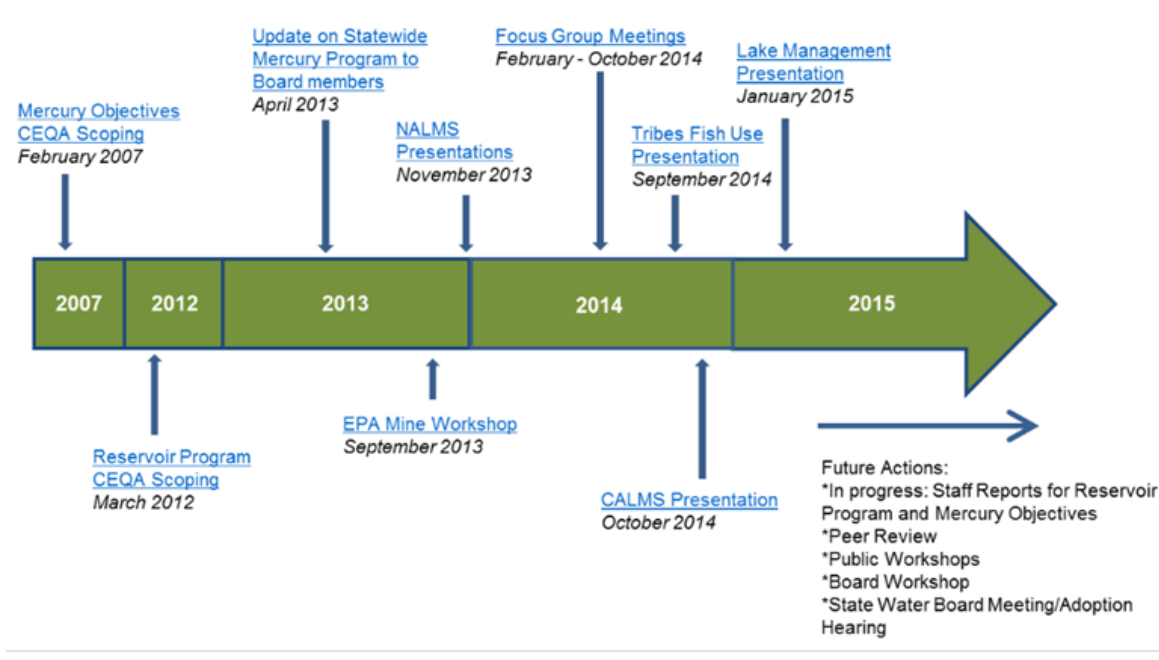
Figure 1. Timeline of California statewide mercury control program activities

Every Reclamation reservoir in the state of California is listed on the Clean Water Act 303(d) list as impaired for mercury. It is imperative that Reclamation collaborate with the state regulatory agency while gathering data and developing tools to understand the mercury cycle in each reservoir. Several other states have initiated mercury management programs including Washington, Oregon

and Colorado. The tool developed as a result of this project will undoubtedly aid Reclamation and the larger reservoir operations community in understanding mercury in their own reservoirs and developing effective mercury management strategies.

1.3 Scope and objective

In this study, we propose to develop an integrated mercury transport and transformation model, involving flow hydrodynamics, sediment transport, water quality (nutrient), and mercury cycling and transport, to answer the following question:

- Can a reliable integrated mercury dynamic model be developed that can be used to assess the feasibility and effectiveness of mercury management measures in reservoirs?

The research will focus on the integrated model development with its initial target applications for streams and reservoirs. The overall thrust is to enable the prediction of future environmental conditions resulting from both human and natural influences and to provide information that could be used to guide decision-making. Such capabilities also allow the stakeholders to predict and assess the impacts of operational/engineering alternatives.

1.4 Technical approach

There are many existing water quality models for reservoir assessment, but only a few have the capability of modeling mercury cycling and transport.

Dynamic Mercury Cycling Model (D-MCM) (EPRI, 2009) is one of the models which has been used extensively in mercury research studies. D-MCM simulates mercury cycling and bioaccumulation in aquatic systems and can simulate three different forms of mercury in water, sediments and food web. D-MCM has been applied to the Gulf of Mexico, Florida Everglades and Great Lakes. It has also been used in regulatory studies in Florida, Wisconsin and California. However, D-MCM is limited at present as it does not simulate hydrodynamics or sediment particle transport in space and fluxes of water and sediment, as well as other constituents reply mostly on user inputs. Other models containing the mercury component are the Water Quality Simulation Program (WASP) developed by the U.S. Environmental Protection Agency (Wool et al., 2006), and the Environmental Fluid Dynamics Code (EFDC) developed by USACE. The depth of development and practical application for mercury processes of WASP and EFDC are not as far-reaching as the D-MCM.

Our team members at the U.S. Army Engineering Research and Development Center (ERDC) have developed several water quality modules that may be integrated with the Reclamation multi-dimensional flow and sediment models. The aquatic Nutrient Simulation Module (NSM) (Zhang and Johnson, 2015a), Contaminant Simulation Module (CSM) and Mercury Simulation Module (HgSM) (Zhang and Johnson, 2015b) have been developed and incorporated into the popular 1D HEC-RAS model. In this project, the HgSM developed by ERDC has been adopted for SRH-2D's mercury module. The HgSM module adopted the mercury kinetic algorithms and formulations used by WASP and D-MCM.

At present, no integrated hydrodynamic, sediment transport, water quality and mercury cycling and transport models exist which may be used to simulate mercury processes in reservoirs. There is an urgent need to develop such an integrated modeling tool. A reliable tool will enable engineers to assess the feasibility of mercury management measures in Reclamation facilities. Without such tools to evaluate reservoir mercury processes, Reclamation may be compelled by water quality regulators to implement unreasonable mercury control practices.

Our research strategy is as follows:

- We will adopt the Reclamation model SRH-2D, a widely used 2D flow and sediment transport model developed by Dr. Yong Lai. STH-2D is used as a platform for developing the integrated mercury model. SRH-2D is robust and reliable in predicting flow and sediment transport and it will enhance the mercury modeling as well as fish tissue accumulation.

- Our team members at Environmental Laboratory of ERDC have developed and will continue to develop their water quality modules including NSM and HgSM. These modules will be integrated into SRH-2D to form an integrated model for mercury modeling in reservoirs. The integration will be achieved by developing a 2D transport module that provides reliable mercury transport through the aquatic system.

- Our Mid-Pacific region research teams at Reclamation will work with various agencies to select specific reservoir sites, gather existing data, and carry out additional field data collection so that the integrated mercury model may be tested, verified and validated against actual reservoirs after its development and test.

2. Review of Literature

2.1 Introduction

Mercury is a potent and dangerous neurotoxin for humans, especially developing fetuses and children who are the most susceptible cohort to suffer mercury toxicity (NRC, 2000). The most direct and important exposure pathway is through the consumption of methylmercury in fish tissue although inhalation of elemental mercury fumes can also be harmful. Mercury toxicity is well documented in populations that consume contaminated fish (Davidson et al., 1998; Grandjean et al., 1997; Kjellstrom et al., 1989; Tsubaki and Irukayama, 1977). Some of the serious impacts associated with consumption of contaminated fish include tingling or loss of tactile sensation (paresthesia), loss of muscle control, blindness, paralysis, birth defects and death. Children whose mothers ate fish during pregnancy may be at risk for more subtle behavioral and neurodevelopmental impairments (Crump et al., 1998; Davidson et al., 1998; NRC, 2000). Children who eat fish themselves are also believed to be more sensitive than adults to mercury because their neural systems are still developing and they tend to consume more fish per body weight than adults (Grandjean et al., 1999; Mahaffey, 1999). Effects in children exposed early in development appear at dose levels five to ten times lower than dose levels associated with toxicity in adults (NRC, 2000).

Mercury (Hg) can exist in a number of forms in the environment, existing naturally in many minerals such as cinnabar (HgS), corderoite ($Hg_3S_2Cl_2$) and livingstonite ($HgSb_4S_8$) - cinnabar is the most common mercury-bearing ore mostly associated with recent volcanic activity and alkaline hot springs although mercury also occurs as an impurity in fossil ores like coal and in certain non-ferrous metals (Gaffney and Marley, 2014). Mercury is somewhat similar to selenium in its hydrochemistry. Mercury is a metalloid – it has the properties of a metal in that it persists in the environment without being readily broken down. Mercury shares some unique hydrophobic chemical properties with selenium in that it can be methylated via a bacterial process. Mercury may be present in air as mercury vapor, dissolved in the water column, or associated with solid particles in air, water, or soil. Mercury has three main oxidation states: elemental (Hg^0), mercurous ion (monovalent, Hg_2^{+2}), or mercuric ion (divalent, Hg^{+2}). Ionic mercury reacts with other compounds in the environment to form organic and inorganic complexes which include methylmercury (CH_3Hg^+), and dimethylmercury. Hg^{2+} is the most abundant mercury species in aquatic systems. Mercury, in inorganic form (Hg and MeHg), are major contaminants of concern for water quality in the Sacramento-San Joaquin River Delta ("the Delta"). Considerable Hg was released into the Delta watershed from historic Hg mining and the historic use of Hg for gold mining. Windham- Myers et al. (2014) identified legacy Hg from gold and Hg mining as a significant source in the "Yolo Bypass" within the Delta. Other studies suggest that Hg in ecosystems of the western U.S. results from a combination of global atmospheric sources such as coal combustion, regional industrial and mining sources, and local cycling (Reinemann, 2014; Tsui, 2014; Wright, 2014).

2.2 Atmospheric mercury flux and deposition to land and water

The primary pathway of mercury into aquatic systems and the environment is through deposition from the atmosphere. Mercury is released into the atmosphere for example from volcanic activities, wildfires, and coal combustion. Mercury deposited from the atmosphere is transformed and bioaccumulated by various processes into aquatic and terrestrial ecosystems from which it can be resuspended and re-emitted back into the atmosphere (Gaffney and Marley, 2014). Mercury However, most of the new emissions today are due to human activities. In 2005 burning coal and other fossils accounted for most of the mercury emissions in the US(Wentz, Brigham, Chasar, Lutz, & Krabbenhoft, 2014).

Gaffney and Marley (2014) have completed a thorough review of atmospheric mercury sources and trends looking at both natural and anthropogenic sources of mercury. According to their analysis atmospheric deposition of mercury increased from 1848 to 1885 which roughly corresponds to the active gold rush mining period and the increased use of mercury in hydraulic (placer) gold mining operations. Use of mercury ceased in 1884 with legislation which banned the use of mercury for placer gold mining due to the environmental pollution it caused, recognized even then. The eruption of Krakatoa in 1883 produced a distinct mercury signal in atmospheric mercury which finally dissipated around 1885 returning mean mercury levels in the atmosphere to around 6 – 7 ng/l (Gaffney and Marley, 2014). Mercury deposition increased to around10 ng/l in the period between 1930 and the end of World War II in 1945 after which it has steadily increased to peak in the 1980's at levels twenty times higher than pre-industrial levels and declined since to current levels about eleven times pre-industrial levels (Gaffney and Marley, 2014).

Besides the occasional volcanic eruption natural sources of mercury flux to the atmosphere also include geothermal emissions, natural volatilization from the ocean and weathering of minerals with mercury content. These natural emissions are low compared to total global mercury flux to the atmosphere (Pirrone et al., 2009; Pacyna et al., 2010) and have been estimated by Gaffney and Marley at 643 tonnes annually for the planet . Geothermal fluids may be enriched in trace metals including mercury – dissolution and transport of mercury in these fluids is a function of pH, redox potential and the concentrations of complexing agents and other minerals (Varekamp and Buseck, 1984). The formation of elemental mercury is supported by high temperature, high pH, low ionic strength, low partial pressure of oxygen and low sulfur concentrations. When these fluids are in contact with oxidizing or acidic water the conversion to mercury II is likely which results in the re-precipitation of the compound cinnabar. Volatilization of elemental mercury to the atmosphere is driven by heat which in turn is related to the age of the geothermal system. Gaffney and Marley (2014) estimate the global emission of mercury from geothermal sources to be approximately 60 tonnes/year.

Mercury emissions from active volcanos is more difficult to estimate given the infrequency of these events and the wide range in number, relative magnitude and duration of these eruptions. Gaffney and Marley (2014) estimate the range of total global emissions from all volcanic sources at between 1 and 700 tonnes/year – there are currently 50-70 active volcanos around the world at the present time and the large explosive eruptions only account for about 15% of the total mercury emission flux (Gustin et. al., 2008). These authors estimate the average emission from volcanic sources

globally at 112 tonnes/year. They claim there is little evidence of elemental mercury occurring naturally in large amounts in either minerals or soils outside local highly enriched sites such as the New Idria mine in the California Coast Range where the elemental mercury present is the result of past mining activities.

The largest source of mercury flux to the atmosphere is from mercury present in the ocean where it is volatilized from the ocean surface. Submarine geothermal vents resulting from tectonic volcanic activity produce geothermal fluids enriched 1000 times over ambient seawater concentrations that mix with cold oxidized seawater to form Hg^{2+} and precipitate cinnabar in the vicinity of the hydrothermal vents. Current estimates of mercury burial of mercury contaminated sediments on the ocean floor (effective mercury sink) is between 180 and 260 tonnes/year (Amos et al., 2013; Gaffner and Marley, 2014). The naturally-derived mercury flux from ocean to atmosphere has been estimated at 456 tonnes/year (Pironne et al., 2010; Amos et. Al., 2013; Gaffney and Marley, 2014) – which is about 71% of the mercury flux from all natural sources (Gaffney and Marley, 2014).

Current anthropogenic sources of mercury have been divided into two categories: (a) industrial byproducts or raw fuels or raw material processing such as coal burning (33%), mining and smelting (22%) and oil and gas refining (2%)– also termed "unintentional emissions" and (b) activities such as small-scale gold mining (37%) and processing and disposal of consumer products (5%) which have also been termed "intentional emissions" (Gaffney and Marley, 2014). Mercury amalgam in mercury fillings amounts to less than 1% of the total. Small scale gold mining produces the greatest anthropogenic flux mainly as a result of amalgam burning and volatilization from mine tailings (Pirronne et al., 2010; Gaffney and Marley, 2014) and is regarded as one of the most critical environmental issues world-wide – a problem in more than 70 countries.

2.3 Mercury in soils and sediments

Sediments of lakes, reservoirs, and rivers, as well as soils throughout the US serve as stores of mercury contamination, as can be seen in Figure 2. Regions of the US with important coal industry show high concentrations of mercury in soils. Besides atmospheric deposition, mercury is brought into the environment through mining. Mercury was released into the environment through mercury and gold mining. Figure 3 shows mercury and gold mines in 2004 in the United States. In California and the western part of the US mining was carried out in an extensive amount and legacy mercury can be found in the soils (Alpers, Hunerlach, May, & Hothem, 2005).
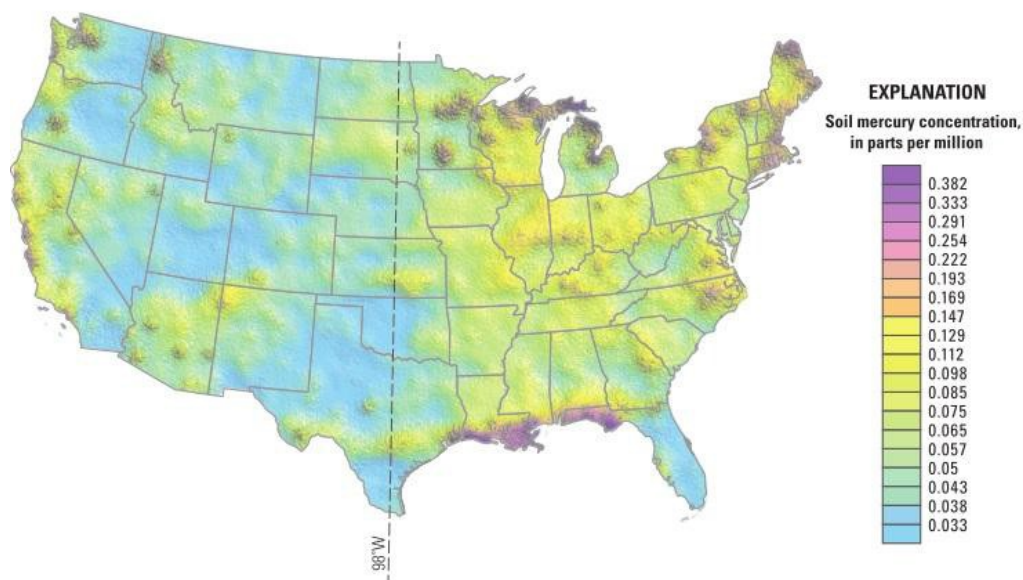
Figure 2: Mercury concentration in soils throughout the US (Wentz et al., 2014)

Mercury and methylmercury form strong complexes with organic substances (including humic acids) and strongly sorb onto soils and sediments. Once sorbed to organic matter, invertebrates can ingest mercury, thus entering it into the food chain. Some of the sorbed mercury will settle to the lake bottom; if buried deeply enough, mercury in bottom sediments will become unavailable to the mercury cycle. Burial in bottom sediments is an important route of removal of mercury from the aquatic environment.
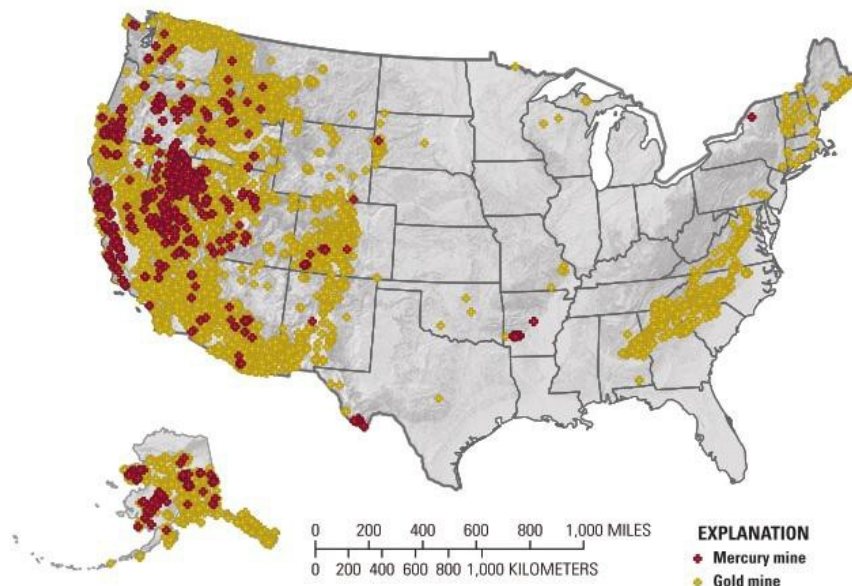
Figure 3: Mercury and gold mines in 2004 in the US (Wentz, Brigham, Chasar, Lutz, & Krabbenhoft, 2014).

2.4 Mercury in water, wetlands, rivers, lakes and reservoirs

Aquatic environments are important sites for methylation, the process transforming mercury into the most toxic form methylmercury. Sulfate-reducing bacteria convert inorganic mercury to methylmercury as a by-product of their normal respiration (Gilmour et al., 1992). Important factors controlling the methylation rate include temperature, percent organic matter, redox potential, salinity, pH, ratio of sulfate to sulfide, and mercury concentration (Barkay et al., 1997; Xun et al., 1987). In lakes, methylation occurs mainly at the sediment water interface and at the oxic-anoxic boundary within the water column. Methylmercury can also be converted back into Hg^{+2}, primarily via bacterial degradation, in a process known as demethylation (Oremland et al., 1995). Dissolved methylmercury is quickly taken up into the food web or demethylated.

Among aquatic environments, wetlands are known to provide conditions promoting methylation(Windham-Myers, 2014). Factors favoring methylation are a good supply of inorganic mercury as a mercury source and organic materials as energy source. We can find these conditions in seasonal wetlands during flood-up and indeed, seasonal wetlands were found to have higher net methylmercury production than permanent wetlands. It was found that output from rice fields is highest during winter flooding. Despite, an enhanced bacteria activity in summer, mercury production decreases due to limited mercury availability in summer and intensified solar radiation(Windham-Myers & Jabusch, 2012). Slow moving shallow water, low oxygen concentrations, and abundant labile plant matter, both present in seasonal managed wetlands, are also considered to enhance methylation (Foresman, 2012; Windham-Myers et al., 2014).

The mercury TMDL and control program adopted for the Delta require substantial reductions in methylmercury sources within the Delta and in its tributary inputs (Wood et al., 2008). Methylmercury is typically produced in anaerobic aquatic sediments of wetlands, lakes and reservoirs where inorganic Hg is converted to MeHg primarily by bacteria during sulfate reduction (Driscoll, 2013; Hsu-Kim, 2013). Wetlands in the San Joaquin and Sacramento Basin are important sources of MeHg loading to the Delta (Alpers et al., 2014, 2005). Furthermore, the San Joaquin River Basin, which includes the Los Banos Wildlife Management Area (WMA), contributes nearly half of all MeHg loading to the Delta, even though it supplies less than 20% of the water flow (Foe et al., 2008). Because the San Joaquin River is a significant Hg source to the Delta, the Hg cycle in wetland tributaries is an important target for science-based management. Monthly measurements of MeHg in filtered and unfiltered samples from Mud Slough and Salt Slough (the primary source of salt, nutrient and trace element contaminants discharged to the San Joaquin River) were collected between April 2003 and July 2006 (Foe et al., 2008).

Methyl-mercury (MeHg) poses a significant health risk to fish and wildlife. This form of mercury is a potent neurotoxin and biomagnifies in the food web, often resulting in elevated levels in fish consumed by wildlife and humans. In 2003, Hg contamination led to 2,140 fish and wildlife consumption advisories, accounting for 76% of all advisories in the State California (Alpers, Hunerlach, May, & Hothem, 2005). Figure 4 provides an overview of methylmercury concentrations in fish throughout the U.S.
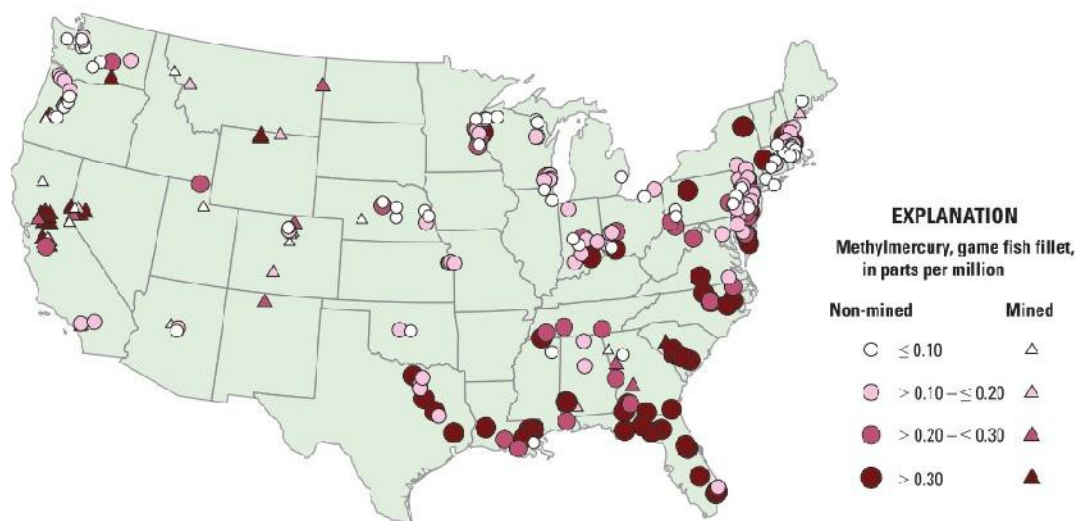
Figure 4: Fish methylmercury concentrations, (Wentz et al., 2014)

The proportion of total mercury in the methylated form typically increases with level of the food chain, and can reach near 90% in top trophic level fish (Nichols et al., 1999). Field research has shown that diet is the primary route of mercury uptake by fish (Wiener and Spry, 1996) and that methylmercury is the predominant form of organic mercury present in most biological systems. In contrast - dimethylmercury, which is an unstable compound that dissociates to methylmercury at neutral or acid pH, is not considered to be a concern in the majority of freshwater systems

10

(USEPA, 1997a). Although diet is also the primary route of methylmercury exposure for organisms that consume fish and aquatic invertebrates - a few studies have indicated that methylmercury directly impairs reproduction of some fish (Huber, 1997; Wiener and Spry, 1996) – hence the greatest concern for mercury toxicity is in higher trophic-level organisms that consume aquatic life. The aquatic food web provides more than 95% of humans' intake of methylmercury (USEPA, 1997c). Wildlife potentially at risk for mercury toxicity includes herons, egrets, grebes, mergansers and other fish-eating waterfowl, kingfishers, bald eagles, osprey, mink, raccoons, bats, and otters.

2.5 Mercury model overview

2.5.1 WARMF Mercury Model

The WARMF model is a water quality simulation model that has been extensively used for salinity and phytoplankton simulation modeling in the San Joaquin River Basin for well over a decade. WARMF is a watershed model that accounts for the contributions of various watershed contaminants and constituents that drain into the river system. Millions of dollars have been invested to improve the calibration of the model for salinity and phytoplankton loading, to use WARMF as a platform for analyzing real-time flow and salinity data, and to make informed forecasts of short-term river assimilative capacity for salt. A submodel to simulate mercury(Hg) hydrochemistry was added to WARMF (C. W. Chen & Herr, 2010). Unlike all other water quality models that have been applied to the San Joaquin Basin, only WARMF considers chemical deposition and makes computations of Hg loading by summing the individual ions in solution. This makes the model a powerful tool in helping to improve the understanding of wetland Hg hydrochemistry and the dynamics of wetland Hg loading to the San Joaquin River.

WARMF is a deterministic flux model that relies on a variety of hydrologic, atmospheric, and aqueous chemical data to parameterize watershed processes, and then uses the parameterized model to simulate future scenarios. Parameters involving Hg were calibrated in WARMF based on data from watersheds in the Lake Superior Basin (Michigan) (EPRI Technical Report, 2006).

In 2006, the WARMF software was enhanced to consider elemental Hg [Hg(0)], inorganic Hg[Hg(2)], and MeHg, and includes parameterized reactions for atmospheric Hg deposition using available precipitation data, Hg adsorption to total suspended solid and dissolved organic carbon, Hg methylation, MeHg adsorption to algae, photo-demethylation of MeHg to Hg(2), and photo-reduction of Hg(2) to Hg(0) (Chen, 2006). However, Hg methylation is primarily a bacterial process linked to sulfate reduction and/or iron reduction, with MeHg concentrations proportional to the concentration of dissolved neutral Hg complexes (e.g. $HgS0$ and $Hg(HS)2$) (Gilmour, 2008; Bessinger, 2012) and possibly thiol-complexed Hg and nano-HgS (i.e. colloidal) that may be bioavailable to methylating bacteria (Schaefer, 2009; Schaefer, 2011; Hsu-Kim, 2013). Likewise, rates of MeHg demethylation depend on temperature, pH, and other environmental variables (Ullrich, 2001). Seasonal wetlands are known sites of MeHg production, but accurate quantification of net production requires a more complete thermodynamic and kinetic description of these biogeochemical processes that are controlled by the local chemical environment.

2.5.2 WASP Mercury Module

The WASP mercury module was developed as a companion to the other two WASP water quality submodels: EUTRO and TOXI. The WASP simulates the transport and fate of Hg0, HgII, and MeHg in surface water. The WASP simulates three mercury components — elemental mercury, Hg0, inorganic divalent mercury, Hg(II), and monomethyl mercury, MeHg. Hg(II) and MeHg are partitioned to suspended and benthic solids and to dissolved organic carbon (DOC) with user-specified partition coefficients for each sorbent type.

The following transformation reactions are simulated in WASP: oxidation of Hg0 in the water column, reduction and methylation of Hg(II) in the water column and sediment layers, and demethylation of MeHg in the water column and sediment layers. These transformation processes are represented as first-order reactions operating on the total pool of the reactants with rate constants that can vary spatially and temperature correction coefficients that adjust the rates with variations in water temperature. Water column reduction and demethylation reactions are driven by sunlight, and so their input surface rate constants are attenuated through the water column using specified light extinction coefficients. Hg0 is subject to volatile exchange between the water column the atmosphere governed by a transfer rate calculated from velocity and depth, and by its Henry's Law constant. Rate constants can be applied to the dissolved, DOC-complexed, and solids-sorbed phases at varying strengths (0 to 1), as specified by the user. WASP computes mercury species and solids concentrations in the water column and sediments of each reach throughout the simulation period. A detailed description of WASP and its mercury module is provided in WASP 6 manual and the overview of the WASP Mercury Module.

2.5.3 D-MCM

The Dynamic Mercury Cycling Model (D-MCM) (Tetra-Tech, 1996, EPRI, 2013) is a time-dependent mechanistic mass balance model for mercury cycling and bioaccumulation. D-MCM simulates a number of major processes involved in the mercury cycle. The model is proprietary and licensed through the Electric Power Research Institute (EPRI) and Reed Harris Environmental Ltd. And is a model that has been used extensively in mercury research studies primarily in the Gulf of Mexico, Florida Everglades and Great Lakes as well as California. The model is capable of simulating three forms of mercury in water, sediments and food web. D-MCM has been applied to It has also been used in regulatory studies in Florida, Wisconsin and California. The major processes simulated are listed in EPRI (2013) as follows:

- inflows and outflows (both surface water and groundwater)
- instantaneous adsorption/desportion
- slow adsorption/desorption of a component of Hg(II) on a particle
- particle settling
- particle decomposition at sediment/water interface and within sediments
- particle resuspension and burial
- atmospheric deposition
- air/water gaseous exchange, industrial mercury sources
- in-situ transformations (*e.g.* biological methylation and demethylation, MeHg photodegradation, Hg(II) reduction and oxidation)

- mercury kinetics in plankton
- methylmercury bioenergetics and fluxes in fish
- Fluxes associated with macrophytes include root uptake, conversion of inorganic Hg(II) to elemental Hg within the plant, air/leaf exchange of elemental Hg related to transpiration, leaf accumulation of atmospheric deposition, and die-off of macrophytes to sediments.
- Four types of particles including labile organics, refractory organics, inorganic fines and coarse fines.
- Other particle properties including carbon content, density, settling and resuspension velocity, Hg partitioning, slow inorganic Hg(II), elemental Hg(0), and MeHg in water, sediments (solids and pore water).
- Simplified foodweb dynamics that include phytoplankton, zooplankton, benthos and three fish species.
- MeHg dynamics in individual fish cohorts are followed for each species using a bioenergetics approach (Harris and Bodaly, 1998).

The model has been provided with an impressive interactive graphical user interface running under Windows XP, Vista and 7 that allows 1D - 3D model system visualization (Figure 5). Model compartments are specified as layers within the water column and sediments, macrophytes – the food web is largely defined by the user. Examples of these compartments are illustrated in Table 1 (EPRI, 2013).
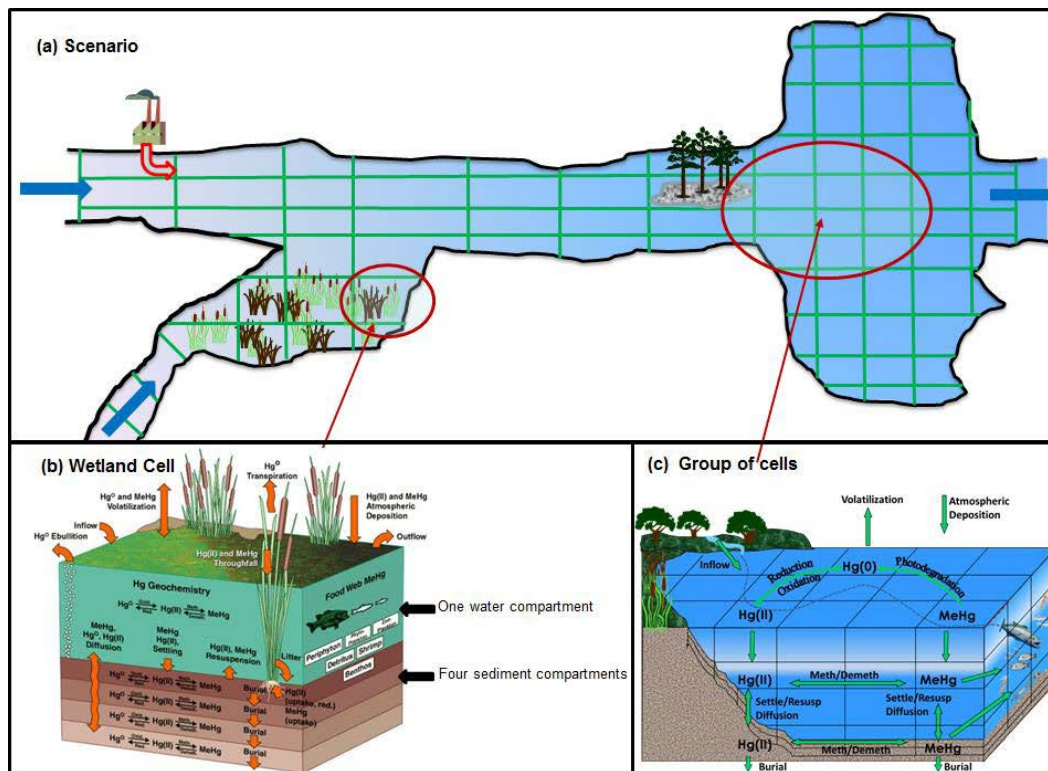
Figure 5. Graphical representation of a D-MCM application including a river, wetland and downstream receiving water (EPRI, 2013).

Table 1. Table 1. D-MCM model structure and compartment characteristics

Compartment	Mercury Form			
	MeHg	Hg(II)	Elemental Hg	Solid HgS
Water Column Abiotic (multiple layers possible)				
Dissolved	●	●	●	
Non-living suspended particles (readily exchangeable) – 4 types of particles	●	●		●
Non-living suspended particles (slowly exchanging) - 4 types of particles		●		
Sediments (multiple layers possible)				
Sediment porewater	●	●	●	
Sediment solids (readily exchangeable) - 4 types of particles	●	●		●
Sediment solids (slowly exchanging) - 4 types of particles		●		
Macrophytes (multiple species possible)_	●	●	●	
Foodweb example (up to 30 organisms)				
Phytoplankton	●	●		
Periphyton	●	●		
Zooplankton	●	●		
Benthos 1	●	●		
Benthos 2	●	●		
Finescale dace	●			
Yellow perch	●			
Walleye	●			

The model's major strength is as a systems analysis tool and decision support system allowing the user to explore the impact of mercury contamination on foodweb dynamics and response. Since in many systems mercury concentration in sediments tends to increase with age, the model is able to track each year class using bioenergetics equations. Two types of mercury binding sites are simulated in sediments and in the water column –solids can have fast exchanging sites represented using an instantaneous equilibrium approach or slower exchanging sites that are simulated using traditional kinetics of adsorption, desorption, and particle decomposition (EPRI, 2013). Most water and sediment fluxes are not computed – rather are added as source, sink terms to the model – hence mercury concentrations in the atmosphere are provided to the model as boundary conditions in order to estimate fluxes across the air/water interface (including gaseous, wet deposition, dry deposition). The current version of the model, as previously noted, does not simulate hydrodynamics or sediment particle transport. This model simplification reduces the complexity of the model and improves computation time – however it potentially detracts from the accuracy of the model in situations where mercury hydrogeochemistry is significantly impacted by changes in system hydrodynamics.

The food web simulated by the current version of the D-MCM model can include multiple trophic levels (*e.g.* plankton, benthos, several fish species) with up to 30 food web compartments. Version 4 of the D-MCM model also is able to simulate fish migration.

The current user interface provided in the D-MCM model was designed to allow users to operate at two levels of detail - standard or advanced. The standard list of inputs shows only those likely

to be modified by most users. This is of benefit to novice users and practitioners who need to make standardized model runs. The advanced level provides the user access to all inputs. The model inputs can be customized for a given site and application depending on the site-specific data that are available.

The proprietary nature of the model and its expense for the user limit the D-MCM model utility for use by some State and Federal agencies, especially those that are mandated to use open-source, public domain codes such as the current HgSM model under development and described in this document (Carol DiGorgio, personal communication, California Department of Water Resources, 2016). The proprietary nature of the D-MCM model code also limits the use of the model in academic research.

2.5.4 Other coupled modeling approaches

Coupled thermodynamic and kinetic reaction models have been developed (Bessinger et al., 2012; O'Day, 2015) to simulate net MeHg production in wetlands during wet and dry cycles. These biogeochemical reaction models provide a quantitative framework describing the processes affecting partitioning, transformation, and fate of Hg and MeHg in the the terrestrial and aquatic environment. Several of these models build upon the USGS-supported PHREEQC model, (Parkhurst, 1999), which focused on the impact of biogeochemical redox zonation on the fate of Hg and Me-Hg in capped sediments (Bessinger, 2012). The accuracy of all biogeochemical reaction models depends on: (a) the establishment of a reliable, internally consistent thermodynamic database for relevant reactions between aqueous, solid and gaseous species and (b) on a biogeochemical reaction matrix related by kinetic rate laws incorporating mechanistic descriptions of the processes (O'Day, 2015). Databases should include the best available equilibrium constants for Hg aqueous inorganic complexes (except sulfur-based ligands), Hg and MeHg sorption to sediment organic matter (SOM) and dissolved organic matter (DOM) (Skyllberg, 2008. O'Day, 2015), and precipitation of mercuric sulfides (cinnabar and metacinnabar) (Bessinger, 2012). Hg sulfide complex stability constants and HgS solubility products were recently critical reevaluated (Drott, 2013). The reaction matrix for Hg methylation is being expanded to include rate laws for methylation by iron-reducing bacteria as well as sulfate-reducing bacteria (O'Day, 2015).

2.5.5 O'Day- biogeochemical modeling framework model

O'Day (2015) has developed a model, which is based on prior studies by Van Cappellen, (1996), Hunter (1998) and Canavan (2006) that uses a Monod-type description of biogeochemical reactions and rates with both primary reduction and secondary oxidation reactions. The overall degradation rate of organic matter (OM), expressed as either SOM or DOM, is treated as the sum of individual reaction rates of successive terminal electron acceptors. The rate of MeHg formation is calculated using a modified equation from Gilmour (2008), which depends on the rate of bacterial sulfate reduction and the total concentration of dissolved neutral Hg sulfide complexes computed for the system based on thermodynamic speciation. The model is adaptable to describe sediment and sediment-water interface processes in waterbodies such as lakes and seasonally flooded wetlands relying on field measurements before and during water level drawdown and re-

flooding. For model data input - in addition to total Hg, MeHg, DOM, SOM, and standard water quality parameters, sediments and sediment pore waters should be sampled for sulfide, polysulfides, reduced iron, manganese, and other redox-active species to quantify reducing conditions during stagnant periods and water drawdown. For managed seasonal wetlands - flooding in the fall is expected to potentially mobilize and transport Hg and MeHg.

2.6 Model Comparison

A comparison of HgSM, WASP and D-MCM mercury model kinetics and aquatic processes is shown in Table 2. All three models simulate mercury in the water column and benthic sediments and simulate air deposition of mercury, sediment-water diffusion, water column settling and sediment resuspension/ deep burial. The hydrogeochemical dynamics of all three main mercury species are also simulated by all three models. Only the HgSM model is able to track linear equilibrium partitioning of HgII and MeHg that includes both organic and inorganic solids sorption on multi-solids. The HgSM model simulates non-linear equilibrium partitioning of HgII and MeHg chemical species – this is a feature that neither the WASP nor D-MCM models can emulate. This distinction also applies to non-equilibrium partitioning of HgII. All three models have capabilities of simulating transformations of the three mercury species Hg0, HgII and MeHg.Sulfide complexation with HgII and MeHg is important to the complex food web dynamics simulations performed by D-MSM and this is a feature unique to this model. As previously mentioned, D-MSM has the ability to define complex food webs and track the interaction between components of the food web assigned to various stacked compartments.

The HgSM model, with its emphasis on hydrodynamics as a mechanism for mercury hydrogeochemical dynamics in the water column and benthic sediments, has the ability to communicate with water quality modules TEMP and NSM and with hydrologic and hydraulic routing models including HEC-RAS and SWAP and the flow and water quality model CE-QUAL-W2.

Table 2. Mercury hydrogeochemistry model comparisons

Feature	HgSM	WASP mercury module	D-MCM
	Dynamic linked library	Dynamic linked library	Independent model
Dimension	Box	1D, 2D, 3D	1D, 2D, 3D
Water Column	Yes	Yes	Yes
Benthic sediments	Yes	Yes	Yes
Air deposition	Yes	Yes	Yes
Sediment-water diffusion	Yes	Yes	Yes
Water column settling and sediment resuspension/ deep burial	Yes	Yes	Yes
Hg species	Hg0, HgII, MeHg	Hg0, HgII, MeHg	Hg0, HgII, MeHg
Linear equilibrium partitioning of HgII and MeHg	User-defined multi-phases: Dissolved in water Sorbed on DOC Sorbed on algae Sorbed on multi-solids including organic and inorganic solids	5 phases: Dissolved in water Sorbed on DOC Sorbed on biotic solids Sorbed on silt and sand particles	User-defined multi-phases: Dissolved in water Sorbed on DOC Sorbed on algae Sorbed on solids particles
Non-linear equilibrium partitioning of HgII and MeHg	Langmuir and Freundlich partitioning between dissolved and solids	No	No
Non-equilibrium partitioning of HgII	Yes	No	Yes
Hg0 transformations	Volatilization Oxidation in water (Hg0-->HgII)	Volatilization Oxidation in water (Hg0-->HgII)	Volatilization Photochemical oxidation in water (Hg0-->HgII)
HgII transformations	Photoreduction reduction in water (HgII-->Hg0) Methylation in water and sediments (HgII-->MeHg)	Photoreduction reduction in water (HgII-->Hg0) Methylation in water and sediments (HgII-->MeHg)	Photochemical reduction in water (HgII-->Hg0) Methylation in water and sediments (HgII-->MeHg)
MeHg transformations	Volatilization Light demethylation (MeHg-->Hg0) Bacterial demethylation (MeHg-->HgII)	Light demethylation (MeHg-->Hg0) Bacterial demethylation (MeHg-->HgII)	Volatilization Photodegradation (MeHg-->Hg0) in water Biological demethylation in

			sediments (MeHg->HgII)
Sulfide complexation with HgII and MeHg	No	No	$Hg(SH)_2$ $Hg(SH)^+$ $Hg(HS)S^-$ $Hg(S)_2^{2-}$ HgS HgOHHS $(CH_3Hg)S^-$, $(CH_3Hg)_2S$
Food web (phytoplankton, zooplankton, fish)	No	No	Yes
Water quality Q linkage	TEMP NSM	EUTRO TOXI	No
Hydro linkage	HEC-RAS CE-QUAL-W2 SWAT	EFDC	Not sure

Acronyms and abbreviations in the above Table:

TEMP   temperature module developed by HEC and ERDC
NSM   nutrient simulation module developed by ERDC
HgSM   mercury simulation module developed by ERDC
WASP   water quality analysis program developed by USEPA
EUTRO   eutrophication module in WASP
TOXI   toxicant module in WASP
D-MCM   dynamic mercury cycling model developed by EPRI

3. A 2-D Flow, Sediment Transport Model and 2D Constituent Transport Module

An integrated flow, sediment, water quality and mercury model will be developed in this study which has the following features:

- Transport of mercury in aquatic system is closely linked to water and sediment movement in the system. A reliable flow and sediment transport model in the riverine and reservoir/lake environment is needed. Flow and sediment transport in aquatic system, such as reservoirs and streams, are simulated using the 2D, depth-averaged flow and sediment transport model SRH-2D. With SRH-2D model results, reliable water and sediment movement and distribution results are computed. Existing models reply mostly on user inputs of flow and sediment fluxes which are often unavailable and they ignore flow advection and dispersion and sediment interactions.
- Mercury and nutrient modules (HgSM and NSM) developed by USACE will be coupled with SRH-2D so that mercury cycling processes are simulated based on the current state of the art.
- A separate 2D transport module will be developed that is used for mercury and other scalar transport modelling in space and time.

The integrated model will be called SRH-HgSM, and some of the physical processes are described below.

3.1 SRH-2D Overview

SRH-2D, Sedimentation and River Hydraulics - Two-Dimension, is a 2D depth-averaged hydraulic and sediment transport model for river systems. It was developed at the Bureau of Reclamation and has since been widely used. Its flow modeling theory and usage were described by Lai (2008), while its sediment module theory and applications were documented by Lai and Randle (2007), Greimann et al. (2008), Lai and Greimann (2008, 2010), Lai (2010; 2011), and Lai et al. (2011).

3.1.1 Features and Capabilities

A major feature of SRH-2D is the use of a flexible mesh for modeling. The arbitrarily shaped element method of Lai et al. (2003) is adopted for geometry representation. This essentially allows the use of most existing meshes available: structured quadrilateral mesh, purely triangular finite element mesh, Cartesian mesh, or hybrid mesh. Our experience shows that a hybrid mesh which uses quadrilateral meshes along main channel and triangular meshes in the remaining zones is the best choice; it often leads to increased accuracy and efficiency. Samples meshes are shown in Figure 6 and Figure 7.
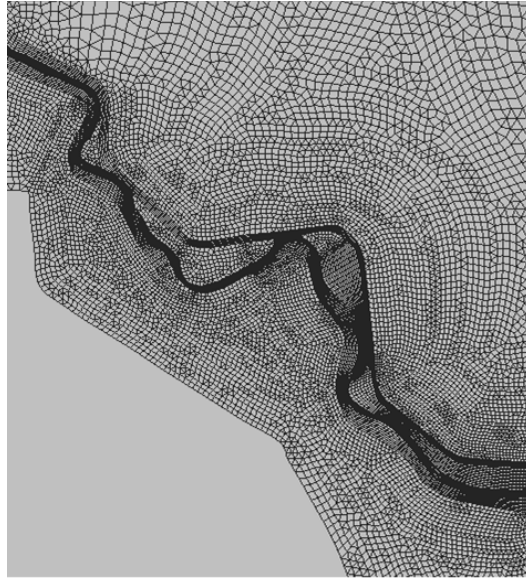
Figure 6. A sample mesh used by SRH-2D; quadrilateral cells are used along the main channel and levees and mixed coarser cells are in the floodplains
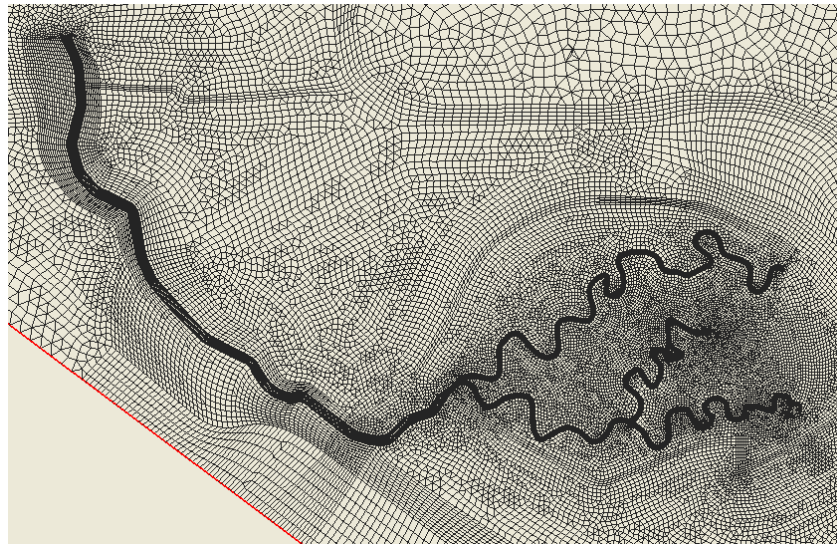
Figure 7. A sample SRH-2D mesh that uses a combination of structured and unstructured meshes

Major capabilities of SRH-2D are listed below:

- 2D depth-averaged solution of the dynamic wave equations for flow hydraulics;

- An implicit solution scheme for solution robustness and efficiency;

- Hybrid mesh methodology which uses the arbitrary mesh cell shapes. In most applications, a combination of quadrilateral and triangular meshes works the best;

- Steady or unsteady flows;

20

- All flow regimes simulated simultaneously: subcritical, supercritical, or transcritical flows;

- Mobile bed modeling of alluvial rivers with a steady, quasi-unsteady, or unsteady hydrograph.

- Non-cohesive or cohesive sediment transport;

- Non-equilibrium sediment transport;

- Multi-size sediment transports with bed sorting and armoring;

- A single sediment transport governing equation for both bed load, suspended load, and mixed load;

- Effects of gravity and secondary flows at curved bends; and

- Granular bed, erodible rock bed, or non-erodible bed.

SRH-2D is a two-dimensional (2D) model, and it is particularly useful for problems where 2D effects are important. Examples include flows with in-stream structures such as weirs, diversion dams, release gates, coffer dams, etc.; bends and point bars; perched rivers; and multi-channel systems. 2D models may also be needed if some hydraulic characteristics are important such as flow recirculation and eddy patterns, lateral variations, flow overtopping banks and levees, differential flow shears on river banks, and interaction between the main channel, vegetated areas and floodplains. Some of the scenarios listed above may be modeled in 1D, but additional empirical models and input parameters are used and extra calibration must be carried out with unknown accuracy.

In the following, only the basic governing equations solved by SRH-2D are presented and the specifics about the numerical discretization and solution schemes may be found in Lai (2008).

3.1.2 Flow Equations

Most open channel flows are relatively shallow and the effect of vertical motions is negligible. As a result, the three-dimensional Navier-Stokes equations may be vertically averaged to obtain a set of depth-averaged 2D equations, leading to the following standard St. Venant equations:

$$\frac{\partial h}{\partial t} + \frac{\partial hU}{\partial x} + \frac{\partial hV}{\partial y} = 0 \tag{3.1a}$$

$$\frac{\partial hU}{\partial t} + \frac{\partial hUU}{\partial x} + \frac{\partial hVU}{\partial y} = \frac{\partial hT_{xx}}{\partial x} + \frac{\partial hT_{xy}}{\partial y} - gh\frac{\partial z}{\partial x} - \frac{\tau_{bx}}{\rho} \tag{3.1b}$$

$$\frac{\partial hV}{\partial t} + \frac{\partial hUV}{\partial x} + \frac{\partial hVV}{\partial y} = \frac{\partial hT_{xy}}{\partial x} + \frac{\partial hT_{yy}}{\partial y} - gh\frac{\partial z}{\partial y} - \frac{\tau_{by}}{\rho} \tag{3.1c}$$

In the above, x and y are horizontal Cartesian coordinates, t is time, h is water depth, U and V are depth-averaged velocity components in x and y directions, respectively, g is gravitational acceleration, T_{xx}, T_{xy}, and T_{yy} are depth-averaged stresses due to turbulence as well as dispersion,

$z = z_b + h$ is water surface elevation, z_b is bed elevation, ρ is water density, and τ_{bx}, τ_{by} are bed shear stresses. The bed stresses are obtained using the Manning's resistance equation as:

$$(\tau_{bx}, \tau_{by}) = \rho U_*^2 \frac{(U,V)}{\sqrt{U^2 + V^2}} = \rho C_f \sqrt{U^2 + V^2}(U,V) \qquad (3.2)$$

where $C_f = \dfrac{gn^2}{h^{1/3}}$, n is Manning's roughness coefficient, and U_* is bed frictional velocity. Effective stresses are calculated with the Boussinesq's formulation as:

$$T_{xx} = 2(\upsilon + \upsilon_t)\frac{\partial U}{\partial x} - \frac{2}{3}k\ ;$$

$$T_{xy} = (\upsilon + \upsilon_t)(\frac{\partial U}{\partial y} + \frac{\partial V}{\partial x}) \qquad (3.3)$$

$$T_{yy} = 2(\upsilon + \upsilon_t)\frac{\partial V}{\partial y} - \frac{2}{3}k$$

where υ is kinematic viscosity of water, υ_t is eddy viscosity, and k is turbulent kinetic energy.

The eddy viscosity is calculated with a turbulence model. Two models are used in SRH-2D (Rodi, 1993): the depth-averaged parabolic model and the two-equation k-ε model. For the parabolic model, the eddy viscosity is calculated as $\upsilon_t = C_t U_* h$ and the frictional velocity U_* is defined in equation (3.2). The model constant C_t may range from 0.3 to 1.0; a default value of $C_t = 0.7$ is used by SRH-2D. For the two-equation k-ε model, the eddy viscosity is calculated as $\upsilon_t = C_\mu k^2 / \varepsilon$ with the two additional equations as follows:

$$\frac{\partial hk}{\partial t} + \frac{\partial hUk}{\partial x} + \frac{\partial hVk}{\partial y} = \frac{\partial}{\partial x}(\frac{h\upsilon_t}{\sigma_k}\frac{\partial k}{\partial x}) + \frac{\partial}{\partial y}(\frac{h\upsilon_t}{\sigma_k}\frac{\partial k}{\partial y}) + P_h + P_{kb} - h\varepsilon \qquad (3.4)$$

$$\frac{\partial h\varepsilon}{\partial t} + \frac{\partial hU\varepsilon}{\partial x} + \frac{\partial hV\varepsilon}{\partial y} = \frac{\partial}{\partial x}(\frac{h\upsilon_t}{\sigma_\varepsilon}\frac{\partial \varepsilon}{\partial x}) + \frac{\partial}{\partial y}(\frac{h\upsilon_t}{\sigma_\varepsilon}\frac{\partial \varepsilon}{\partial y})$$

$$+ C_{\varepsilon 1}\frac{\varepsilon}{k}P_h + P_{\varepsilon b} - C_{\varepsilon 2}h\frac{\varepsilon^2}{k} \qquad (3.5)$$

The expressions of some terms, along with the model coefficients, follow the recommendation of Rodi (1993); they are listed below:

$$P_h = h\upsilon_t\left[2\left(\frac{\partial U}{\partial x}\right)^2 + 2\left(\frac{\partial V}{\partial y}\right)^2 + \left(\frac{\partial U}{\partial y} + \frac{\partial V}{\partial x}\right)^2\right] \qquad (3.6a)$$

$$P_{kb} = C_f^{-1/2}U_*^3\ ; \qquad P_{\varepsilon b} = C_{\varepsilon\Gamma}C_{\varepsilon 2}C_\mu^{1/2}C_f^{-3/4}U_*^4 / h \qquad (3.6b)$$

$$C_\mu = 0.09,\ C_{\varepsilon 1} = 1.44,\ C_{\varepsilon 2} = 1.92, \sigma_k = 1, \sigma_\varepsilon = 1.3, C_{\varepsilon\Gamma} = 1.8 \sim 3.6 \quad (3.6c)$$

22

The terms P_{kb} and P_{kb} are added to account for the generation of turbulence energy and dissipation due to bed friction in case of uniform flows.

3.1.3 Sediment Transport Equations

Sediment transport in a mobile-bed river depends on several key input variables such as topographic and bathymetric features, flow hydraulics, bed gradation, and upstream sediment supply. The bed gradation changes from its initial state as sediment particles are eroded from or deposited on the bed, which in turn changes flow hydraulics and fractional sediment transport rates.

In general, a water column and a river bed may be divided into four separate vertical layers, from a computational point of view:

- Suspended Load Layer: a top layer in the water column where sediment particles are in suspension and are transported as suspended load (including wash load);

- Bed Load Layer: a layer near the bed where sediment particles roll, slide, or saltate. Particles are transported as bed load. Total load refers to the sum of suspended load and bed load;

- Active Layer: a layer on the top surface of the bed where sediment exchange occurs between the sediment load above and the bed underneath; and

- Subsurface Layers: one or several bed layers, which have not been mobilized by flow and are underneath the active layer.

With SRH-2D, transport of the bed material load is considered. That is, the combined suspended load and bed load, but without the wash load, is simulated. The wash load refers to those fine sediments that are transported from the upstream boundary to the downstream exit without interaction with the bed sediments. Wash load is ignored as it does not contribute to the bed morphological changes.

Furthermore, the general modeling approach of the non-uniform and non-equilibrium sediment transport is adopted. Non-uniform transport refers to the representation of sediments with multiple sediment size classes and transport of each size class is tracked separately. The non-uniform approach may be compared with the alternative of the uniform transport method in which all sediments are represented by one size class (d_{50} is usually used). The non-uniform approach is closer to field conditions and is the choice if sediment sorting and other related features are of interest. Non-equilibrium transport refers to the use of the full sediment transport equation in which the sediment concentration does not equal the sediment transport capacity. This is in contrast to the commonly used Exner equation, an equilibrium model, which assumes instant exchange between the transported loads and the bed materials. With the non-equilibrium method, the sediment concentration is allowed to vary in response to local flow features such as convection and dispersion, local transport capacity, and local bed gradation.

In contrast to many existing mobile bed models, a single sediment transport governing equation is used by SRH-2D with different size classes of sediments. The details of the method and its advantages were reported by Greimann et al. (2008). With this approach, a clear cut of suspended bed or bed load is not used. Instead, a load parameter, f ranging from 0 to 1, is used to represent the transport property of a given sediment size class. Zero load parameter indicates a pure bed load while $f =1$ refers to a purely suspended load. The load parameter may be interpreted statistically as the probability a given sediment class will be transported as suspended load.

If all sediments are divided into a number of size classes and each sediment size class (k) obeys the following transport equation derived from mass conservation:

$$\frac{\partial hC}{\partial t} + \frac{\partial \cos(\alpha)V_t hC}{\partial x} + \frac{\partial \sin(\alpha)V_t hC}{\partial y} = S_E \tag{3.7}$$

where C is the depth-averaged sediment concentration, h is water depth, t is time, x and y are two horizontal Cartesian coordinates, respectively, V_t is the depth-averaged total sediment velocity, α is the angle of sediment transport direction relative to the x-axis, and S_E is the sediment exchange rate between the transported sediments and those in the active layer. Specific models for a number of variables in the above equation will not be discussed and may be found in Greimann et al. (2008). It is sufficient to point out a few main features of the above equation: (1) the angle of sediment transport direction is not the same as the water flow. Instead, the angle depends on whether or not the size class is suspended load, bed load, or mixed load, and the impacts of secondary flows and gravity may be included; and (2) The transport velocity of sediment does not have to be the same as water flow velocity. An empirical expression may be used to compute the sediment velocity.

The sediment exchange term is discussed next. For non-cohesive sediments, the exchange term may be expressed as:

$$S_E = \frac{1}{L_{tot}}(q_{tot}^* - V_t hC) \tag{3.8}$$

where q_{tot}^* is the equilibrium transport capacity and L_{tot} is the adaptation length which is calculated as:

$$L_{tot} = (1 - f)L_b + f \zeta V_t h / \omega_s \tag{3.9}$$

where f is the load parameter representing the probability for the sediment to be suspended, ζ is the parameter for the rate of suspended load exchange, L_b is the bed load adaptation length, and ω_s is the particle fall velocity. The bed load adaptation length characterizes the distance for sediments to adjust from the non-equilibrium state to the equilibrium state, and is related to river geometry and the scales of sediment transport characteristics such as saltation and bedform. In this study, a constant L_b was specified. The suspended sediment coefficient, ζ, equals 1.0 for net erosion and 0.25 for net deposition.

A number of sediment capacity equations are available with SRH-2D. For example, the Parker (1990) capacity equation is adopted for gravel river or mixed sand/gravel rivers. The Parker

24

equation is well suited to rivers composed of both coarse sediments (e.g., gravels) and fine sediments (e.g., sands). The transport equation for sediment size class k may be expressed as:

$$\frac{q_{t,k}^* g(s-1)}{(\tau_b/\rho)^{1.5}} = p_{ak}G(\phi_k); \qquad \phi_k = \frac{\theta_k}{\theta_r}\left(\frac{d_k}{d_{50}}\right)^\alpha \qquad (3.10)$$

In the above, $q_{t,k}^*$ is the volumetric sediment transport rate per unit width, p_{ak} is the volumetric fraction of sediment size class k on the bed surface, $s = \rho_S/\rho$, ρ and ρ_S are the water and sediment density, respectively, g is the gravitational acceleration, τ_b is bed shear stress, $\theta_k = \tau_b/\left[\rho g(s-1)d_k\right]$ is Shield's parameter of sediment size class k; θ_r is the reference Shield's parameter, d_k is diameter of sediment size class k, and d_{50} is the median diameter of the sediment mixture in bed. The function in the transport equation was fit to the field data by Parker (1990) and is expressed as:

$$G=\begin{cases} 11.933(1-0.853/\phi)^{4.5}, & \phi>1.59 \\ .00218\exp\left[14.2(\phi-1)-9.28(\phi-1)^2\right], & 1.0\le\phi\le1.59 \\ .00218\,\phi^{14.2}, & \phi<1.0 \end{cases} \qquad (3.11)$$

Two parameters must be defined by a user to apply the Parker equation: θ_r and α. The parameter θ_r is a reference value above which sediment is mobilized and α is the exposure (or hiding) factor to account for reduction in critical shear stress for larger particles and increase in critical shear stress for smaller particles. In this project, the same values adopted by Greimann and Vandeburg (2008) are used: θ_r =0.0385 and α =0.905.

Dynamics of the bed sediments and the bed interaction with the sediment load are also simulated, and details may be found in Greimann et al. (2008).

3.2 2-D Transport Module

A separate 2D depth-averaged transport module is developed that may be used to transport scalar variables such as mercury, temperature, and other water quality variables. The governing equations and the numerical method are documented in detail next.

The 2D transport module solves the following generic convection-diffusion equation:

$$\frac{\partial h\Phi}{\partial t} + \nabla\bullet(h\vec{V}\Phi) = \nabla\bullet(\Gamma\nabla\Phi) + S_\Phi^* \qquad (3.12)$$

Here Φ denotes a scalar variable, h is water depth, t is time, $\vec{V}$ is the velocity vector, Γ is diffusivity coefficient, and S_Φ^* is the source/sink term.

We adopt the finite-volume method to carry out the discretization of the above equation, consistent with the approach of SRH-2D. That is, the governing equation is integrated over an arbitrarily shaped polygon P as shown in 8. This leads to:

$$\frac{(h_P^{n+1}\Phi_P^{n+1} - h_P^n\Phi_P^n)A}{\Delta t} + \sum_{all-sides}(h_C V_C |\vec{s}|)^{n+1}\Phi_C^{n+1} = \sum_{all-sides}(\Gamma_C^{n+1}\nabla\Phi^{n+1}\bullet\vec{n}|\vec{s}|) + S_\Phi \quad (3.13)$$

In the above, Δt is time step, A is cell area, $V_C = \overrightarrow{V_C}\bullet\vec{n}$ is velocity component normal to the polygonal side (e.g., P_1P_2 in Figure 8) and is evaluated at the side center C, $\vec{n}$ is unit normal vector of a polygon side, $\vec{s}$ is the polygon side distance vector (e.g., from P_1 to P_2 in Figure 8), and $S_\Phi = S_\Phi^* A$. Subscript C indicates a value evaluated at the center of a polygon side and superscript, n or $n+1$, denotes the time level. In the remaining discussion, superscript $n+1$ will be dropped for ease of notation. The first-order Euler implicit time discretization is adopted. The remaining task is to obtain appropriate expressions for the convective and diffusive fluxes at each polygon side.
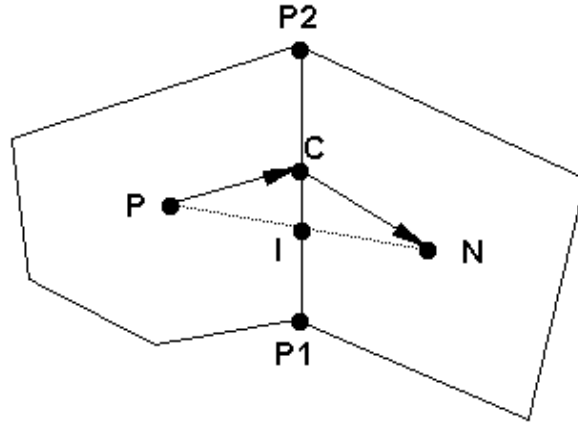
Figure 8. Schematic illustrating a polygon cell P along with one of its neighboring polygons N

Discretization of the dispersion term, the first on the right hand side of (3.13), is carried out first and the final expression is derived as:

$$\nabla\Phi\bullet\vec{n}\,|\vec{s}| = D_n(\Phi_N - \Phi_P) + D_c(\Phi_{P2} - \Phi_{P1}) \quad (3.14a)$$

$$D_n = \frac{|\vec{s}|}{(\vec{r}_1 + \vec{r}_2)\bullet\vec{n}} \quad ; \qquad D_c = -\frac{(\vec{r}_1 + \vec{r}_2)\bullet\vec{s}/|\vec{s}|}{(\vec{r}_1 + \vec{r}_2)\bullet\vec{n}} \quad (3.14b)$$

In the above, $\vec{r}_1$ is the distance vector from P to C and $\vec{r}_2$ is from C to N. The "normal" and "cross" diffusion coefficients, D_n and D_c, at each polygon side involve only geometric variables; they are calculated only once in the beginning of the computation.

Computation of a variable, say Y, at the center C of a polygon side invokes interpolations, and it is computed by:

$$Y_C = \frac{\delta_1 Y_N + \delta_2 Y_P}{\delta_1 + \delta_2} \tag{3.15}$$

in which $\delta_1 = \vec{r}_1 \bullet \vec{n}$ and $\delta_2 = \vec{r}_2 \bullet \vec{n}$. Φ_C in the convective term of (3.13) needs further discussion. If the second-order central scheme is used directly, spurious oscillations may occur for flows with a high cell Peclet number. Therefore, a damping term is added to the central difference scheme similar to the concept of artificial viscosity. The damped scheme is as follows:

$$\Phi_C = \Phi_C^{CN} + d(\Phi_C^{UP} - \Phi_C^{CN}) \tag{3.16}$$

$$\Phi_C^{UP} = \frac{1}{2}(\Phi_P + \Phi_N) + \frac{1}{2} sign(V_C)(\Phi_P - \Phi_N) \tag{3.17}$$

where Φ_C^{CN} is omputed by eqn (3.15). In the above, d defines the amount of damping. Note that d is not a calibration parameter and a non-zero d makes the convective scheme less than second-order accuracy.

The final discretized equation at mesh cell P may be organized as a linear equation:

$$A_P \Phi_P = \sum_{nb} A_{nb} \Phi_{nb} + S_\Phi \tag{3.18}$$

where "nb" refers to all neighbor cells surrounding cell P. The implicit solver requires the solution of non-symmetric sparse matrix linear equations (3.18). In this study, the standard conjugate gradient solver with the Incomplete Lower-Upper (ILU) preconditioning is used.

4. Water Quality Modules

4.1 General Approach

The Environmental Laboratory of U.S. Army Engineer Research and Development Center (ERDC) has developed a set of "plug in" water quality modules for a variety of hydrologic and hydraulic (H&H) models. These modules were designed to be independent of the dimensionality of the spatial domain and only compute the speciation and biochemical reactions in aquatic systems. The transport component in H&H models is responsible for simulating the physical processes of advection, dispersion, and boundary inflow across the model domain. All "plug in" water quality modules are written as dynamic link libraries (DLLs) and have been integrated into HEC-RAS. To describe the transport and transformations of mercury in reservoirs, two water quality modules will be integrated into SRH-2D: nutrient simulation module (NSMI) and mercury simulation module (HgSM). NSMI models algae and benthic algae biomass, simple nitrogen and phosphorus cycles, organic carbon, carbonaceous biochemical oxygen demand, dissolved oxygen and pathogen using 16 state variables. The NSMI is well-documented in Zhang and Johnson (2015a). This Chapter describes the theory and mathematical formulations used in HgSM. The HgSM can also be found in Zhang and Johnson (2015b).

4.2 NSMI Overview

The NSMI was designed to conduct an aquatic eutrophication simulation with simplified processes and minimum state variables. The algorithms that are incorporated into NSMI were derived, in part, from QUAL2E (Brown and Barnwell 1987), QUAL2K (Chapra et al. 2008), WASP (Wool et al. 2006), and CE-QUAL-RIV1 (EL 1995a). Figure 9 provides an overview of the NSMI representation of water quality state variables and major processes involved in the water column.
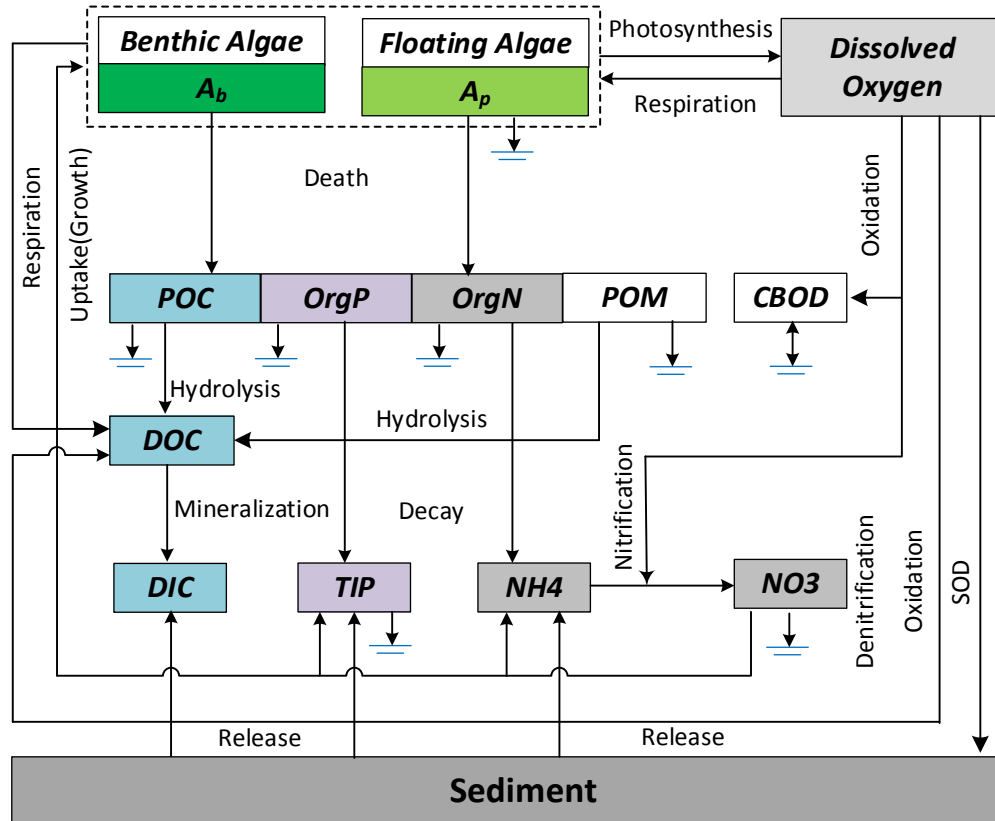
Figure 9. Water quality state variables and major processes modeled in NSMI.

NSMI models up to 16 state variables. Table 3 lists the NSMI's state variables and the symbols. Chla, D, C, N, P and O_2 under the units refer to chlorophyll-a, dry weight, carbon, nitrogen, phosphorus, and oxygen, respectively. The colony forming unit (CFU) is a measure of viable bacterial numbers. The NSMI allows the user to selectively turn on and off each state variable, providing increased flexibility in its application. A discussion of each of the kinetic equations can be found in Zhang and Johnson (2015a).

Table 3. Water quality state variables modeled in NSMI.

Variable	Definition	Units	Option
A_p	Algae (Phytoplankton)	µg-Chla L^{-1}	On/Off
A_b	Benthic algae	g-D m^{-2}	On/Off
$OrgN$	Organic nitrogen	mg-N L^{-1}	On/Off
$NH4$	Ammonium	mg-N L^{-1}	On/Off
$NO3$	Nitrate	mg-N L^{-1}	On/Off
$OrgP$	Organic phosphorous	mg-P L^{-1}	On/Off
TIP	Total inorganic phosphorous	mg-P L^{-1}	On/Off
POC	Particulate organic carbon	mg-C L^{-1}	On/Off
DOC	Dissolved organic carbon	mg-C L^{-1}	On/Off
DIC	Dissolved inorganic carbon	mol L^{-1}	On/Off
POM	Particulate organic matter	mg-D L^{-1}	On/Off
POM_2	Sediment particulate organic matter	mg-D L^{-1}	On/Off
$CBOD_i$	Carbonaceous biochemical oxygen demand	mg-O_2 L^{-1}	0-10
DO	Dissolved oxygen	mg-O_2 L^{-1}	On/Off
PX	Pathogen	cfu $(100\ mL)^{-1}$	On/Off
Alk	Alkalinity	mg-$CaCO_3$ L^{-1}	On/Off

4.3 HgSM Overview

This section provides a brief overview of HgSM. A more detailed discussion can be found in Zhang and Johnson (2015b). The HgSM was designed to model three species in the water column: Hg0, HgII, and MeHg and two species in the sediment layer: HgII and MeHg. In HgSM, Hg0 is used to represent the elemental mercury. HgII is used to represent inorganic mercury that can exist as Hg^{2+} susch as $HgCl_2$, $Hg(OH)_2$, HgS, etc. MeHg is used to represent methylmercury. HgII and MeHg cen be adsorbed by DOC, algae, POM and inorganic solids. Physical and biochemical processes modeled in HgSM include (1) adsorption and desorption of mercury, (2) volatilization, (3) atmospheric deposition, (4) diffusive exchange between the water column and sediment layer, (5)

deposition and resuspension, (6) sediment burial of sorbed mercury, and (7) biogeochemical transformations among three species. The HgSM models several transformations of mercury cycling in the water column and sediment layer. Figure 10 provides an overview of the HgSM representation of mercury species and major processes involved in aquatic systems, with the exception of transport and external sources.
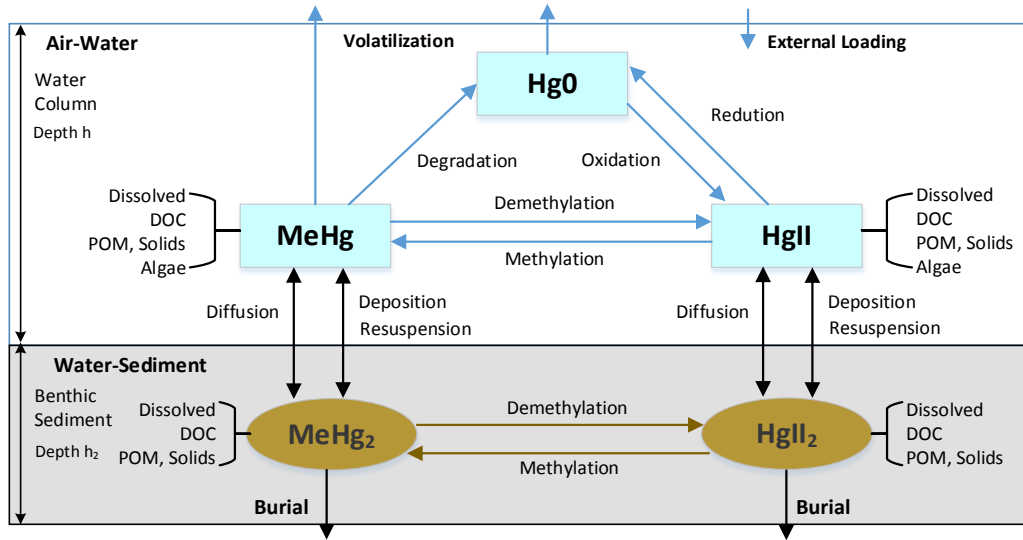
Figure 10. Mercury speciation and major processes modeled in HgSM.

The transformation processes of Hgo, HgII and MeHg and their rates are described using simple kinetc equations adopted from the WASP mercury module (Wool et al. 2006) and Dynamic Mercury Cycling Model (D-MCM) (ERPI 2009; 2013). Due to the small concentration of mercury species compared to the major water quality constituents, its concentration is normally on the order of nanograms per liter (10^{-9} g/l) in solution. Therefore the concentrations of mercury species in HgSM are expressed in volumetric units of nanograms per liter (ng L^{-1}).

4.4 Mercury Speciation and Partitioning

4.4.1 Mercury speciation

Because the relative distribution of the different species control the bioavailability and affects the transport and fate of mercury in the environment (Jackson 1997), the HgSM models three primary mercury species of environmental concern: Hg0, HgII, and MeHg. Gaseous Hg0 is the dominant form in the atmosphere (Nater and Grigal 1992). Hg0 is slightly water soluble and has a high Henry's Law constant (Schrosder and Munthe 1998). Hg0 constitutes very little of the total mercury in the surface water but may provide a significant pathway for the evolution of mercury out of the water body. In HgSM, Hg0 is assumed to exist in the dissolved phase and only in the water column.

Hg^{2+} is soluble, and its compounds exist in gaseous, dissolved, and solid forms. In natural waters, HgII generally persists in the form of aqueous mercury−ligand complexes (e.g., Hg^{2+} complexes with chloride, inorganic sulfide, or dissolved organic matter). HgII sorbs on solids (Morel et al. 1998; Boszke et al. 2002; Skyllberg 2012). The relative partitioning of HgII in various dissolved and particulate forms will govern the overall mobility and the bioavailability of HgII to methylation in aquatic systems. Hg^{2+} can form compounds with a methyl group and other alkyl groups (Puk and Weber 1994). In oxidizing conditions, the dominant forms are Hg^{2+} and $Hg2^{2+}$ as chloride and hydroxide complexes, while in reducing conditions, the dominant are sulphur-mercury compounds such as mono- and bi-sulphide complexes such as HgS (s), HgS_2H_2, HgS_2H^- and HgS_2^{2-} (Morel et al. 1998). In intermediate conditions, the most common forms are alkyl mercury compounds (Tyler 1992). The HgSM combines all Hg^{2+} species of mercury into a state variable identified by HgII. HgII is modeled for the water column and sediment layer.

MeHg accounts for the majority of the organic mercury species in freshwater systems - mainly methylmercury (CH_3Hg^+) or dimethylmercury (($CH_3)_2Hg$). MeHg may exist in various dissolved and particulate forms in aquatic systems. MeHg can be consumed by organisms and move up the food chain. Even with very low concentrations of MeHg in water, bioaccumulation through the food web may cause high levels of mercury contamination in fish (Zillioux et al. 1993, Carroll et al. 2000, Wang et al. 2004). So, MeHg is the species of greatest concern for both human health and ecosystems. The effects of mercury in fish and wildlife have been documented (Evers 2005). MeHg is included for the water column and sediment layer.

4.4.2 Partitioning of HgII and MeHg

It has been well documented that DOC and solids are two principal carriers of MeHg and HgII (Lyon et al. 1997). In HgSM, all Hg0 is assumed in dissolved phase, HgII and MeHg can be partition between dissolved phase and DOC, algae, and solids sorbed phases. Similar to the CSM, solids can be assigned to mineral abiotic solids, detrital, or various classes or size categories of suspended solids. In HgSM, partitioning of HgII and MeHg is handled in the same manner in the sediment layer as in the water column. HgII and MeHg are allowed to be partitioned between dissolved, DOC and solids sorbed phases. Under an equilibrium partitioning, all HgII and MeHg on solids are assumed to be instantly exchangeable between the dissolved and adsorbed phases.

It is recognized that sorbed HgII may be not at true "equilibrium" with the dissolved phase. Alternatively, sorption of HgII on algae organic and inorganic solids can be simulated according to non-equilibrium adsorption/desorption kinetics.

Linear equilibrium partitioning

Partitioning factions of HgII and MeHg in the water column and sediment layer are identically calculated based on the formulations of contaminants in CSM (refer to Chapter 3.3). Table 4 summarizes formulations for calculating linear equilibrium partitioning fractions of HgII and MeHg. The symbols in these formulations are defined in Table 5.

Table 4. Linear partitioning fractions of HgII and MeHg computed in HgSM

32

HgII	MeHg
Water column	
$$f_{d-HgII} = \frac{10^6}{R_{HgII}}$$	$$f_{d-MeHg} = \frac{10^6}{R_{MeHg}}$$
$$f_{doc-HgII} = \frac{K_{doc-HgII}DOC}{R_{HgII}}$$	$$f_{doc-MeHg} = \frac{K_{doc-MeHg}DOC}{R_{MeHg}}$$
$$f_{ap-HgII} = \frac{K_{ap-HgII}A_{pd}}{R_{HgII}}$$	$$f_{ap-MeHg} = \frac{K_{ap-MeHg}A_{pd}}{R_{MeHg}}$$
$$f_{pom-HgII} = \frac{K_{pom-HgII}POM}{R_{HgII}}$$	$$f_{pom-MeHg} = \frac{K_{pom-MeHg}POM}{R_{MeHg}}$$
$$f_{pn-HgII} = \frac{K_{pn-HgII}m_n}{R_{HgII}}$$	$$f_{pn-MeHg} = \frac{K_{pn-MeHg}m_n}{R_{MeHg}}$$

$$R_{HgII} = 10^6 + K_{doc-HgII}DOC + K_{ap-HgII}A_{pd} + K_{pom-HgII}POM + \sum_{n=1}^{N} K_{pn-HgII}m_n$$

$$R_{MeHg} = 10^6 + K_{doc-MeHg}DOC + K_{ap-MeHg}A_{pd} + K_{pom-MeHg}POM + \sum_{n=1}^{N} K_{pn-MeHg}m_n$$

HgII	MeHg
Sediment layer	
$$f_{d-HgII2} = \frac{10^6\phi}{R_{HgII2}}$$	$$f_{d-MeHg2} = \frac{10^6\phi}{R_{MeHg2}}$$
$$f_{doc-HgII2} = \frac{K_{doc-HgII2}\phi DOC_2}{R_{HgII2}}$$	$$f_{doc-MeHg2} = \frac{K_{doc-MeHg2}\phi DOC_2}{R_{MeHg2}}$$
$$f_{pom-HgII2} = \frac{K_{pom-HgII2}POM_2}{R_{HgII2}}$$	$$f_{pom-MeHg2} = \frac{K_{pom-MeHg2}POM_2}{R_{MeHg2}}$$
$$f_{pn-HgII2} = \frac{K_{pn-HgII2}m_{n2}}{R_{HgII2}}$$	$$f_{pn-MeHg2} = \frac{K_{pn-MeHg2}m_{n2}}{R_{MeHg2}}$$

$$R_{HgII2} = 10^6\phi + K_{doc-HgII2}\phi DOC_2 + K_{pom-HgII2}POM_2 + \sum_{n=1}^{N} K_{pn-HgII2}m_{n2}$$

$$R_{MeHg2} = 10^6\phi + K_{doc-MeHg2}\phi DOC_2 + K_{pom-MeHg2}POM_2 + \sum_{n=1}^{N} K_{pn-MeHg2}m_{n2}$$

Table 5. Definition of symbols used in Table 4

Name	Definition	Units
Water column		
$f_{d\text{-}HgII}$	Fraction of dissolved HgII in water	-
$f_{doc\text{-}HgII}$	Fraction of DOC sorbed HgII in water	-
$f_{ap\text{-}HgII}$	Fraction of algae sorbed HgII in water	-
$f_{pom\text{-}HgII}$	Fraction of POM sorbed HgII in water	-
$f_{pn\text{-}HgII}$	Fraction of solids sorbed HgII in water	-
$K_{doc\text{-}HgII}$	HgII equilibrium partition coefficient for DOC in water	L kg^{-1}
$K_{ap\text{-}HgII}$	HgII equilibrium partition coefficient for algae in water	L kg^{-1}
$K_{pom\text{-}HgII}$	HgII equilibrium partition coefficient for POM in water	L kg^{-1}
$K_{pn\text{-}HgII}$	HgII equilibrium partition coefficient for solids in water	L kg^{-1}
$f_{d\text{-}MeHg}$	Fraction of dissolved MeHg in water	-
$f_{doc\text{-}MeHg}$	Fraction of DOC sorbed MeHg in water	-
$f_{ap\text{-}MeHg}$	Fraction of algae sorbed MeHg in water	-
$f_{pom\text{-}MeHg}$	Fraction of POM sorbed MeHg in water	-
$f_{pn\text{-}MeHg}$	Fraction of solids sorbed MeHg in water	-
$K_{doc\text{-}MeHg}$	MeHg equilibrium partition coefficient for DOC in water	L kg^{-1}
$K_{ap\text{-}MeHg}$	MeHg equilibrium partition coefficient for algae in water	L kg^{-1}
$K_{pom\text{-}MeHg}$	MeHg equilibrium partition coefficient for POM in water	L kg^{-1}
$K_{pn\text{-}MeHg}$	MeHg equilibrium partition coefficient for solids in water	L kg^{-1}
Sediment layer		
$f_{d\text{-}HgII2}$	Fraction of dissolved HgII in sediment	-
$f_{doc\text{-}HgII2}$	Fraction of DOC sorbed HgII in sediment	-
$f_{pom\text{-}HgII2}$	Fraction of POM sorbed HgII in sediment	-
$f_{pn\text{-}HgII2}$	Fraction of solids sorbed HgII in sediment	-

$K_{doc\text{-}HgII2}$	HgII equilibrium partition coefficient for sediment DOC	L kg^{-1}
$K_{pom\text{-}HgII2}$	HgII equilibrium partition coefficient for sediment POM	L kg^{-1}
$K_{pn\text{-}HgII2}$	HgII equilibrium partition coefficient for sediment solids	L kg^{-1}
$f_{d\text{-}MeHg2}$	Fraction of dissolved MeHg in sediment	-
$f_{doc\text{-}MeHg2}$	Fraction of DOC sorbed MeHg in sediment	-
$f_{pom\text{-}MeHg2}$	Fraction of POM sorbed MeHg in sediment	-
$f_{pn\text{-}MeHg2}$	Fraction of solids sorbed MeHg in sediment	-
$K_{doc\text{-}MeHg2}$	MeHg equilibrium partition coefficient for sediment DOC	L kg^{-1}
$K_{pom\text{-}MeHg2}$	MeHg equilibrium partition coefficient for sediment POM	L kg^{-1}
$K_{pn\text{-}MeHg2}$	MeHg equilibrium partition coefficient for sediment solids	L kg^{-1}

Concentrations of HgII and MeHg in each phase in the water column and sediment layer can be calculated from the partitioning factions that are listed in Table 6. Dissolved concentrations of HgII and MeHg in the sediment layer are the mass of dissolved and DOC sorbed phases relative to the total volume of solids and water.

Table 6. Linear partitioning concentrations of HgII and MeHg computed in HgSM

HgII	MeHg
Water column	
$HgII_d = f_{d-HgII}HgII$	$MeHg_d = f_{d-MeHg}MeHg$
$HgII_{doc} = f_{doc-HgII}HgII$	$MeHg_{doc} = f_{doc-MeHg}MeHg$
$HgII_{pt} = \sum_{n=1}^{N} f_{pn-HgII}HgII$	$MeHg_{pt} = \sum_{n=1}^{N} f_{pn-MeHg}MeHg$
$HgII_{pts} = 10^3 \sum_{n=1}^{N} \dfrac{1}{m_n} f_{pn-HgII}HgII$	$MeHg_{pts} = 10^3 \sum_{n=1}^{N} \dfrac{1}{m_n} f_{pn-MeHg}MeHg$
Sediment layer	
$HgII_{d2} = f_{d-HgII2}HgII_2$	$MeHg_{d2} = f_{d-MeHg2}MeHg_2$
$HgII_{doc2} = f_{doc-HgII2}HgII_2$	$MeHg_{doc2} = f_{doc-MeHg2}MeHg_2$

$HgII_{pt2} = \sum_{n=1}^{N} f_{pn-HgII2} HgII_2$	$MeHg_{pt2} = \sum_{n=1}^{N} f_{pn-MeHg2} MeHg_2$
$HgII_{pts2} = 10^3 \sum_{n=1}^{N} \frac{1}{m_{n2}} f_{pn-HgII2} HgII_2$	$MeHg_{pts2} = 10^3 \sum_{n=1}^{N} \frac{1}{m_{n2}} f_{pn-MeHg2} MeHg_2$
Pore water	
$HgII_{dp2} = HgII_{d2} / \phi$	$MeHg_{dp2} = MeHg_{d2} / \phi$
$HgII_{docp2} = HgII_{doc2} / \phi$	$MeHg_{docp2} = MeHg_{doc2} / \phi$

Table 7. Definition of symbols used in Table 6

Name	Definition	Units
Water column		
HgII	Concentration of total HgII in water	ng L^{-1}
HgII$_d$	Concentration of dissolved HgII in water	ng L^{-1}
HgII$_{doc}$	Concentration of DOC sorbed HgII in water	ng L^{-1}
HgII$_{pt}$	Total concentration of sorbed HgII on solids in water	ng L^{-1}
HgII$_{pts}$	Total mass of HgII sorbed on solids in water	ng g^{-1}
MeHg	Concentration of total MeHg in water	ng L^{-1}
MeHg$_d$	Concentration of dissolved MeHg in water	ng L^{-1}
MeHg$_{doc}$	Concentration of DOC sorbed MeHg in water	ng L^{-1}
MeHg$_{pt}$	Total concentration of sorbed MeHg on solids in water	ng L^{-1}
MeHg$_{pts}$	Total mass of MeHg sorbed on solids in water	ng g^{-1}
Sediment layer		
HgII$_2$	Concentration of total HgII in sediment	ng L^{-1}
HgII$_{dp2}$	Concentration of dissolved HgII in pore water	ng L^{-1}
HgII$_{docp2}$	Concentration of DOC sorbed HgII in pore water	ng L^{-1}

HgII$_{pt2}$	Total concentration of solids sorbed HgII in sediment	ng L^{-1}
HgII$_{pts2}$	Total mass of solids sorbed HgII in sediment	ng g^{-1}
MeHg$_2$	Concentration of total MeHg on in sediment	ng L^{-1}
MeHg$_{dp2}$	Concentration of dissolved MeHg in pore water	ng L^{-1}
MeHg$_{docp2}$	Concentration of DOC sorbed MeHg in pore water	ng L^{-1}
MeHg$_{pt2}$	Total concentration of solids sorbed MeHg in sediment	ng L^{-1}
MeHg$_{pts2}$	Total mass of solids sorbed MeHg in sediment	ng g^{-1}

Non-linear equilibrium partitioning

Two of the most popular adsorption isotherms including the Langmuir and Freundlich isotherms are included for HgII and MeHg. Similarly with CSM, concentrations of HgII and MeHg for each phase must be solved numerically once the total concentration of HgII and MeHg are known. With the Freundlich equilibrium partitioning, concentrations of total HgII and MeHg in the water column and sediment layer are defined as follows.

Total HgII:

$$HgII_d + 10^{-6}k_{doc-HgII}HgII_d DOC + 10^{-3bpom}k_{fpom-HgII}HgII_d^{bpom}POM$$
$$+ 10^{-3bap}k_{fap-HgII}HgII_d^{fap}A_{pd} + 10^{-3bpn}\sum_{n=1}^{N}k_{fpn-HgII}HgII_d^{bpn}m_n = HgII \qquad (4.1a)$$

$$HgII_{d2} + 10^{-6}k_{doc-HgII2}HgII_{d2}DOC_2 + 10^{-3bpom2}k_{fpom-HgII2}\left(HgII_{d2}/\phi\right)^{bpom2}POM_2$$
$$+ 10^{-3bpn}\sum_{n=1}^{N}k_{fpn-HgII2}\left(HgII_{d2}/\phi\right)^{bpn2}m_{n2} = HgII_2 \qquad (4.1b)$$

Total MeHg:

$$MeHg_d + 10^{-6}k_{doc-MeHg}MeHg_d DOC + 10^{-3bpom}k_{fpom-MeHg}MeHg_d^{bpom}POM$$
$$+ 10^{-3bap}k_{fap-MeHg}MeHg_d^{bap}A_{pd} + 10^{-3bpn}\sum_{n=1}^{N}k_{fpn-MeHg}MeHg_d^{bpn}m_n = MeHg \qquad (4.2a)$$

$$MeHg_{d2} + 10^{-6}k_{doc-MeHg2}MeHg_{d2}DOC_2 + 10^{-3bpom2}k_{fpom-MeHg2}\left(MeHg_{d2}/\phi\right)^{bpom2}POM_2$$
$$+ 10^{-3bpn2}\sum_{n=1}^{N}k_{fpn-MeHg2}\left(MeHg_{d2}/\phi\right)^{bpn2}m_{n2} = MeHg_2 \qquad (4.2b)$$

where:

$K_{fpom\text{-}HgII}$ = HgII Freundlich adsorption constant for POM in water $(((\mu g\ g^{-1})(\mu g\ L^{-1})^{-b}$,

$K_{fpom\text{-}HgII2}$ = HgII Freundlich adsorption constant for sediment POM $(((\mu g\ g^{-1})(\mu g\ L^{-1})^{-b}$,

$K_{fap\text{-}HgII}$ = HgII Freundlich adsorption constant for algae in water $(((\mu g\ g^{-1})(\mu g\ L^{-1})^{-b}$,

$K_{fpn\text{-}HgII}$ = HgII Freundlich adsorption constant for solid "n" in water $(((\mu g\ g^{-1})(\mu g\ L^{-1})^{-b}$,

$K_{fpn\text{-}HgII2}$ = HgII Freundlich adsorption constant for sediment solid "n" $(((\mu g\ g^{-1})(\mu g\ L^{-1})^{-b}$,

$K_{fpom\text{-}MeHg}$ = MeHg Freundlich adsorption constant for POM in water $(((\mu g\ g^{-1})(\mu g\ L^{-1})^{-b}$,

$K_{fpom\text{-}MeHg2}$ = MeHg Freundlich adsorption constant for sediment POM $(((\mu g\ g^{-1})(\mu g\ L^{-1})^{-b}$,

$K_{fap\text{-}MeHg}$ = MeHg Freundlich adsorption constant for algae in water $(((\mu g\ g^{-1})(\mu g\ L^{-1})^{-b}$,

$K_{fpn\text{-}MeHg}$ = MeHg Freundlich adsorption constant for solid "n" in water $(((\mu g\ g^{-1})(\mu g\ L^{-1})^{-b}$,

$K_{fpn\text{-}MeHg2}$ = MeHg Freundlich adsorption constant for sediment solid "n" $(((\mu g\ g^{-1})(\mu g\ L^{-1})^{-b}$,

b_{pom} = Freundlich exponent for POM in water (uniteless),

b_{pom2} = Freundlich exponent for sediment POM (uniteless),

b_{ap} = Freundlich exponent for algae in water (uniteless),

b_{pn} = Freundlich exponent for solid "n" in water (uniteless),

b_{pn2} = Freundlich exponent for sediment solid "n" (uniteless).

With the Langmuir equilibrium partitioning, concentrations of total HgII and MeHg in the water column and sediment layer are defined as follows.

Total HgII:

$$HgII_d + 10^{-6}K_{doc-HgII}DOC \cdot HgII_d + \frac{K_{lap-HgII}q_{cap-HgII}A_{pd}HgII_d}{10^3 + K_{lap-HgII}HgII_d}$$

$$+ \frac{K_{lpom-HgII}q_{cpom-HgII}POM \cdot HgII_d}{10^3 + K_{lpom-HgII}HgII_d} + \sum_{n=1}^{N}\frac{K_{lpn-HgII}q_{cn-HgII}m_n HgII_d}{10^3 + K_{lpn-HgII}HgII_d} = HgII \qquad \textbf{(4.3a)}$$

$$HgII_{d2} + 10^{-6}K_{doc-HgII2}DOC_2 HgII_{d2} + \frac{K_{lpom-HgII2}q_{cpom-HgII2}POM_2(HgII_{d2}/\phi)}{10^3 + K_{lpom-HgII2}(HgII_{d2}/\phi)}$$

$$+ \sum_{n=1}^{N}\frac{K_{lpn-HgII2}q_{cn-HgII2}m_{n2}(HgII_{d2}/\phi)}{10^3 + K_{lpn-HgII2}(HgII_{d2}/\phi)} = HgII_2 \qquad \textbf{(4.3b)}$$

Total MeHg:

$$MeHg_d + 10^{-6}K_{doc-MeHg}DOC \cdot MeHgI_d + \frac{K_{lap-MeHgI}q_{cap-MeHgI}A_{pd}MeHg_d}{10^3 + K_{lap-MeHgI}MeHg_d}$$

$$+ \frac{K_{lpom-MeHgI}q_{cpom-MeHgI}POM \cdot MeHgI_d}{10^3 + K_{lpom-MeHgI}MeHgI_d} + \sum_{n=1}^{N}\frac{K_{lpn-MeHg}q_{cn-MeHgI}m_n MeHg_d}{10^3 + K_{lpn-MeHgI}MeHg_d} = MeHg \qquad \textbf{(4.4a)}$$

$$MeHg_{d2} + 10^{-6} K_{doc-MeHg2} DOC_2 \cdot MeHg_{d2} + \frac{K_{lpom-MeHg2} q_{cpom-MeHg2} POM_2 (MeHg_{d2}/\phi)}{10^3 + K_{lpom-MeHg2} (MeHg_{d2}/\phi)}$$

$$+ \sum_{n=1}^{N} \frac{K_{lpn-MeHg2} q_{cn-MeHg2} m_{n2} (MeHg_{d2}/\phi)}{10^3 + K_{lpn-MeHg2} (MeHg_{d2}/\phi)} = MeHg_2 \qquad \textbf{(4.4b)}$$

where

$K_{lap-HgII}$ = HgII Langmuir adsorption constant for algae in water (L µg^{-1}),

$K_{lpom-HgII}$ = HgII Langmuir adsorption constant for POM in water (L µg^{-1}),

$K_{lpom-HgII2}$ = HgII Langmuir adsorption constant for sediment POM (L µg^{-1}),

$K_{lpn-HgII}$ = HgII Langmuir adsorption constant for solid "n" in water (L µg^{-1}),

$K_{lpn-HgII2}$ = HgII Langmuir adsorption constant for sediment solid "n" (L µg^{-1}),

$q_{cap-HgII}$ = maximum amount of HgII adsorbed by algae in water (µg g^{-1}),

$q_{cpom-HgII}$ = maximum amount of HgII adsorbed by POM in water (µg g^{-1}),

$q_{cpom-HgII2}$ = maximum amount of HgII adsorbed by sediment POM (µg g^{-1}).

$q_{cn-HgII}$ = maximum amount of HgII adsorbed by solid "n" in water (µg g^{-1}),

$q_{cn-HgII2}$ = maximum amount of HgII adsorbed by sediment solid "n" (µg g^{-1}),

$K_{lap-MeHg}$ = MeHg Langmuir adsorption constant for algae in water (L µg^{-1}),

$K_{lpom-MeHg}$ = MeHg Langmuir adsorption constant for POM in water (L µg^{-1}),

$K_{lpom-MeHg2}$ = MeHg Langmuir adsorption constant for sediment POM (L µg^{-1}),

$K_{lpn-MeHg}$ = MeHg Langmuir adsorption constant for solid "n" in water (L µg^{-1}),

$K_{lpn-MeHg2}$ = MeHg Langmuir adsorption constant for sediment solid "n" (L µg^{-1}),

$q_{cap-MeHg}$ = maximum amount of MeHg adsorbed by algae in water (µg g^{-1}),

$q_{cpom-MeHg}$ = maximum amount of MeHg adsorbed by POM in water (µg g^{-1}),

$q_{cpom-MeHg2}$ = maximum amount of MeHg adsorbed by sediment POM (µg g^{-1}).

$q_{cn-MeHg}$ = maximum amount of MeHg adsorbed by solid "n" in water (µg g^{-1}),

$q_{cn-MeHg2}$ = maximum amount of MeHg adsorbed by sediment solid "n" (µg g^{-1}).

Non-equilibrium partitioning

As indicated by some researchers (EPRI 2013), HgII sorption onto solids is partially instantaneous and partially rate limited (slow). HgII species are strongly adsorbed by soils and sediments and are desorbed slowly. Clay minerals adsorb mercury maximally at pH 6. In acid soils, most mercury is adsorbed by organic matter. When organic matter is not present, mercury becomes relatively more mobile in acid soils. Non-equilibrium sorption of HgII onto POM, algae and inorganic solids can be simulated in HgSM. In the water column, rate limited adsorption and desorption of HgII onto algae, POM and suspended solids are described by

$$\frac{\partial HgII_{ap}}{\partial t} = 10^{-3} k_{adap} (q_{cap-HgII} A_{pd} - HgII_{ap}) HgII_d - k_{daap} HgII_{ap} \qquad \textbf{(4.5a)}$$

$$\frac{\partial HgII_{pom}}{\partial t} = 10^{-3} k_{adpom} (q_{cpom-HgII} POM - HgII_{pom}) HgII_d - k_{dapom} HgII_{pom} \qquad \textbf{(4.5b)}$$

$$\frac{\partial HgII_{pn}}{\partial t} = 10^{-3} k_{adn} \left(q_{cn-HgII} m_n - HgII_{pn} \right) HgII_d - k_{dan} HgII_{pn} \tag{4.5c}$$

where

k_{adn} = adsorption coefficient for solid "n" in water (L µg^{-1} d^{-1}),
k_{adap} = adsorption coefficient for algae in water (L µg^{-1} d^{-1}),
k_{adpom} = adsorption coefficient for POM in water (L µg^{-1} d^{-1}),
k_{dan} = desorption rate for solid "n" in water (d^{-1}),
k_{daap} = desorption rate for algae in water (d^{-1}),
k_{dapom} = desorption rate for POM in water (d^{-1}).

Rate limited adsorption and desorption of HgII onto POM and solids in the sediment layer can be described by

$$\frac{\partial HgII_{pom2}}{\partial t} = 10^{-3} k_{adpom2} \left(q_{cpom-HgII2} POM_2 - HgII_{pom2} \right) \frac{HgII_{d2}}{\phi} - k_{dapom2} HgII_{pom2} \tag{4.6a}$$

$$\frac{\partial HgII_{pn2}}{\partial t} = 10^{-3} k_{adn2} \left(q_{cn-HgII2} m_{n2} - HgII_{pn2} \right) \frac{HgII_{d2}}{\phi} - k_{dan2} HgII_{pn2} \tag{4.6b}$$

where

k_{adn2} = adsorption coefficient for sediment solid "n" (L µg^{-1} d^{-1}),
k_{adpom2} = adsorption coefficient for sediment POM (L µg^{-1} d^{-1}),
k_{dan2} = desorption rate for sediment solid "n" (d^{-1}),
k_{dapom2} = desorption rate for sediment POM (d^{-1}).

4.5 Mercury Transformations

Mercury brought into water bodies undergoes many transformations (EPRI 2006, 2013). One of the major concerns of mercury and its impact to the environments is its transformation to MeHg, a highly toxic form of mercury. Any form of mercury entering surface waters can be microbially converted to MeHg, given favorable conditions. MeHg concentrations depend on available HgII, methylation rate, and on dilution and dispersion of produced MeHg. Dissolved inorganic mercury is found to be the form of mercury that acts as a direct precursor for the formation of MeHg by microorganisms (Benoit et al. 2003). Photolysis of MeHg has been shown to occur in water (Callahan et al. 1979). Hg0 may be formed through the demethylation of MeHg or the reduction of HgII (Allard and Arsenie 1991).

Within the sediment layer, biotic and abiotic reactions can result in methylation, demethylation, and reduction, just as in the water column. Environmental factors such as redox conditions, pH, and presence of soluble organics and sulfate contribute to the transformation of mercury species. Speciation plays a major role in determining the MeHg transformation (Turner 1987, Stein et al. 1996, Morel et al. 1998). Table 8 summarizes key transformation processes among three mercury

species included in HgSM. Mercury transformation processes and their kinetics are described in more detail in the following sections.

Table 8. Major mercury species and transformations in HgSM

Species	Water column			Sediment layer	
	HgO	HgII	MeHg	HgII	MeHg
HgO		Oxidation (Hg0-->HgII)			
HgII	Photoreduction (HgII-->Hg0)		Methylation (HgII-->MeHg)		Methylation (HgII-->MeHg)
MeHg	Photoreduction (MeHg-->Hg0)	Demethylation (MeHg-->HgII)		Demethylation (MeHg-->HgII)	

4.5.1 Elemental mercury (Hg0)

In waters with good access to oxygen, Hg0 can be relatively quickly oxidized by different reagents - mainly oxygen but also nitrates, nitrites, iron hydroxides, iron phosphates, sulphates, sulphur, carbon dioxide (Stein et al. 1996). Similar to WASP model, oxidation from Hg0 to HgII in the water column is calculated by a first order kinetics

$$Hg0 \rightarrow HgII = k_{12}(T) \cdot Hg0 \qquad\qquad (4.7)$$

where

$Hg0$-->$HgII$ = oxidation rate from Hg0 to HgII in water (ng L^{-1} d^{-1}),
$k_{12}(T)$ = oxidation rate from Hg0 to HgII in water (d^{-1}).

The oxidation yield, $Hg0$-->$HgII$, is subtracted from the Hg0 as a sink (-) and added to the HgII as a source (+) with a specified yield coefficient (Y_{12}) of 1.0.

4.5.2 Inorganic mercury (HgII)

Reduction of HgII in the water column and methylation of HgII in the water column and sediments are simulated. In most cases, the transformations of dissolved mercury include mercury complexes with dissolved organic carbon (DOC) (Nriagu 1979, Bloom et al. 1991). In HgSM, the user can assign the DOC sorbed HgII that is available for reduction and methylation.

HgII reduction

On the basis of experimental data some authors indicate the biological processes as the most important, while others suggest that photoredution reactions play the dominant role (Costa and

Liss 2000). Photoreduction of HgII to Hg0 is light dependent. Thus reduction of HgII is expected to peak at midday. In HgSM, HgII reduction is assumed to be driven by sunlight, and the surface reduction rate is attenuated through the water column using a specified light extinction coefficient. Similar to WASP model, photoreduction from HgII to Hg0 in the water column is calculated by

$$HgII \rightarrow Hg0 = 1.33 \frac{I_0}{I_{0pht}} \frac{1-e^{-\lambda_{max} \cdot h}}{\lambda_{max} \cdot h} (1-0.56C_L)(k_{d21}f_{d-HgII} + k_{doc21}f_{doc-HgII})HgII \qquad \textbf{(4.8)}$$

where

> $HgII \text{-->} Hg0$ = photoreduction rate from HgII to Hg0 in water (ng L^{-1} d^{-1}),
> k_{d21} = photoreduction rate from dissolved HgII to Hg0 in water (d^{-1}),
> k_{doc21} = photoreduction rate from DOC sorbed HgII to Hg0 in water (d^{-1}).

The surface photoreduction rates (k_{d21}, k_{doc21}) are specified by the user and are not adjusted for temperature. The photoreduction yield, $HgII \text{-->} Hg0$, is subtracted from the HgII as a sink (-) and added to the Hg0 as a source (+) with a specified yield coefficient (Y_{21}) of 1.0.

HgII methylation

Several studies indicated that methylation of HgII is the dominant source of MeHg in aquatic systems (USEPA 1997; EPRI 2013). HgII can be methylated to MeHg in water phase through biotic pathways or abiotic pathways (photo-mediated or non photo-mediated chemical methylation) (Stein 1996; Ullrich 2001). Methylation takes place mainly in sediments and in soils, but it can also take place in water although more weakly (Regnell et al. 1996). The mechanisms of mercury methylation in water have not been fully recognized yet, but it is assumed that they involve microorganisms, similarly as in bed sediments (Morel et al. 1998). Chemical speciation of HgII affects methylation and bioavailability. HgII must be in solution or easily transferrable form for methylation (Marvin-DiPasquale et al. 2009). DOC interacts strongly with dissolved HgII and likely affects methylation rate and MeHg production. Similar to WASP model, methylation from HgII to MeHg in the water column is calculated by the first-order kinetics

$$HgII \rightarrow MeHg = (k_{d23}(T)f_{d-HgII} + k_{doc23}(T)f_{doc-HgII})HgII \qquad \textbf{(4.9)}$$

where

> $HgII \text{-->} MeHg$ = methylation rate from HgII to MeHg in water (ng L^{-1} d^{-1}),
> $k_{d23}(T)$ = methylation rate from dissolved HgII to MeHg in water (d^{-1}),
> $k_{doc23}(T)$ = methylation rate from DOC sorbed HgII to MeHg in water (d^{-1}).

Gilmour and Henry (1991) reported that increased DOC in the water column may increase ligand formation between DOC and dissolved HgII, making it unavailable for microbial methylation.

For the biological methylation of HgII in anaerobic conditions the most important are sulphate reducing bacteria (SRB) (Langer et al. 2001, Mason et al. 2005, Lin et al. 2012). Sulfur, organic carbon, sediment structure, and composition in the sediment layer all affect MeHg production by changing the amount of bioavailable HgII and by stimulating SRB activity. HgII methylation is

directly tied to sulfate reduction rates in sediments (King et al., 1999, King et al., 2001) and is also influenced by pore water sulfide concentrations (Benoit et al. 1999).

Langer et al (2001) drew a diagram showing the relationship between HgII methylation and sulfate in sediments (Figure 11). At low sulfate concentrations, HgII is methylated at faster rates as sulfate concentration increase. At high sulfate concentrations, sulfide concentrations in pore water increase, which inhibites the methylation. Methylation rates consequently peak at a sulfate concentration above which excessive sulfide is produced. The amount of MeHg increased in proportion to the concentration of sulfate, then the MeHg decreased (Craig and Moreton 1986, Gilmour et al. 1998).
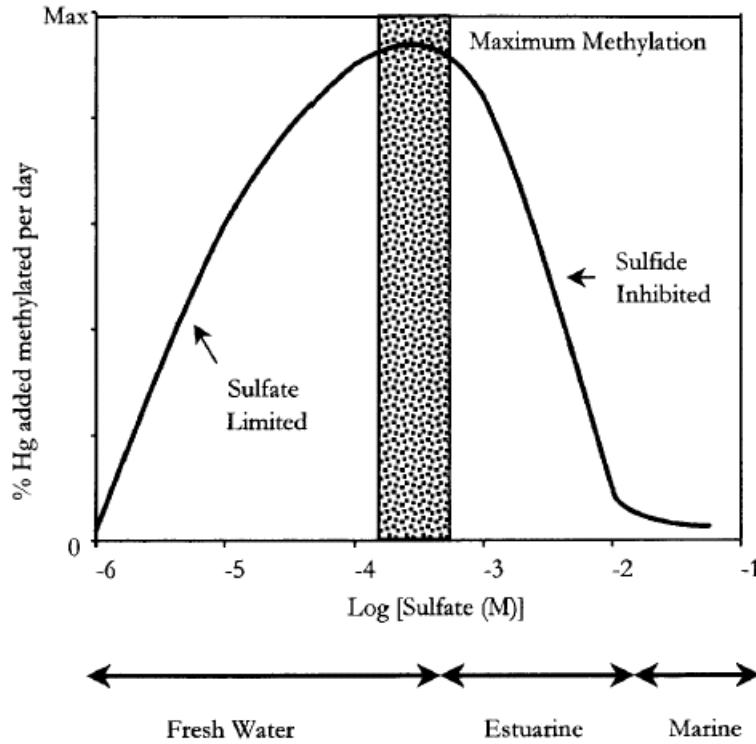
Figure 11. Relationship between HgII methylation and sulfate in sediments.

Similar to D-MCM (EPRI 2013), sediment methylation rate is calculated as a function of sulfate reduction.

$$(HgII \rightarrow MeHg)_2 = POM_2 k_{dom2}(T) Y_{m2} \left(\frac{SO4_2}{K_{SO4} + SO4_2} \right) \left(f_{d-HgII2} + f_{mdoc2} f_{doc-HgII2} \right) HgII_2 \quad \textbf{(4.10)}$$

where

$(HgII-->MeHg)_2$ = methylation rate from HgII to MeHg in sediment (ng L^{-1} d^{-1}),
$k_{dom2}(T)$ = sediment organic matter decomposition rate (d^{-1}),
Y_{m2} = sediment methylation efficiency ((ng-MeHg ng-HgII^{-1}) (mg L^{-1})$^{-1}$),
$SO4_2$ = sediment pore water sulfate concentration (mg-O$_2$ L^{-1}),

K_{SO4} = half-saturation constant for the effect of sulfate on methylation (mg-O_2 L^{-1}),
f_{mdoc2} = fraction of DOC sorbed HgII methylation (0 – 1.0).

The above equation relates methylation to overall carbon decomposition. Increased DOC at the sediment-water interface may act as a substrate for bacteria, thereby increasing microbial methylation (Stein et al., 1996). A half-saturation constant is used to represent the sulfate effect. This relationship results in methylation rate dependencies which are nearly linear when sulfate concentrations are much less than K_{so4}. Conversely, methylation rate does not vary with sulfate if sulfate is much greater than K_{so4}.

A "Q_{10}" approach is used to adjust methylation rate according to local temperature (Wool et al. 2006, EPRI 2013). The methylation rate for a base temperature is a user-specified parameter. The methylation yield, *HgII-->MeHg*, is subtracted from the HgII as a sink (-) and added to the MeHg as a source (+) with a specified yield coefficient (Y_{23}) of 1.07.

4.5.3 Methylmercury (MeHg)

MeHg can be reduced by sunlight to Hg0 (photoreduction) and reduced by bacteria to HgII (demethylation). Both processes are modeled in HgSM. The user can assign the DOC sorbed MeHg that is available for these transformations.

MeHg photoreduction

Photoreduction from MeHg to Hg0 is simulated as a light dependent process. This process occurs primarily in the water surface due to light attenuation. Similar to WASP model, photoreduction rate is calculated based on the rate of light attenuation and available MeHg in the water column

$$MeHg \rightarrow Hg0 = 1.33 \frac{I_0}{I_{0pht}} \frac{1-e^{-\lambda_{max} \cdot h}}{\lambda_{max} \cdot h} (1-0.56 C_L)\left(k_{d31} f_{d-MeHg} + k_{doc31} f_{doc-MeHg}\right) MeHg \qquad \textbf{(4.11)}$$

where

    MeHg-->Hg0 = photoreduction rate from MeHg to Hg0 in water (ng L^{-1} d^{-1}),
    k_{d31} = photoreduction rate from dissolved MeHg to Hg0 in water (d^{-1}),
    k_{doc31} = photoreduction rate from DOC sorbed MeHg to Hg0 in water (d^{-1}).

The surface photoreduction rates (k_{d31}, k_{doc31}) are specified by the user and are not adjusted for temperature. The photoreduction yield is subtracted from the MeHg as a sink (-) and added to the Hg0 as a source (+) with specified yield coefficient (Y_{31}) of 0.93.

MeHg demethylation

Methylation and demethylation are concurrent reactions. Demethylation is a reverse process of HgII methylation. Similar to methylation of HgII, demethylation of MeHg can also proceed through biotic or abiotic pathways (photodemethylation or non photo-mediated demethylation

(Hobman et al. 2000). Demethylation by photolysis is assumed to occur in the water column. Similar to WASP model, demethylation rate from MeHg to HgII in the water column is calculated by

$$MeHg \rightarrow HgII = 1.33 \frac{I_0}{I_{0pht}} \frac{1 - e^{-\lambda_{max} \cdot h}}{\lambda_{max} \cdot h} (1 - 0.56 C_L)(k_{d32} f_{d-MeHg} + k_{doc32} f_{doc-MeHg}) MeHg \qquad (4.12)$$

where

$MeHg \text{-->} HgII$ = demethylation rate from MeHg to HgII in water (ng L^{-1} d^{-1}),
$\quad k_{d32}$ = demethylation rate from dissolved MeHg to HgII in water (d^{-1}),
$\quad k_{doc32}$ = demethylation rate from DOC sorbed MeHg to HgII in water (d^{-1}).

The demethylation rates (k_{d32}, k_{doc32}) are specified by the user and are not adjusted for temperature.

There are several possible pathways for MeHg demethylation that are discussed in the literature (Marvin-DiPasquale et al. 2000). Biotic process was suggested to be the dominant pathway of MeHg demethylation in the sediment layer. The biological demethylation of MeHg is a slow process and in contrast to methylation is most effective in aerobic conditions (Gilmour and Henry 1991). The turnover time of MeHg demethylation in sediments is on the order of days to weeks. The sediment demethylation rate from MeHg to HgII is calculated based on carbon diagenesis rate (EPRI 2013)

$$(MeHg \rightarrow HgII)_2 = POM_2 k_{dom2}(T) Y_{dm2} (f_{d-MeHg2} + f_{dmdoc2} f_{doc-MeHg2}) MeHg_2 \qquad (4.13)$$

where:

$\quad (MeHg \text{-->} HgII)_2$ = demethylation rate from MeHg to HgII in sediment (ng L^{-1} d^{-1}),
$\quad Y_{dm2}$ = sediment demethylation efficiency ((ng-HgII ng-MeHg^{-1}) (mg L^{-1})$^{-1}$),
$\quad f_{dmdoc2}$ = fraction of sediment DOC sorbed MeHg demethylation (0 – 1.0).

The demethylation yield, $MeHg \text{-->} HgII$, is subtracted from the MeHg as a sink (-) and added to the HgII as a source (+) with a specified yield coefficient (Y_{32}) of 0.93.

4.6 Volatilization

Volatilization of Hg0 and MeHg are simulated in HgSM at the surface of the water column. Volatilization of HgII is ignored in the model since HgII has much lower Henry's Law Constants (USEPA 1997). The Henry's Law constant is 0.29 for Hg0, 1.9 x 10^{-5} for MeHg and 3.17 x 10^{-8} for HgII (EPRI 2006). The volatilization rate is calculated using a transfer velocity and its Henry's Law constant given as in CSM. In HgSM, volatilization rates can also be defined by the user. The volatilization rate, which is referenced to 20 °C, is adjusted for ambient water temperature.

4.6.1 Element mercury (Hg0)

Hg0 is a liquid in water at ambient temperatures and can emit to the air via volatilization. The volatilization of Hg0 represents the most important part of the exchange between water and the air. The source-sink term of Hg0 volatilization can be calculated by

$$Atm \rightarrow Hg0 = v_{v-Hg0}(T)\frac{1}{h}\left(Hg0 - \frac{Hg0_0}{K_H/(R \cdot T_{wk})}\right) \tag{4.14}$$

where

$Atm\text{-->}Hg0$ = Hg0 volatilization rate (ng L^{-1} d^{-1}),
$v_{v-Hg0}(T)$ = volatilization velocity of Hg0 across air-water interface (m d^{-1}),
$Hg0_0$ = air concentration of Hg0 (gaseous) (ng L^{-1}),
K_{H-Hg0} = Henry's Law constant of Hg0 (Pa m^3 mol^{-1}).

Air-surface exchange of Hg0 can occur bi-directionally, allowing transfer of mercury from the atmosphere. Ambient air concentrations of Hg0$_0$ are reported to range from about 2 to 10 ng/m^3, with the higher end of this range reflecting contributions from specific local sources (ATSDR 2005).

4.6.2 Methylmercury (MeHg)

Analagous to Hg0, the source-sink term of MeHg volatilization is calculated by

$$Atm \rightarrow MeHg = v_{v-MeHg}\frac{1}{h}\left(f_{d-MeHg}MeHg - \frac{MeHg_0}{K_H/(R \cdot T_{wk})}\right) \tag{4.15}$$

where

$Atm\text{-->}MeHg$ = MeHg volatilization rate (ng L^{-1} d^{-1}),
$v_{v-MeHg}(T)$ = volatilization velocity of MeHg across air-water interface (m d^{-1}),
$MeHg_0$ = air concentration of MeHg (gaseous) (ng L^{-1}),
K_{H-MeHg} = Henry's Law constant of MeHg (Pa m^3 mol^{-1}).

4.7 Air Deposition, Settling and Sedimentation

Atmospheric deposition of HgII and MeHg is included in HgSM. Mercury settling, sediment resuspension and burial processes are assumed to operate on all particulate fractions of HgII and MeHg in aquatic systems.

4.7.1 Air deposition

Mercury may be added to a water body by both wet and dry atmospheric deposition. Atmospheric deposition of HgII and MeHg represents the sum of wet and dry mercury deposition. Source-sink terms for HgII and MeHg deposition are calculated by

$$Atm \rightarrow HgII = \frac{1}{h} L_{HgII} \qquad (4.16a)$$

$$Atm \rightarrow MeHg = \frac{1}{h} L_{MeHg} \qquad (4.16b)$$

where

$Atm\text{-->}HgII$ = HgII atmospheric deposition (ng L^{-1} d^{-1}),
$Atm\text{-->}MeHg$ = MeHg atmospheric deposition (ng L^{-1} d^{-1}),
L_{HgII} = HgII atmospheric deposition load (μg m^{-2} d^{-1}),
L_{MeHg} = MeHg atmospheric deposition load (μg m^{-2} d^{-1}).

4.7.2 Settling

When sorbed on suspended solids, mercury species can settle from the water column, and they may eventually become a part of the bed sediment. Settling of suspended solids will remove sorbed mercury species in proportion to their bulk concentration. Settling rates of solids sorbed mercury species (HgII and MeHg) from the water column are calculated by

$$HgII \rightarrow Bed = -\frac{1}{h}\left(\sum_{n=1}^{N} v_{pn} f_{pn-HgII} + v_{sap} f_{ap-HgII} + v_{som} f_{pom-HgII}\right) HgII \qquad (4.17a)$$

$$MeHg \rightarrow Bed = -\frac{1}{h}\left(\sum_{n=1}^{N} v_{pn} f_{pn-MeHg} + v_{sap} f_{ap-MeHg} + v_{som} f_{pom-MeHg}\right) MeHg \qquad (4.17b)$$

where

$HgII\text{-->}Bed$ = HgII settling rate (ng L^{-1} d^{-1}),
$MeHg\text{-->}Bed$ = MeHg settling rate (ng L^{-1} d^{-1}).

4.7.3 Sediment resuspension

Erosion or resuspension of bed material due to bed shears in excess of a user-defined critical shear of erosion causes the reentrainment of sorbed mercury species into the water column. The resuspension rate of mercury species (HgII and MeHg) is calculated as the product of sediment sorbed concentration and the resuspension velocity

$$Bed \rightarrow HgII = \frac{1}{h_2}\left(\sum_{n=1}^{N} v_{rn} f_{pn-HgII2}\right) HgII_2 \qquad (4.18a)$$

$$Bed \rightarrow MeHg = \frac{1}{h_2}\left(\sum_{n=1}^{N} v_{rn} f_{pn-MeHg2}\right) MeHg_2 \qquad (4.18b)$$

where

$Bed \text{-->} HgII$ = HgII resuspension rate (ng L^{-1} d^{-1}),
$Bed \text{-->} MeHg$ = MeHg resuspension rate (ng L^{-1} d^{-1}).

4.7.4 Sediment burial

As new sediments are deposited, an equal mass of sediment is lost to burial. The flux of mercury out of the active sediment layer and into underlying sediments is calculated as the product of active sediment sorbed mercury concentration and burial velocity

$$HgII_2 \; burial = \frac{1}{h_2} v_b \left(\sum_{n=1}^{N} f_{pn-HgII2} + f_{pom-HgII2} \right) HgII_2 \tag{4.19a}$$

$$MeHg_2 \; burial = \frac{1}{h_2} v_b \left(\sum_{n=1}^{N} f_{pn-MeHg2} + f_{pom-MeHg2} \right) MeHg_2 \tag{4.19b}$$

where

$HgII_2 \; burial$ = HgII burial rate (ng L^{-1} d^{-1}),
$MeHg_2 \; burial$ = MeHg burial rate (ng L^{-1} d^{-1}).

4.7.5 Sediment-water transfer

Dissolved mercury species are carried through the bed by pore water flow and are exchanged between bed sediment and the water column by the diffusion process. Pore water diffusion is assumed to operate on all dissolved fractions of HgII and MeHg. Sediment-water fluxes of HgII and MeHg are calculated by

$$HgII \leftrightarrow HgII_2 = \frac{v_m}{h} \left[\begin{array}{c} \left(f_{d-HgII2} + f_{doc-HgII2} \right) HgII_2 / \phi \\ - \left(f_{d-HgII} + f_{doc-HgII} \right) HgII \end{array} \right] \tag{4.20a}$$

$$MeHg \leftrightarrow MeHg_2 = \frac{v_m}{h} \left[\begin{array}{c} \left(f_{d-MeHg2} + f_{doc-MeHg2} \right) MeHg_2 / \phi \\ - \left(f_{d-MeHg} + f_{doc-MeHg} \right) MeHg \end{array} \right] \tag{4.20b}$$

where

$HgII \text{<-->} HgII_2$ = sediment-water flux of dissolved and DOC sorbed HgII (ng L^{-1} d^{-1}),
$MeHg \text{<-->} MeHg_2$ = sediment-water flux of dissolved and DOC sorbed MeHg (ng L^{-1} d^{-1}).

A positive flux results in the transport of mercury from the sediment to the overlying water, a negative flux means the transport of mercury from the overlying water to the sediment. The sediment-water mass-transfer velocity is a user specified parameter or internally computed in HgSM. Similar to the CSM, three alternative formulations are available.

4.8 Water Column Source and Sink Equations of Mercury Species

The sources and sinks for three mercury species are depicted in Figure 5. Major processes modeled in HgSM are partitioning of HgII and MeHg, particulate settling, resuspension and burial, sediment-water diffusion, volatilization, and transformations (*e.g.* biological methylation and demethylation, MeHg photoreduction, HgII reduction and oxidation). Meanwhile, mercury species can be transported together with water, DOC and suspended solids.

All concentrations in following source and sink term equations, including those for sediment mercury species, are expressed in terms of mass per unit volume of water and solids (ng L^{-1}). The method employed here is numerically equivalent and simpler because all the state variables are in the same units, and no correction term is needed in the mass balance equations. Furthermore, this method is more amenable to integration with the SRH-2D transport model, for which the common concentration units are mass per unit volume.

4.8.1 Elemental mercury (Hg0)

Hg0 is the predominant mercury cycling product in the water column. Major processes involved in Hg0 cycling in the water column include HgII reduction to Hg0, demethylation, and volatilization. The sum of internal source and sink terms of Hg0 in the water column is written as:

$$SS_{Hg0} = -v_{v-Hg0}\frac{1}{h}\left(Hg0 - \frac{Hg0_0}{K_H/RT_K}\right)$$ Hg0 volatilization   **(4.21)**

$$-k_{12}(T)\cdot Hg0$$ Hg0 oxidation

$$+1.33\frac{I_0}{I_{0pht}}\frac{1-e^{-\lambda_{max}\cdot h}}{\lambda_{max}\cdot h}(1-0.56C_L)$$

$$\left(k_{d21}f_{d-HgII} + k_{doc21}f_{doc-HgII}\right)HgII\cdot Y_{21}$$ HgII photoreduction

$$+1.33\frac{I_0}{I_{0pht}}\frac{1-e^{-\lambda_{max}\cdot h}}{\lambda_{max}\cdot h}(1-0.56C_L)$$

$$\left(k_{d31}f_{d-MeHg} + k_{doc31}f_{doc-MeHg}\right)MeHg\cdot Y_{31}$$ MeHg photoreduction

where

SS_{Hg0} = sum of internal source and sink terms of Hg0 in water (ng L^{-1} d^{-1}),
Y_{21} = photoreduction yield coefficient from HgII to Hg0 in water,
Y_{31} = photoreduction yield coefficient from MeHg to Hg0 in water.

4.8.2 Inorganic mercury (HgII)

Both equilibrium and non-equilibrium partitioning of HgII is modeled in HgSM. Under a non-equilibrium partitioning, the internal source and sink term must be tracked separately for dissolved and sorbed phases.

Equilibrium partitioning

Major processes involved in HgII cycling in the water column include HgII reduction, methylation, settling of sorbed particulates into the underlying sediment layer, HgII diffusion across the sediment-water interface, and sediment resuspension and burial. HgII may be adsorbed by DOC, algae, POM and suspended solids. The internal source (+) and sink (-) equation of total HgII in the water column is written as

$$SS_{HgII} = \frac{1}{h} L_{HgII} \qquad\qquad \text{Atmospheric HgII deposition} \qquad \textbf{(4.22)}$$

$$-\frac{1}{h}\left(\sum_{n=1}^{N} v_{pn} f_{pn-HgII} + v_{sap} f_{ap-HgII} + v_{som} f_{pom-HgII}\right) HgII \quad \text{HgII settling}$$

$$+\frac{1}{h}\left(\sum_{n=1}^{N} v_{rn} f_{pn-HgII2}\right) HgII_2 \qquad\qquad \text{HgII resuspension}$$

$$+\frac{v_m}{h}\left[\begin{array}{l}\left(f_{d-HgII2} + f_{doc-HgII2}\right) HgII_2 / \phi \\ -\left(f_{d-HgII} + f_{doc-HgII}\right) HgII\end{array}\right] \qquad \text{HgII sediment-water transfer}$$

$$+ k_{12}(T) \cdot HgO \cdot Y_{12} \qquad\qquad \text{Hg0 oxidation}$$

$$-1.33\frac{I_0}{I_{0pht}}\frac{1-e^{-\lambda_{max}\cdot h}}{\lambda_{max}\cdot h}\left(1-0.56 C_L\right)$$
$$\left(k_{d21} f_{d-HgII} + k_{doc21} f_{doc-HgII}\right) HgII \qquad \text{HgII photoreduction}$$

$$-\left(k_{d23}(T) f_{d-HgII} + k_{doc23}(T) f_{d-HgII}\right) HgII \qquad \text{HgII methylation}$$

$$+1.33\frac{I_0}{I_{0pht}}\frac{1-e^{-\lambda_{max}\cdot h}}{\lambda_{max}\cdot h}\left(1-0.56 C_L\right)$$
$$\left(k_{d32} f_{d-MeHg} + k_{doc32} f_{doc-MeHg}\right) MeHg \cdot Y_{32} \qquad \text{MeHg demethylation}$$

Where:

SS_{HgII} = sum of internal source and sink terms of total HgII in water (ng L^{-1} d^{-1}),
Y_{12} = oxidation yield coefficient from Hg0 to HgII in water ($Y_{12} = 1.0$),
Y_{32} = demethylation yield coefficient from MeHg to HgII in water.

Non-equilibrium partitioning

Under a non-equilibrium partitioning state, sorption and desorption of HgII are represented separately in kinetic formulations. The HgSM must compute the rate change of HgII in each phase separately. The internal source and sink equations for dissolved, DOC sorbed, algae sorbed, POM sorbed, and solids sorbed phases in the water column are written as:

Dissolved HgII:

$$SS_{HgIId} = \frac{1}{h}L_{HgII} \qquad \text{Atmospheric HgII deposition} \quad (4.23)$$

$$+\frac{v_m}{h}\left[HgII_{d2}/\phi - HgII_d\right] \qquad \text{HgII sediment-water transfer}$$

$$+ k_{12}(T)\cdot HgO \cdot Y_{12} \qquad \text{Hg0 oxidation}$$

$$-1.33\frac{I_0}{I_{0pht}}\frac{1-e^{-\lambda_{max}\cdot h}}{\lambda_{max}\cdot h}(1-0.56C_L)k_{d21}HgII_d \quad \text{HgII photoreduction}$$

$$- k_{d23}(T)HgII_d \qquad \text{HgII methylation}$$

$$+1.33\frac{I_0}{I_{0pht}}\frac{1-e^{-\lambda_{max}\cdot h}}{\lambda_{max}\cdot h}(1-0.56C_L) \qquad \text{MeHg demethylation}$$
$$\left[(k_{d32}(T)MeHg_d)+(k_{doc32}(T)MeHg_{doc})\right]Y_{32}$$

$$-\left(\begin{array}{l}10^{-3}k_{adap}(T)HgII_d\left(q_{cap}A_{pd}-HgII_{ap}\right)\\-k_{daap}(T)HgII_{ap}\end{array}\right)$$

$$-\left(\begin{array}{l}10^{-3}k_{adpom}(T)HgII_d\left(q_{cpom}POM-HgII_{pom}\right)\\-k_{dapom}(T)HgII_{pom}\end{array}\right) \qquad \text{Adsorption-desorption}$$

$$-\sum_{n=1}^{N}\left[\begin{array}{l}10^{-3}k_{adn}(T)HgII_d\left(q_{cn}m_n-HgII_{pn}\right)\\-k_{dan}(T)HgII_{pn}\end{array}\right]$$

DOC sorbed HgII:

$$SS_{HgIIdoc} = \frac{v_m}{h}\left[HgII_{doc2}/\phi - HgII_{doc}\right] \qquad \text{HgII sediment-water transfer (4.24)}$$

$$-1.33\frac{I_0}{I_{0pht}}\frac{1-e^{-\lambda_{max}\cdot h}}{\lambda_{max}\cdot h}(1-0.56C_L)k_{doc21}HgII_{doc} \quad \text{HgII photoreduction}$$

$$- k_{doc23}(T)HgII_{doc} \qquad \text{HgII methylation}$$

Algae sorbed HgII:

$$SS_{HgIIap} = -\frac{1}{h}v_{sap}HgII_{ap} \qquad\qquad \text{HgII settling} \qquad\qquad \textbf{(4.25)}$$

$$+10^{-3}k_{adap}(T)HgII_d\left(q_{cap}A_{pd} - HgII_{ap}\right) \quad \text{Adsorption-desorption}$$
$$-k_{daap}(T)HgII_{ap}$$

POM sorbed HgII:

$$SS_{HgIIpom} = -\frac{1}{h}v_{som}HgII_{pom} \qquad\qquad \text{HgII settling} \qquad\qquad \textbf{(4.26)}$$

$$+10^{-3}k_{adpom}(T)HgII_d\left(q_{cpom}POM - HgII_{pom}\right) \quad \text{Adsorption-desorption}$$
$$-k_{dapom}(T)HgII_{pom}$$

Solids sorbed HgII:

$$SS_{HgIIpn} = -\frac{1}{h}v_{pn}HgII_{pn} \qquad\qquad \text{HgII settling} \qquad\qquad \textbf{(4.27)}$$

$$+\frac{1}{h}v_{rn}HgII_{pn2} \qquad\qquad \text{HgII resuspension}$$

$$+10^{-3}k_{adn}(T)HgII_d\left(q_{cn}m_n - HgII_{pn}\right) \quad \text{Adsorption-desorption}$$
$$-k_{dan}(T)HgII_{pn}$$

where

SS_{HgIId} = sum of internal source and sink terms of dissolved HgII in water (ng L^{-1} d^{-1})
$SS_{HgIIdoc}$ = sum of internal source and sink terms of DOC sorbed HgII in water (ng L^{-1} d^{-1})
SS_{HgIIap} = sum of internal source and sink terms of algae sorbed HgII in water (ng L^{-1} d^{-1})

$SS_{HgIIpom}$ = sum of internal source and sink terms of POM sorbed HgII in water (ng L^{-1} d^{-1})

SS_{HgIIp} = sum of internal source and sink terms of solids sorbed HgII in water (ng L^{-1} d^{-1}).

4.8.3 Methylmercury (MeHg)

Only equilibrium partitioning of MeHg is modeled in HgSM. Major processes involved in MeHg cycling in the water column include volatilization, methylation, photodegradation, settling of sorbed particulates into the sediment layer, MeHg diffusion across the sediment-water interface, and sediment resuspension and burial. MeHg may be adsorbed by DOC, algae, POM, and suspended solids. The internal source and sink equation of total MeHg in the water column is writtern as

$$SS_{MeHg} = \frac{1}{h} L_{MeHg} \qquad \textbf{Atmospheric MeHg deposition} \qquad \textbf{(4.28)}$$

$$-\frac{1}{h}\left(\sum_{n=1}^{N} v_{pn} f_{pn-MeHg} + v_{sap} f_{ap-MeHg} + v_{som} f_{pom-MeHg} \right) MeHg \quad \text{MeHg settling}$$

$$+\frac{1}{h}\left(\sum_{n=1}^{N} v_{rn} f_{pn-MeHg2} \right) MeHg_2 \qquad \textbf{MeHg resuspension}$$

$$+\frac{v_m}{h}\left[\begin{array}{c} \left(f_{d-MeHg2} + f_{doc-MeHg2} \right) MeHg_2 / \phi \\ -\left(f_{d-MeHg} + f_{doc-MeHg} \right) MeHg \end{array} \right] \qquad \textbf{MeHg sediment-water transfer}$$

$$-v_{v-MeHg}\frac{1}{h}\left(f_{d\text{-}MeHg} MeHg - \frac{MeHg_0}{K_H / RT_K} \right) \qquad \text{MeHg volatilization}$$

$$+\left(k_{d23}(T) f_{d-HgII} + k_{doc23}(T) f_{doc-HgII} \right) HgII \cdot Y_{23} \qquad \textbf{HgII methylation}$$

$$-1.33 \frac{I_0}{I_{0pht}} \frac{1 - e^{-\lambda_{max} \cdot h}}{\lambda_{max} \cdot h}\left(1 - 0.56 C_L \right) \qquad \textbf{MeHg demethylation}$$
$$\left(k_{d32} f_{d-MeHg} + k_{doc32} f_{doc-MeHg} \right) MeHg$$

$$-1.33 \frac{I_0}{I_{0pht}} \frac{1 - e^{-\lambda_{max} \cdot h}}{\lambda_{max} \cdot h}\left(1 - 0.56 C_L \right) \qquad \text{MeHg photoreduction}$$
$$\left(k_{d31} f_{d-MeHg} + k_{doc31} f_{doc-MeHg} \right) MeHg$$

where

SS_{MeHg} = sum of internal source and sink terms of total MeHg in water (ng L^{-1} d^{-1}),
Y_{23} = methylation yield coefficient from HgII to MeHg in water.

4.9 Sediment Mass Balance Equations of Mercury Species

Important sediment processes that are modeled include diffusive exchange of dissolved mercury species between sediment pore water and the water column, and sediment mixing processes of solids-bound mercury species. Similar to the CSM, the sediment layer is assumed to have constant properties including the thickness, volume, porosity, and bulk density. HgII and MeHg are modeled, Hg0 is not included for the sediment layer.

4.9.1 Inorganic mercury (HgII)

Equilibrium partitioning

Major processes involved in HgII cycling in the sediment layer include methylation, demethylation, water column settling, pore water diffusion across the sediment-water interface, sediment resuspension and burial. HgII may be adsorbed by DOC, sediment POM and solids. Because of varying environmental conditions, the rate of these reactions can vary dramatically from those in the water column. The mass balance equation of sediment total HgII is written as

$$SS_{HgII2} = \frac{1}{h_2}\left(\sum_{n=1}^{N} v_{dn} f_{pn-HgII} + v_{sap} f_{ap-HgII} + v_{som} f_{pom-HgII}\right) HgII \qquad \textbf{HgII deposition} \qquad \textbf{(4.29)}$$

$$-\frac{1}{h_2}\left(\sum_{n=1}^{N} v_{rn} f_{pn-HgII2}\right) HgII_2 \qquad \textbf{HgII resuspension}$$

$$-\frac{v_m}{h_2}\left[\frac{\left(f_{d-HgII2} + f_{doc-HgII2}\right) HgII_2 / \phi}{-\left(f_{d-HgII} + f_{doc-HgII}\right) HgII}\right] \qquad \textbf{HgII sediment-water transfer}$$

$$-\frac{v_b}{h_2}\left(\sum_{n=1}^{N} f_{pn-HgII2} + f_{pom-HgII2}\right) HgII_2 \qquad \textbf{HgII deep burial}$$

$$-POM_2 k_{dom2}(T) Y_{m2}\left(\frac{SO4_2}{K_{SO4} + SO4_2}\right) \qquad \textbf{HgII methylation}$$
$$\left(f_{d-HgII2} + f_{mdoc2} f_{doc-HgII2}\right) HgII_2$$

$$+POM_2 k_{dom2}(T) Y_{dm} \qquad \text{MeHg demethylation}$$
$$\left(f_{d-MeHg2} + f_{dmdoc2} f_{doc-MeHg2}\right) MeHg_2 \cdot Y_{32}$$

where

SS_{HgII2} = sum of source and sink terms of total HgII in sediment (ng L^{-1} d^{-1}).

Non-equilibrium partitioning

Non-equilibrium of HgII onto sediment solids is modeled identically to the partitioning of HgII onto suspended solids in the water column. However, the values for the number of binding sites for sediments can be different, thus providing the ability to reflect the difference in adsorption characteristics between sediment solids and solids suspended in the water column. Under a non-equilibrium partitioning, the mass balances of HgII in each phase must be solved simultaneously. The mass balance equations for HgII dissolved, DOC sorbed, POM and solids sorbed phases in the sediment layer are writtern as follows.

<u>**Dissolved HgII**</u>:

$$SS_{HgIId2} = -\frac{v_m}{h_2}\left[HgII_{d2}/\phi - HgII_d\right] \qquad \text{HgII sediment-water transfer} \qquad \textbf{(4.30)}$$

$$- POM_2 k_{dom2}(T)Y_{m2}\left(\frac{SO4_2}{K_{SO4}+SO4_2}\right)HgII_{d2} \quad \text{HgII methylation}$$

$$+ POM_2 k_{dom2}(T)Y_{dm} \atop \left(f_{d-MeHg2}+f_{dmdoc2}f_{doc-MeHg2}\right)MeHg_2 \cdot Y_{32} \quad \text{MeHg demethylation}$$

$$-\left(\begin{array}{c}10^{-3}k_{adpom2}(T)HgII_{d2}\left(q_{cpom2}POM_2 - HgII_{pom2}\right)\\ -k_{dapom2}(T)HgII_{pom2}\end{array}\right) \quad \text{Adsorption-desorption}$$

$$-\sum_{n=1}^{N}\left[\begin{array}{c}10^{-3}k_{adn2}(T)HgII_{d2}\left(q_{cn2}m_{n2} - HgII_{pn2}\right)\\ -k_{dan2}(T)HgII_{pn2}\end{array}\right]$$

DOC sorbed HgII:

$$SS_{HgIIdoc2} = -\frac{v_m}{h_2}\left[HgII_{doc2}/\phi - HgII_{doc}\right] \qquad \text{HgII sediment-water transfer} \qquad \textbf{(4.31)}$$

$$- POM_2 k_{dom2}(T)Y_{m2}\left(\frac{SO4_2}{K_{SO4}+SO4_2}\right)f_{mdoc2}HgII_{doc2} \quad \text{HgII methylation}$$

POM sorbed HgII:

$$SS_{HgIIpom2} = \frac{1}{h_2}\left(v_{sap}HgII_{ap} + v_{som}HgII_{pom}\right) \qquad \text{HgII deposition} \qquad \textbf{(4.32)}$$

$$-\frac{v_b}{h_2}HgII_{pom2} \qquad \text{HgII deep burial}$$

$$+10^{-3}k_{adpom2}(T)HgII_{d2}\left(q_{cpom2}POM_2 - HgII_{pom2}\right) \atop -k_{dapom2}(T)HgII_{pom2} \quad \text{Adsorption-desorption}$$

Solids sorbed HgII:

$$SS_{HgIIpn2} = \frac{1}{h_2}v_{dn}HgII_{pn} \qquad \text{HgII deposition} \qquad \textbf{(4.33)}$$

$$-\frac{1}{h_2}v_{rn}HgII_{pn2} \qquad \text{HgII resuspension}$$

$$-\frac{v_b}{h_2}HgII_{pn2} \qquad \text{HgII deep burial}$$

$$+ 10^{-3}k_{adn2}(T)HgII_{d2}\left(q_{cn2}m_{n2} - HgII_{pn2}\right)$$ Adsorption-desorption
$$- k_{dan2}(T)HgII_{pn2}$$

where

SS_{HgIId2} = sum of source and sink terms of dissolved HgII in sediment (ng L^{-1} d^{-1}),
$SS_{HgIIdoc2}$ = sum of source and sink terms of DOC sorbed HgII in sediment (ng L^{-1} d^{-1}),
$SS_{HgIIpom2}$ = sum of source and sink terms of POM sorbed HgII in sediment (ng L^{-1} d^{-1}),
SS_{HgIIp2} = sum of source and sink terms of solids sorbed HgII in sediment (ng L^{-1} d^{-1}).

4.9.2 Methylmercury (MeHg)

Major processes involved in MeHg cycling in the sediment layer include methylation, biological demethylation, pore water diffusion across the sediment-water interface, water column settling, sediment resuspension, and burial. MeHg may be adsorbed by DOC, sediment POM and solids. The mass balance equation of sediment total MeHg is written as

$$SS_{MeHg2} = \frac{1}{h_2}\left(\sum_{n=1}^{N}v_{dn}f_{pn-MeHg} + v_{sap}f_{ap-MeHg} + v_{som}f_{pom-MeHg}\right)MeHg \quad \textbf{MeHg deposition} \quad (4.34)$$

$$- \frac{1}{h_2}\left(\sum_{n=1}^{N}v_{rn}f_{pn-MeHg2}\right)MeHg_2 \quad \text{MeHg resuspension}$$

$$- \frac{v_m}{h_2}\left[\frac{\left(f_{d-MeHg2} + f_{doc-MeHg2}\right)MeHg_2/\phi}{-\left(f_{d-MeHg} + f_{doc-MeHg}\right)MeHg}\right] \quad \text{MeHg sediment-water transfer}$$

$$- \frac{v_b}{h_2}\left(\sum_{n=1}^{N}f_{pn-MeHg2} + f_{pom-MeHg2}\right)MeHg_2 \quad \text{MeHg deep burial}$$

$$+ POM_2 k_{dom2}(T)Y_{m2}\left(\frac{SO4_2}{K_{SO4} + SO4_2}\right) \quad \text{HgII methylation}$$
$$\left(f_{d-HgII2} + f_{mdoc2}f_{doc-HgII2}\right)HgII_2 \cdot Y_{23}$$

$$- POM_2 k_{dom2}(T)Y_{dm} \quad \text{MeHg demethylation}$$
$$\left(f_{d-MeHg2} + f_{dmdoc2}f_{doc-MeHg2}\right)MeHg_2$$

where

SS_{MeHg2} = sum of source and sink terms of total MeHg in sediment (ng L^{-1} d^{-1}).

4.10 HgSM Parameters

Table 9 provides a summary of HgSM model parameters and their default values. Similar to CSM, all of these parameters are spatially-variable parameters by user-defined water quality regions, and do not vary with time. There are three groups of parameters: global, water column and sediment layer. Literature values are taken from a compilation of several studies. It should be noted that suggested values are based on a limited literature review. Most of them are model calibration

parameters in real world applications. This table will be repeated for each water quality region, allow the user to define the different values for input parameters.

Table 9. HgSM input parameters and coefficients

Name	Definition	Default values	Approximate range	Units	Temp correction *	
Global						
D_m	Molecular diffusivity	-	n/a	$m^2\ d^{-1}$		
v_m	Sediment-water mass transfer velocity	-	n/a	$m\ d^{-1}$		
v_{ss}	Solids settling velocity	-	n/a	$m\ d^{-1}$		
v_{som}	Organic matter settling velocity	-	n/a	$m\ d^{-1}$		
$k_{pht}(T)$	Aquatic photolysis rate	-	n/a	d^{-1}	E_a	n/a
I_{0pht}	Light intensity when k_{pht} is measured	-	n/a	$W\ m^{-2}$		
α_l	Light attenuation adjusting coefficient	1.33	1.2 - 1.6	unitless		
Water column						
Elemental mercury						
MW	Hg0 molecular weight[a]	200.6	-	$g\ mol^{-1}$		
S_{Hg0}	Solubility	56	-	$\mu g\ L^{-1}$		
$v_{v\text{-}Hg0}(T)$	Hg0 volatilization velocity[f]	0.006	0.0059 – 0.45	$m\ hr^{-1}$	θ	n/a
K_H	Hg0 Henry's Law constant	0.09[l]	-	$Pa\ m^3\ mol^{-1}$		
$Hg0_0$	Air concentration of Hg0	2×10^{-3}	n/a	$ng\ L^{-1}$		
$k_{12}(T)$	Hg0 oxidation rate[b]	10^{-3}	1×10^{-3} - 1×10^{-1}	d^{-1}	E_a	n/a
Y_{12}	Oxidation yield coefficient	1.0	0 - 2.0	unitless		
Inorganic mercury						
MW	HgII molecular weight[a]	271.52	232.68 (HgS) 271.52 ($HgCl_2$)	$g\ mol^{-1}$		

$K_{p\text{-}HgII}$	Equilibrium partition coefficient for algae[c]	-	1×10^{5} - 1×10^{6}	L kg^{-1}		
$K_{p\text{-}HgII}$	Equilibrium partition coefficient for silt[b]	2×10^{5}	1×10^{3} - 1×10^{6}	L kg^{-1}		
$K_{p\text{-}HgII}$	Equilibrium partition coefficient for clay[b]	2×10^{5}	1×10^{3} - 1×10^{6}	L kg^{-1}		
$K_{p\text{-}HgII}$	Equilibrium partition coefficient for solids[e]	$10^{5.3}$	$10^{4.2}$ - $10^{6.9}$	L kg^{-1}		
b_{HgII}	Freundlich exponent[h]	-	$0.4 - 1.2$	unitless		
$K_{f\text{-}HgII}$	Freundlich adsorption constant[h]	-	$4.5\times10^{4} - 2.52\times10^{8}$	(µg g^{-1}) (µg L^{-1})$^{-b}$		
$K_{l\text{-}HgII}$	Langmuir adsorption constant[h]	-	$1\times10^{6} - 7\times10^{6}$	L µg^{-1}		
$qcn_{\text{-}HgII}$	Adsorption capacity for solid "n"[h]	-	$2.8\times10^{2} - 3.58\times10^{3}$	µg g^{-1}		
$kadn_{\text{-}HgII}$	Adsorption coefficient	-	n/a	L µg^{-1} d^{-1}		
$kdan_{\text{-}HgII}$	Desorption rate	1.0	n/a	d^{-1}		
$k_{doc\text{-}HgII}$	Partition coefficient for DOC[e]	$10^{5.3}$	$10^{5.3}$ - $10^{5.6}$	L kg^{-1}		
k_{d21}	Dissolved photoreduction rate[b]	5×10^{-2}	1×10^{-3} - 5×10^{-1}	d^{-1}		
k_{doc21}	DOC sorbed photoreduction rate[b]	0.0	1×10^{-3} - 5×10^{-1}	d^{-1}		
Y_{21}	Photoreduction yield coefficient	1.0	0 - 2.0	unitless		
$k_{d23}(T)$	Dissolved methylation rate[b]	10^{-3}	1×10^{-5} - 5×10^{-2}	d^{-1}	θ	1.14
$k_{doc23}(T)$	DOC sorbed methylation rate[b]	10^{-3}	1×10^{-5} - 5×10^{-2}	d^{-1}	θ	1.14
Y_{23}	Methylation yield coefficient	1.07	0 - 2.0	unitless		
Methymercury						

58

MW	MeHg molecular weight[a]	230.66 (CH3$_2$Hg)	n/a	g mol^{-1}		
$K_{p\text{-}MeHg}$	Equilibrium partition coefficient for algae[g]	10^5	10^5 - 10^7	L kg^{-1}		
$K_{p\text{-}MeHg}$	Equilibrium partition coefficient for silt[b]	2×10^5	1×10^3 - 1×10^6	L kg^{-1}		
$K_{p\text{-}MeHg}$	Equilibrium partition coefficient for caly[b]	2×10^5	1×10^3 - 1×10^6	L kg^{-1}		
$K_{p\text{-}MeHg}$	Equilibrium partition coefficient for solids[e]	$10^{5.4}$	$10^{4.2}$ - $10^{6.2}$	L kg^{-1}		
$K_{doc\text{-}MeHg}$	Equilibrium partition coefficients for DOC[b]	2×10^5	1×10^5 - 1×10^6	L kg^{-1}		
b_{MeHg}	Freundlich exponent	-	n/a	unitless		
$K_{f\text{-}MeHg}$	Freundlich adsorption constant	-	n/a	(μg g^{-1})(μg L^{-1})$^{-b}$		
$K_{l\text{-}MeHg}$	Langmuir adsorption constant[h]	-	n/a	L μg^{-1}		
$qcn_{\text{-}MeHg}$	Adsorption capacity for solid "n"	-	n/a	μg g^{-1}		
k_{d31}	Dissolved photoreduction rate into Hg0[b]	-	1×10^{-3} - 5×10^{-1}	d^{-1}		
k_{doc31}	DOC sorbed photoreduction rate into Hg0[b]	0.0	1×10^{-3} - 5×10^{-1}	d^{-1}		
Y_{31}	Photoreduction yield coefficient	0.93	0 - 2.0	unitless		
k_{d32}	Dissolved demethylation rate into HgII[b]	5×10^{-2}	1×10^{-3} - 5×10^{-1}	d^{-1}		
k_{doc32}	DOC sorbed demethylation rate into HgII[b]	0.0	1×10^{-3} - 5×10^{-1}	d^{-1}		
Y_{32}	Demethylation yield coefficient	0.93	0 - 2.0	unitless		
$v_{v\text{-}MeHg}(T)$	MeHg volatilization velocity	1.9×10^{-5}	n/a	m d^{-1}	θ	n/a
K_H	MeHg Henry's constant	4.5×10^{-6}[l]	n/a	Pa m^3 mol^{-1}		

$MeHg_0$	Air concentration of MeHg	0.0	n/a	ng L^{-1}		
Sediment layer						
Inorganic mercury						
$K_{p\text{-}HgII2}$	Equilibrium partition coefficient for silt[b]	-	1×10^{3} - 1×10^{6}	L kg^{-1}		
$K_{p\text{-}HgII2}$	Equilibrium partition coefficient for clay[b]	-	1×10^{3} - 1×10^{6}	L kg^{-1}		
$K_{p\text{-}HgII2}$	Equilibrium partition coefficient for solids[e]	$10^{4.9}$	$10^{3.8}$ - 10^{6}	L kg^{-1}		
b_{HgII2}	Freundlich exponent	-	n/a	unitless		
$K_{f\text{-}HgII2}$	Freundlich adsorption constant	-	n/a	(µg g^{-1}) (µg L^{-1})$^{-b}$		
$K_{l\text{-}HgII2}$	Langmuir adsorption constant[d]	-	51 - 390	L µg^{-1}		
$qcn_{\text{-}HgII2}$	Adsorption capacity for solid "n"	-	n/a	µg g^{-1}		
$kadn_{\text{-}HgII}2$	Adsorption coefficient	-	n/a	L µg^{-1} d^{-1}		
$kdan_{\text{-}HgII}2$	Desorption rate	0.1	n/a	d^{-1}		
$k_{doc\text{-}HgII2}$	Partition coefficient for DOC[b]	-	1×10^{4} - 1×10^{5}	L kg^{-1}		
$k_{dom2}(T)$	Sediment organic matter decomposition rate	-	-	d^{-1}	θ	n/a
Y_{m2}	Sediment methylation efficiency	-	-	(ng-MeHg ng-HgII^{-1}) (mg L^{-1})$^{-1}$		
f_{mdoc2}	Fraction of DOC sorbed HgII methylation	0.0	$0 - 1.0$	unitless		
K_{SO4}	Half-saturation constant for the effect of sulfate on methylation	-	-	mg-O$_2$ L^{-1}		
Methymercury						
$K_{p\text{-}MeHg2}$	Equilibrium partition coefficient for silt[b]	-	1×10^{3} - 1×10^{6}	L kg^{-1}		

$K_{p\text{-}MeHg2}$	Equilibrium partition coefficient for clay[b]	-	1×10^3 - 1×10^6	L kg^{-1}	
$K_{p\text{-}MeHg2}$	Equilibrium partition coefficient for solids[e]	$10^{3.6}$	$10^{2.8}$ - 10^5	L kg^{-1}	
$K_{doc\text{-}MeHg2}$	Equilibrium partition coefficients for DOC[b]	-	1×10^5 - 1×10^6	L kg^{-1}	
b_{MeHg2}	Freundlich exponent	-	n/a	Unitless	
$K_{f\text{-}MeHg2}$	Freundlich adsorption constant	-	n/a	(μg g^{-1}) (μg L^{-1})$^{-b}$	
$K_{l\text{-}MeHg2}$	Langmuir adsorption constant[d]	-	n/a	L μg^{-1}	
$qcn_{\text{-}MeHg}2$	Adsorption capacity for solid "n"	-	n/a	μg g^{-1}	
Y_{dm2}	Sediment demethylation efficiency	-	-	(ng-HgII ng-MeHg^{-1}) (mg L^{-1})$^{-1}$	
f_{dmdoc2}	fraction of sediment DOC sorbed MeHg demethylation	-	0 – 1.0	Unitless	

a. ATSDR (2005).
b. Wool (et al., 2006).
c. Hudson et al. (1994).
d. Tsiros and Ambrose (1999).
e. Allison and Allison (2005).
f. Loux (2004).
g. Miles et al. (2001).
h. Chen et al. (2009).
l. Lin et al. (1999).

The sediment layer has a constant volume and thickness during a simulation. Sediment particle density and porosity are fixed. Settling velocities of particles and sediment resuspension rates are required model input parameters.

4.11 HgSM Outputs

This section summarize the model outputs from HgSM. Concentrations of the HgII and MeHg computed for each physical compartment (water column and sediment layer) include dissolved, DOC sorbed, algae, POM and solids sorbed phases. Table 10 lists the HgSM's output concentrations of mercury species with a brief description.

Table 10. Concentrations of mercury species computed in HgSM

Name	Definition	Units
Elemental mercury		
Hg0	Hg0 concentration in water	ng L^{-1}
Inorganic mercury		
HgII	Concentration of total HgII in water	ng L^{-1}
HgII$_d$	Concentration of dissolved HgII in water	ng L^{-1}
HgII$_{doc}$	Concentration of DOC sorbed HgII in water	ng L^{-1}
HgII$_{ap}$	Concentration of algae sorbed HgII in water	ng L^{-1}
HgII$_{pom}$	Concentration of POM sorbed HgII in water	ng L^{-1}
HgII$_{pt}$	Total concentration of solids sorbed HgII in water	ng L^{-1}
HgII$_{pts}$	Total mass of of solids sorbed HgII in water	ng g^{-1}
HgII$_2$	Concentration of total HgII in sediment	ng L^{-1}
HgII$_{dp2}$	Concentration of dissolved HgII in pore water	ng L^{-1}
HgII$_{docp2}$	Concentration of DOC sorbed HgII in pore water	ng L^{-1}
HgII$_{pom2}$	Concentration of POM sorbed HgII in sediment	ng L^{-1}
HgII$_{pt2}$	Total concentration of solids sorbed HgII in sediment	ng L^{-1}
HgII$_{pts2}$	Total mass of solids sorbed HgII in sediment	ng g^{-1}
Methymercury		
MeHg	Concentration of total MeHg in water	ng L^{-1}
MeHg$_d$	Concentration of dissolved MeHg in water	ng L^{-1}
MeHg$_{doc}$	Concentration of DOC sorbed MeHg in water	ng L^{-1}
MeHg$_{ap}$	Concentration of algae sorbed MeHg in water	ng L^{-1}
MeHg$_{pom}$	Concentration of POM sorbed MeHg in water	ng L^{-1}
MeHg$_{pt}$	Total concentration of MeHg sorbed on solids in water	ng L^{-1}
MeHg$_{pts}$	Total mass of MeHg sorbed on solids in water	ng g^{-1}

MeHg$_2$	Concentration of total MeHg in sediment	ng L^{-1}
MeHg$_{dp2}$	Concentration of dissolved MeHg in pore water	ng L^{-1}
MeHg$_{docp2}$	Concentration of DOC sorbed MeHg in pore water	ng L^{-1}
MeHg$_{pom2}$	Concentration of POM sorbed MeHg in sediment	ng L^{-1}
MeHg$_{pt2}$	Total concentration of solids sorbed MeHg in sediment	ng L^{-1}
MeHg$_{pts2}$	Total mass of solids sorbed MeHg in sediment	ng g^{-1}

Mercury pathway fluxes are internally ccomputed in HgSM and can be reported in the model outputs. Table 11 lists the mercury pathway fluxes outputs from HgSM.

Table 11. Mercury pathway fluxes computed in HgSM

Name	Definition	Units
Elemental mercury		
Atm<-->Hg0	Hg0 volatilization in water	ng L^{-1} d^{-1}
Hg0-->HgII	Hg0 oxidation into HgII in water	ng L^{-1} d^{-1}
Inorganic mercury		
HgII-->Hg0	HgII photoreduction into Hg0 in water	ng L^{-1} d^{-1}
HgII-->MeHg	HgII methylation into MeHg in water	ng L^{-1} d^{-1}
HgII-->Bed	HgII settling	ng L^{-1} d^{-1}
Bed-->HgII	HgII resuspension	ng L^{-1} d^{-1}
HgII<-->HgII$_2$	HgII sediment-water transfer	ng L^{-1} d^{-1}
HgII$_2$-->MeHg$_2$	sediment HgII methylation into MeHg	ng L^{-1} d^{-1}
HgII-->Bed	HgII deposition	ng L^{-1} d^{-1}
Bed-->HgII	HgII erosion	ng L^{-1} d^{-1}
HgII<-->HgII$_2$	HgII sediment-water transfer	ng L^{-1} d^{-1}
HgII$_2$ burial	HgII burial	ng L^{-1} d^{-1}
Methymercury		
Atm<-->MeHg	MeHg volatilization in water	ng L^{-1} d^{-1}
MeHg-->Hg0	MeHg photoreduction into Hg0 in water	ng L^{-1} d^{-1}
MeHg-->HgII	MeHg demethylation into HgII in water	ng L^{-1} d^{-1}
MeHg-->Bed	MeHg settling	ng L^{-1} d^{-1}

Bed-->MeHg	MeHg resuspension	ng L^{-1} d^{-1}
MeHg<-->MeHg$_2$	MeHg sediment-water transfer	ng L^{-1} d^{-1}
MeHg$_2$-->HgII$_2$	sediment MeHg bacterial demethylation into HgII	ng L^{-1} d^{-1}
MeHg-->Bed	MeHg deposition	ng L^{-1} d^{-1}
Bed-->MeHg	MeHg erosion	ng L^{-1} d^{-1}
MeHg<-->MeHg$_2$	MeHg sediment-water transfer	ng L^{-1} d^{-1}
MeHg$_2$ burial	MeHg burial	ng L^{-1} d^{-1}

5. Data Requirements for the Model Development, Calibration and Validation

Mercury modeling involves many physical, chemical and biological processes and an extensive set of data needs to be available for a success modeling. In this chapter, the necessary input data requirements are presented which allow a modeler to carry out the mercury modeling. In addition, suggested data that may be needed for model calibration is also discussed.

5.1 Terrain Data

A modeler needs to determine the spatial extent of the modeling first and it is called model domain in this report. In general, the model domain is selected so that it covers, as a minimal, all connected water movement areas so that all important physical, chemical and biological processes are incorporated to answer the study question. For reservoir modeling, for example, the model domain may need to include the entire reservoir, portion of streams connected to the reservoir, and even portion of the upland.

Within the selected model domain, terrain and bathymetric data are needed which can come from a combination of various survey sources ranging from ground based surveys to airborne. It is ideal to process multi-source terrain and bathymetric data within the GIS environment (or other tools) and a single composite terrain model is developed. In gathering and developing the terrain data, some cautions are listed below:

- The model domain may be limited by the availability of the terrain data;
- The horizontal and vertical datum of the terrain data should be clearly checked and documented; it is particularly important with multiple sources of the data;
- The time when a data set was collected should be documented also; when very old terrain data is used, ensure that the area has not subject to dramatic change unless the terrain in the area is less critical.

5.2 Hydraulic and Hydrological Data

All open boundaries of the model domain should be identified. An open boundary is defined as a segment of the boundary through which water and scalars are entering (inlet boundary) or leaving (outlet boundary) the model domain. Some open boundaries can be both: inlet over a period of time and outlet at other time.

At most open boundaries, stream flow data, in the form of flow discharge versus time (flow hydrograph), is required. The data is obtained through a flow gauge station nearby or other means. If a reservoir is connected to a downstream outlet, the stage data is usually needed at the downstream stream location, not the flow hydrograph.

Flow hydrograph is a time series data and hourly or daily time interval is usually used.

At inlet open boundaries, scalar variables such as sediment concentration, temperature, water quality variables, and mercury concentration are also needed. As a thumb of rule, any

66

scalar that is solved by a partial differential equation in the numerical model should have its time series values specified at inlet boundaries.

5.3 Sediment Data

In this study, suspended sediment concentration is simulated and bedload is ignored as only suspended sediment is important for most reservoirs.

Sediment input data include the following:

- Sediment concentration at all inlet open boundaries
- Initial bed gradation of the model domain

5.4 Meteorological data

Meteorological data are an essential part of water temperature models and influences water quality processes. At least one full meteorological data set must be provided to run the SRH-2D and its water quality model. Hourly meteorological data are typically required for modeling water temperature due to large fluctuations in air temperature and solar radiation. As a minimum, a time series consisting of the following information is required:

- Atmospheric Pressure (mb)
- Air Temperature (^{o}C)
- Dew point [°C]
- Humidity (%)
- Short Wave Radiation (W/m^2)
- Cloud cover [%]
- Wind Speed (m/s)

Meteorological data should be assembled from the nearest meteorological station(s) to the reservoirs selected.

5.5 Water Quality Data

The SRH-2D water quality model requires an extensive array of coefficients and measured data that are used to describe hydraulic transport, transfer, and biochemical transformation properties of the simulated reservoirs. Complete sets of water quality data at the appropriate daily or monthly time intervals are required for all low flow or high flow conditions used for the model calibration. At a minimium, daily or monthly, critical water quality constituents on all major branch and tributary inflows are needed for all hydraulic boundaries.

The critical water quality parameters that are to be measured and analyzed from samples collected are listed below (they are variables in the water column needed by the Nutrient Model, NSM):

- Water Temperature
- Dissolved Oxygen
- Chlorophyll-a
- Carbon, Total Organic
- Dissolved Organic Carbon
- Dissolved Organic Matter
- Nitrogen, Total Ammonia
- Nitrogen, Total Kjeldahl
- Nitrogen, Nitrate-Nitrite
- Phosphorus, Dissolved
- Phosphorus, Orthophosphate
- Phosphorus, Total
- Alkalinity
- pH
- Chloride
- Sulfate
- Suspended Solids, Total

5.6 Mercury Data

All inflow boundaries also need observed mercury data. These data include time series concentration measurements for the following species:

- Elementary mercury
- Inorganic mercury, both dissolved and total concentrations
- Methylmercury, organic form of mercury, both dissolved and total concentrations

5.7 Model Calibration and Validation Data

requirements

The SRH-2D water quality model will be run for a period of records, may be three to five years for a selected reservoir. The model output includes flow as well as concentrations of water quality constituents. To assess the model performance with regard to flow and water quality predictions, observed data collected from the reservoir are necessary. Both model calibration and validation periods depended upon observed data availability. First, calibrated flow conditions must be in agreement with observed data. After the model is hydrologically calibrated, water quality calibration will be performed in sequential order until the predictions are in agreement, as much as possible. As for water quality data needed for the model calibration and validation, both spatial and temporal distribution of data collection should be considered.

6. Field Data Acquisition

6.1 Screening Analysis of Potential Reservoir Study Sites – Overview

The ultimate purpose of the mercury transport model under development is to predict runoff containing various forms of mercury and suggest changes that are likely to take place during and after mercury mobilization and transport to terminal facilities such as reservoirs. Once developed, the model will be applied primarily in watersheds with reservoirs managed by the Reclamation. Although it is not a requirement that the watershed(s) selected for model calibration and testing is (are) areas with elevated mercury concentrations, or watersheds with water storage reservoirs, an assumption going into this study was that those watersheds with elevated mercury would be those containing the most extensive monitoring database of mercury and methylmercury concentration and loading. The same mobilization and transport mechanisms could equally apply to watersheds with managed wetlands as a buffer between the watershed and a riverine receiving water.

An ideal data set for model calibration and testing would have water-quality data — including mercury species, suspended sediment and other ancillary parameters — for a wide range of flow conditions. Continuous (15-minute or hourly) flow records are ideal to enable the computation of constituent loads and the investigation of relationships between flow and concentration at various time scales over a wide range of hydrologic conditions. In addition to water-quality data for discrete samples, continuous data for water quality, such as turbidity, temperature, and specific conductance, is beneficial so that detailed relationships of these constituents with flow could be understood and potentially used as model input parameters (i.e., explanatory variables that would help explain variations in mercury species).

Some of the material included in this chapter was assembled for another report entitled "Integrated modeling of mercury transformation and transport in watersheds subject to wildfire" by Dr. Jun Wang (US Bureau of Reclamation, Sacramento, CA), Dr. Charles Alpers (U.S. Geological Survey, Sacramento, CA), Dr.Yong Lai (Technical Services Center, US Bureau of Reclamation, Denver, CO), Dr. Nigel Quinn (Berkeley National Laboratory, Berkeley, CA and US Bureau of Reclamation, Sacramento, CA), Dr. James Weigand (US Bureau of Land Management, Sacramento, CA) and Dr. Joel Sholtes (US Bureau of Reclamation Technical Services Center, Denver, CO). The Wang et al. (2017) report has an emphasis on the impact of wildfire on watershed runoff and mobilization of mercury for transport from watersheds to rivers and creeks with particular focus on soil erodibility and wildfire burn severity. Chapter 8 in the Wang et al. (2017) report, which reviews available data in the Putah and Cache Creek watersheds in California - draws heavily on the research of Dr. Charles Alpers and his staff and on work by Ms. Genevieve Sparks, an MS student from Sacramento State University, who submitted an MS thesis entitled "Mercury and methylmercury related to historical mercury mining in three tributaries to Lake Berryessa, Upper Putah Creek watershed, California" completed in spring 2016. Dr. Alpers served on Ms Sparks' thesis committee and is included in the list of

contributors to this report. As will be described later in this chapter – these studies in Putah Creek and Cache Creek, together with State of California-funded research activities in Clear Lake, CA provide the most useful mercury data resource among watersheds in the Central Valley.

Section 6.10 provides a protocol, developed by Dr. Alpers that suggests techniques using direct and indirect parameter estimation techniques for populating model parameter values for those parameters that are not directly measurable. The chapter deals specifically with a strategy for development of mercury mobilization and transport mechanisms in Cache Creek, which has several long-established flow and water quality monitoring stations and provides a scientifically defensible proxy for the hydrogeochemistry of the Putah Creek watershed and mercury transport to Lake Berryessa. This overview describes available mercury and mercury-related data for major agency owned and managed storage facilities and their watersheds in the State of California.

6.2 Folsom Reservoir

Originally authorized in 1944 as a 355,000 acre-feet flood control unit, Folsom Dam (Figure 12) was reauthorized in 1949 as a 1,000,000 acre-feet multiple-purpose facility. Construction of the dam began in October 1948 and was completed in May 1956. The dam regulates flows of the American River, a tributary of the Sacramento River, for irrigation, power, flood control, municipal and industrial use, fish and wildlife, recreation, and other purposes.

Folsom Dam is a concrete gravity dam 340 feet high and 1,400 feet long. The main section is flanked by two earthfill wing dams. The right wing dam is 6,700 feet long and 145 high, and the left wing dam is 2,100 feet long and 145 feet high. In addition to the main section and wing dams, there is one auxiliary dam and eight smaller earthfill dikes. The Mormon Island Auxiliary Dam is in Blue Ravine, it encloses low lying areas along the circumference of Folsom Lake. The earthfill dikes range in height from 10 feet to 100 feet and in length from 740 feet to 2,060 feet.

The auxillary dam is a rolled earthfill structure 4,820 feet long and 110 feet high. The combined length of the main dam, wing dams, auxiliary dam, and dikes is 26,730 feet, or over five miles. The total volume of materials in the dam, wing dams, auxiliary dam, and dikes is 13,970,000 cubic yards, including 1,050,000 cubic yards of concrete in the main section. The spillway in the concrete main section is divided into eight sections, each controlled by a 42- by 50-foot radial gate. The capacity of the spillway is 567,000 cubic feet per second.

Folsom Reservoir has a capacity of 1,010,00 acre-feet with a surface area of 11,450 acres. Folsom Lake is the most popular multi-use year round unit in the California State Park System. Recreation facilities at the 18,000-acre park, which is administered by the California Department of Parks and Recreation, include 50 miles of trails for hiking and horseback riding, picnicking, fishing, swimming, boating, water skiing, and camping.

Figure 12. Folsom Dam and Reservoir

6.2.1 Folsom Reservoir - Data Resource

Folsom Reservoir is located in a watershed that was once mined for gold and other precious metals. Mercury was used extensively during the peak of the mining activity and is still found at high levels within the watershed. Different organizations have undertaken sampling efforts for various reasons over time to measure mercury in each river and reservoir. Since data samples were taken for many reasons the number of samples taken, constituents measured and duration of sampling varies by data source. Limited mercury data has been gathered from samples taken mostly over the past 10-15 years. The data is scientific in nature and intended to provide profile information for the reservoir. Parameters collected for profile studies include: depth, temperature, dissolved oxygen, pH, specific conductance, total dissolved solids, turbidity. Reclamation also performed a sediment survey of the reservoir in 2005. The sediment survey records the bathymetry of the reservoir during that time period along with other useful information related to the operation of the reservoir.

The Reclamation Mid-Pacific Region Planning Division has established an agreement with the Environmental Affairs Environmental Monitoring Branch to sample mercury and related constituents within the reservoir and major inflows of sediment and mercury into the Reservoir. This monitoring effort would depend on independent funding since no cost authority exists within the Environmental Monitoring Branch to collect these data.

The major issue with the existing data resource is the lack of a systematic monitoring in the reservoir and the lack of time series inflow, sediment and mercury species concentration information entering the reservoir. There have been no long-term data collection activities specifically targeting mercury management that might have provided the funds to develop a longer term and more comprehensive data resource suitable for model calibration and validation.

6.3 Oroville Reservoir

Construction on Oroville Dam first began in 1961 and the dedication ceremony was held in 1968. The dam is a zoned earthfill structure contining 80 million cubic yards of material at a height of 770 feet, crest length of 6,920 feet and crest width of 50.6 feet. The dam and associated reservoir were created for flood control, storage, power generation, recreation, wildlife, and water quality. It is currently a part of the California State Water Project, which supplies water for agriculture, industrial and municipal uses to areas south of the reservoir.

Lake Oroville sits in the Feather River watershed of California and serves as the beginning of the State Water Project. Three smaller lakes sit above Lake Oroville in the watershed: Antelope Lake, Frenchman Lake, and Lake Davis which are all used for recreation, municipal and releases for wildlife. Releases from this reservoir convey down the Feather River to its confluence with the Sacramento. Once in the Sacramento, water proceeds to the Sacramento/San Joaquin Delta where it is pumped into the California Aqueduct via the Banks Pumping Plant.

Oroville Reservoir has a capacity of just over 3.5 million acre feet and a surface area of 15,810 acres. The State of California manages recreational uses of the reservoir and surrounding area. Recreational uses for the area include: hiking trails, picnicking, fishing, swimming, boating, water skiing, and camping.

6.3.1 Oroville Reservoir Data Resource

Sampling data for a variety of constituents have been collected over the last 20 years at Oroville Reservoir (Figure 13). Virtually all of these samples were related to Federal Energy Regulatory Commission (FERC) licensing or scientific characterization of reservoir water. Oroville Lake supplies water for wildlife, temperature control, agriculture and drinking water uses. The Feather River hatchery is located just downstream of the reservoir and is dependent on flows from the reservoir to perform hatchery activities.

Metals sampled for scientific studies and regulatory requirements were: arsenic, aluminum, copper, iron, manganese, mercury and lead. The quality and consistency of mercury sampling varies by project and defined sampling need. While there are mercury concentration data available for the reservoir, much of it is not be of the proper quality or duration to be useful for mercury model development.

Figure 13. Oroville Dam and Reservoir[1]

6.4 Lake Berryessa – Putah Creek Watershed

The Putah Creek watershed (Figure 14) can be divided into an upper watershed (above Lake Berryessa) that is largely contained in Napa County and a lower watershed (below Lake Berryessa) that crosses into Yolo and Solano counties. Drainage from the 576-square-mile Putah Creek watershed originates in the Vaca Mountains and smaller watersheds served by Capell Creek, Pope Creek, and Eticuera Creek flows that into Lake Berryessa. These smaller tributaries are emphemeral, contributing flow during the winter and early spring and remaining dry during the summer months. The Lake is the largest in Napa County, approximately 15.5 miles long and 3 miles wide, covering an area of 20,000 acres with a storage capacity of 1,602,000 acre feet. The dam spillway, an unusual "glory hole" design has a maximum capacity of 48,000 cfs. Monticello Dam, owned and operated by the Reclamation provides water supply to farmland in Solano County and generates power to the North Bay region of northern California. The Solano Project water yield of up to 245,000 acre-feet per year is largely managed by Solano County Water Agency and the Solano Irrigation District for use within the County. Water rights holders include agricultural, and industrial users in addition to municipalities with delivery contracts with the Bureau of Reclamation Water stored in Lake Berressa provides supply to the cities of Vacaville, Suisun City, Vallejo, and Fairfield in Solano County, as well as Travis Air Force Base. Lake Berryessa also has a role in controlling potential flooding for both Solano and Yolo Counties. The Solano County Water Agency (SCWA) and its partners work closely

---

[1] Source: http://water.ca.gov/swp/facilities/Oroville/index.cfm

together to manage the water levels at Lake Berryessa. The highest water level ever recorded at the Lake was 446.7 ft. Other water supply contractors use of up to 1,500 acre-feet of project water per year for Napa County farmland around Lake Berryessa. These 25-year contracts were renewed in 2009. The Monticello Dam Powerplant built in 1983 generated up to 12 MW of hydroelectric power. A settlement of water right claims to lower Putah Creek was made in 2000. Known as the Putah Creek Accord, it allowed for scheduled instream flows in lower Putah Creek flowing to the Yolo Bypass. Water rights for the watershed above Monticello Dam were amended in 1996.
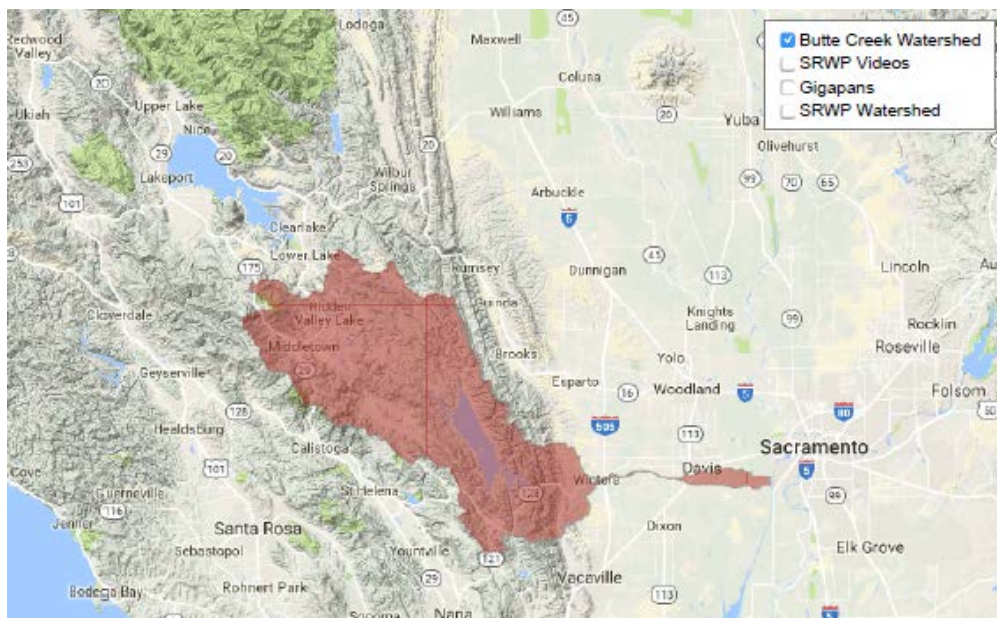
Figure 14. Map of the upper and lower Putah Creek watersheds in Napa, Solano and Yolo Counties

Lake Berryessa (Figure 15) is listed as an impaired waterbody with respect to mercury and appears on the State of California's 303(d) list of impaired waterbodies (SWRCB, 2016). Of 25 reservoirs compared for mercury bioaccumulation in grebes, Lake Berryessa had the highest Hg concentration (Ackerman et al. 2016). The upper Putah Creek watershed is susceptible to wildfire and was recently subjected to the 50,000 acre Valley Fire in summer 2015 (Figure 14). Although wildfire impacts modeling is not the subject of this review and model development enterprise–wildfire is known to increase watershed runoff, sediment erosion and transport of mercury to streams and lakes.

74

Figure 15. Lake Berryessa and "Glory hole" spillway outlet in Monticello Dam[2]

The Lake is monomictic - the water in the lake typically turns once per year usually in the Fall. Turnover occurs when the warmer surface water starts to cool and equilibriates with lower cooler water. The mixing that occurs causes oxygen levels to rise in those parts of the water column where it has been diminished. Lake turnover also tends to scatter fish in the Lake given the monotone temperature and oxygen level conditions. Lake Berryessa is a critical resource for groundwater recharge in lower watershed served by Putah Creek which can become depleted during summer months in dry and critically dry years.

6.4.1 Putah Creek Watershed Data Resource

Available water-quality data for mercury and methylmercury species in Putah Creek are limited to data collected during 2013-14 by Sparks (2016) for her MS thesis research at California State University, Sacramento. Data for unfiltered total mercury THg) and unfiltered methylmercury (MeHg) were collected at six locations (Figure 16) during four sampling events. The six monitoring locations are distributed in the three major tributaries to Lake Berryessa: Pope Creek, Upper Putah Creek and Knoxville-Eticuera Creek (2 locations in each drainage). Suspended

---

[2] Source: Nigel Quinn, public archive.

sediment concentration data are also available for the four sampling events. Field parameters, including water temperature, pH, specific conductance, dissolved oxygen, and turbidity, were measured at the six sampling locations on approximately 65 occasions during 2013-14. This sampling period was during an extended drought and was well below the long-term average for precipitation and stream flow -- there were only two storm events in the two wet seasons combined.

Of the six sampling stations used by Sparks (2016), one is a USGS gaging station with a long term record (USGS gage 11453500, Putah Creek near Guenoc, CA). This station has available discharge data for 1905-06, 1931-76, and 1999-present. Suspended sediment data are available only for 1965. At the other five sampling locations, Sparks (2016) estimated flow with a temporary gage using a pressure transducer.

No water-quality data were available for upper Putah Creek during Water Year 2016. Two water samples were taken by USGS in late February 2017 (Water Year 2017), one at the Guenoc gage on Upper Putah Creek and one on Pope Creek. These samples were taken after the tenth in a series of large storm/runoff events affecting the watershed in 2017, the wettest year on record in the past 100 years in this region. Turbidity in these two water samples was very low (< 10 FNU). Alpers (2017) has suggested that the effects of the extensive 2015 Valley Fire had been largely flushed out by the time that sampling event occurred.
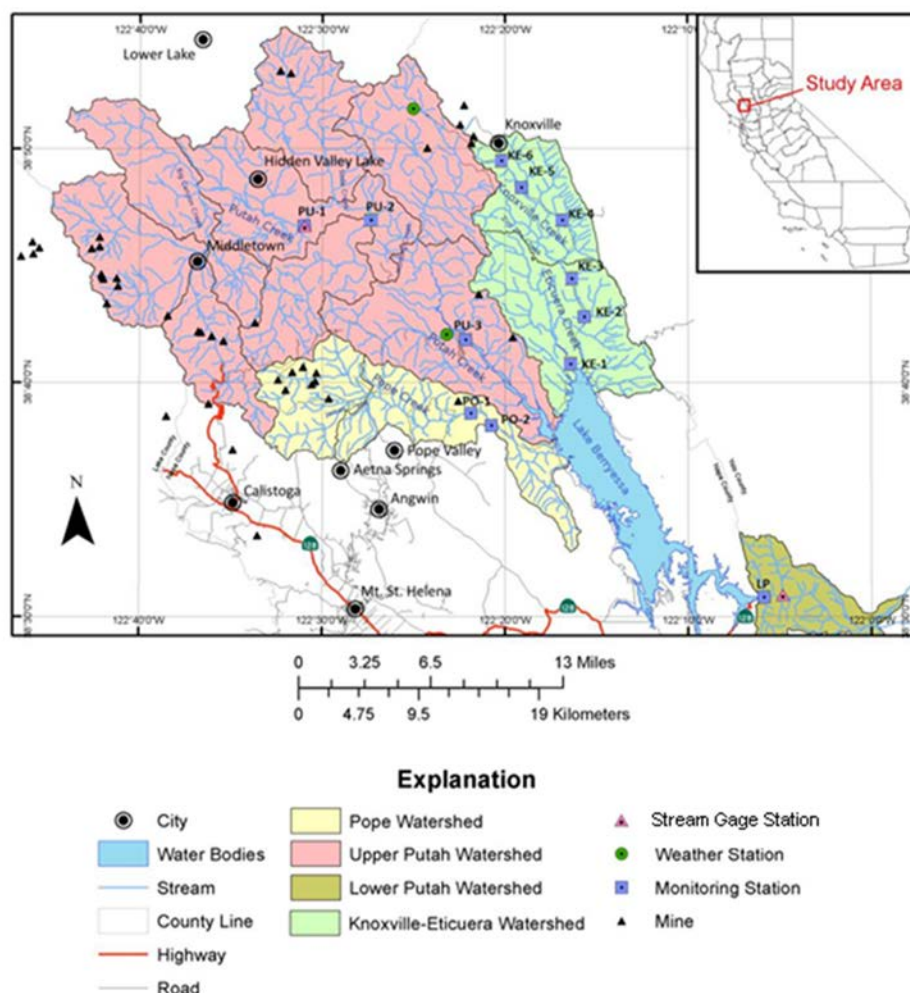
Figure 16. Map of the Upper Putah Creek watershed showing the location of weather stations, monitoring stations and former mercury mines

Historic mining activity in upper Putah Creek

Sparks (2016) developed a detailed history of mining activity in the upper Putah Creek and adjacent watersheds as part of the MS thesis at California State University, Sacramento. This history is useful to gain perspective on both the number of source areas and the potential pollutant load generated in the upper watersheds that has led to current contamination of bed sediments in Lake Berryessa. The following descriptions of mining activity are excerpted from Sparks (2016).

The East Mayacmas Mining District is located in the northwest portions of Napa County and southern Lake County a portion of which lies inside the Upper Putah Creek Watershed boundary and drains into Pope Creek. Several of the mercury mines in this area were major producers, including the former Oat Hill, Great Western, Aetna, and Mirabel Mines (USBM, 1965). The Knoxville Mining District drain into Knoxville-Eticuera Creek and Upper Putah Creek within the Upper Putah Creek Watershed. The major mercury producer within this

mining district was the former Knoxville Mine, cited as California's fifth largest producing mine, with an output of 121,000 flasks of mercury (USBM, 1965) (1 flask of mercury weighs 76 lbs). the Knoxville Mine reached peak production in the 1870's with intermittent production thereafter in response to local demand.

Most of these mines were located in proximity to surface water resources or in areas that could be serviced by appropriated water piped to the mine operation. Runoff or return flows from these operations mobilized productive natural deposits of mercury ore resulting in a release of mercury-bound sediment to the environment. Sparks (2016) was able to locate three mercury-related water and streambed sediment studies, completed within the past twenty years in the upper watersheds and major tributaries to Lake Berryessa and biological food web studies (Littrel, 1991; Slowey, 2007; and Ackerman et al., 2015) that examined conditions with Lake Berryessa and in the Putah Creek watershed below Monticello Dam.
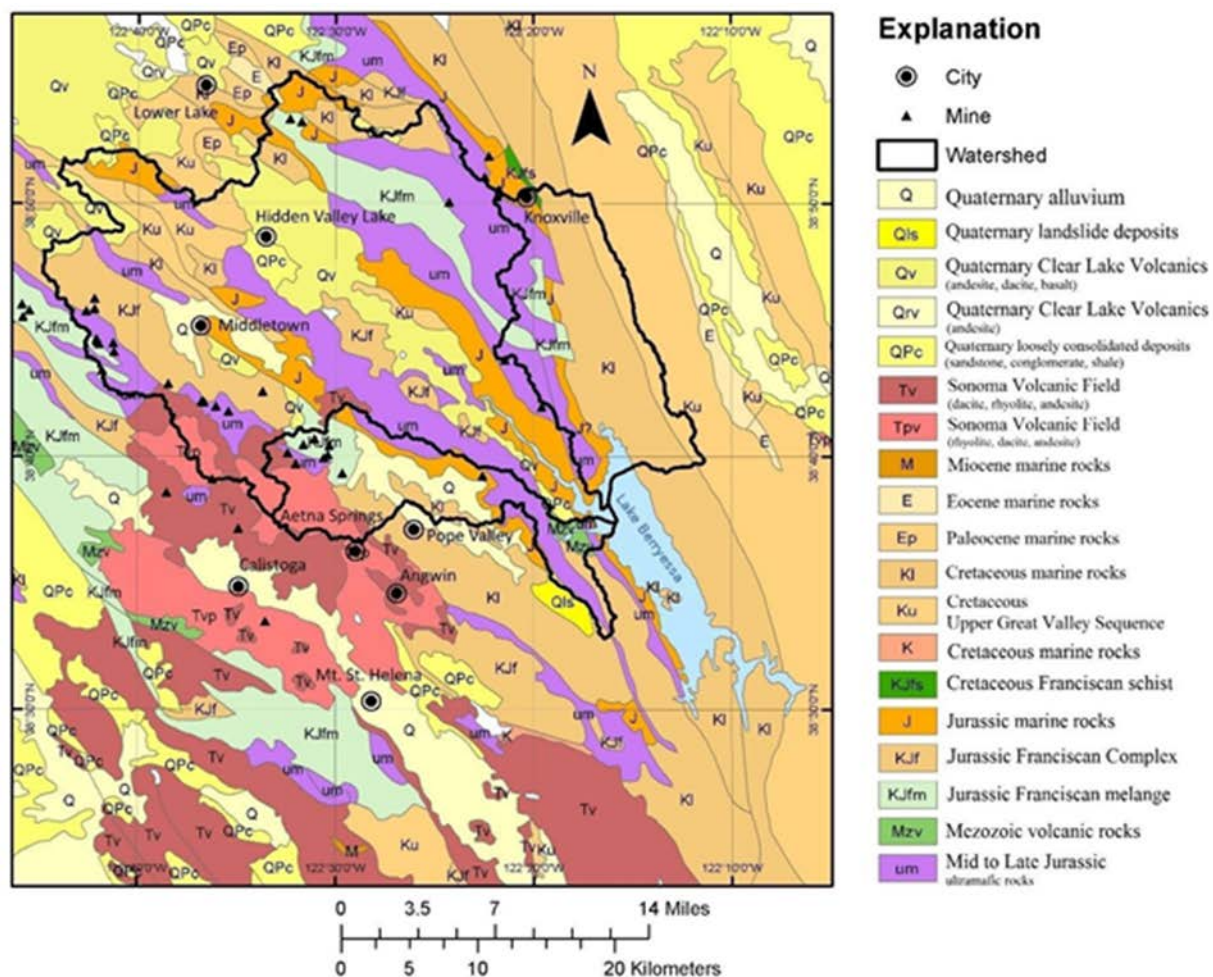
Figure 17. Regional geological map showing Pope Creek, Upper Putah Creek, and Knoxville-Eticuera Creeks subwatersheds and approximate mine locations of mines (Keith Ballard and Genevieve Sparks, 2016).

In the first study Sparks (2016) reports that Wyels (1987) collected sediment samples within Lake Berryessa and in locations within the Upper Putah Creek Watershed.

Sixteen sediment samples were collected along Pope, Upper Putah, and Knoxville-Eticuera Creeks between April 29, 1987 and July 24, 1987. The sediment samples had THg concentrations ranging between <0.02 – 5,600 mg/L dry weight. Sorting the data by tributary resulted in a range of 3.5 to 5,600 mg/L for Pope Creek; 0.31-6.5 mg/L for Upper Putah Creek; and 0.46 mg/l for Eticuera Creek (Wyels, 1987).

The second study by Slowey et al. (2007) reported by Sparks (2016) was conducted in James Creek, a tributary to Pope Creek. This study involved mercury analysis of water, sediment (mine tailings and streambed sediment), and biota from the Oat Hill Mine draining into James Creek. Unfiltered stream water contained THg in the range of 5 to 14 ng/L. More elevated readings in sediment and water were discovered in eroded mine tailings and springs that drained into the creek.

The third study (Rytuba et al. 2003) included stream sediments and water samples collected from Dry Creek a tributary of Upper Putah Creek at Helen, Research and Chicago mine sites . The mercury concentration in the channel sediments at the Research Mine were 3.37 mg/L and 2.99 mg/l and at the Helen Mine site were 0.2 and 90.8 mg/l. During low flow conditions total mercury and MeHg concentrations of water samples in the lower reach of Dry Creek were <3.5 ng/L and <0.09 ng/L, respectively (Rytuba et al. 2003).
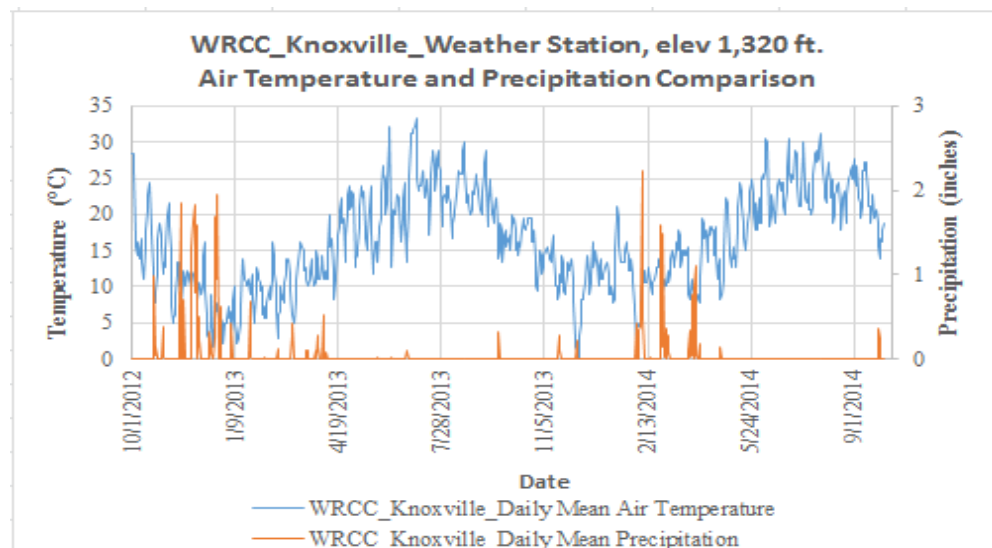
Weather and precipitation data

A weather station located at 1,320 ft elevation, WRCC Knoxville, serves the Upper Putah Creek and Knoxville- Eticuera Creek watersheds. The weather station maintains a reliable record of air temperature, barometric pressure and precipitation (Figure 18a and b). Another weather station, the Mesowest Pope Creek weather station, is situated at a lower altitude (500 ft) in the Pope Creek watershed and measures air temperature and precipitation (Figure 18c).
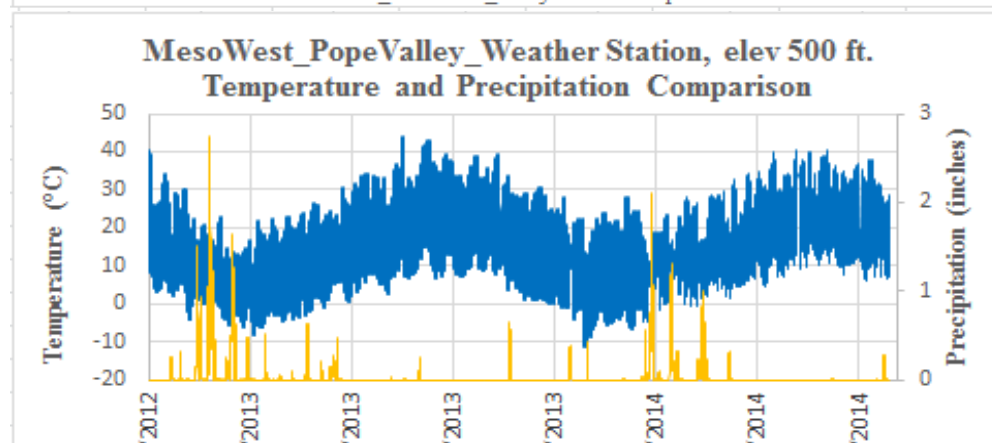
(a)
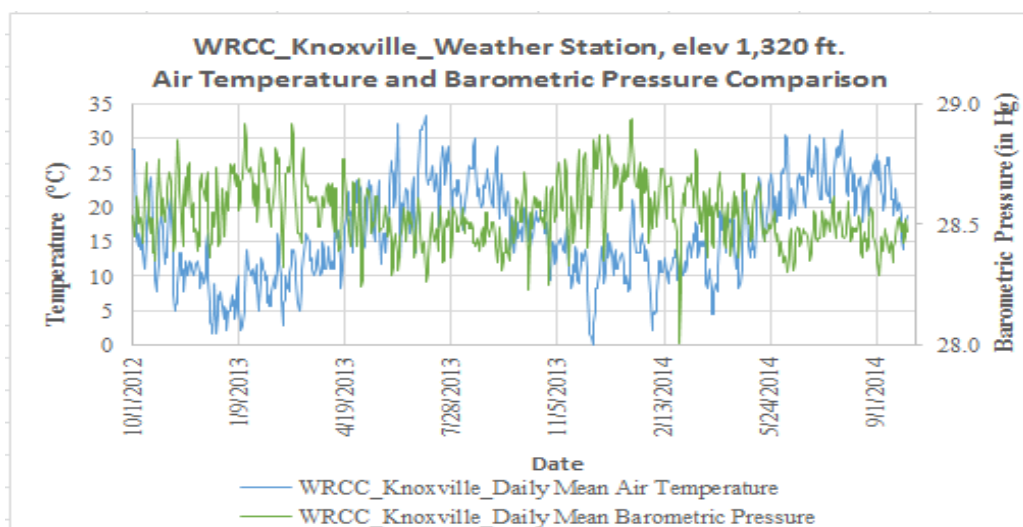
(b)

(c)

Figure 18a,b and c: Air temperature, precipitation, and barometric pressure data from weather stations located along Knoxville-Eticuera Creeks (Western Regional Climate Change, and Pope Creek (MesoWest). Barometric pressure was not available for the Pope Creek weather station (Sparks, 2016)

Research objectives of Sparks (2016) study

The study objectives from Sparks MS thesis were the following: (a) determine if tributaries downstream of historical mercury mining districts and draining to Lake Berryessa were sources of THg and MeHg; (b) identify any correlations in water chemistry among collected water quality parameters; (c) characterize the variability of parameters in upstream and downstream reaches of each tributary; and (d) estimate THg and MeHg loads entering Lake Berryessa from each tributary. The field research ran from October 2012 to September 2014 during which time 55 non-storm and 9 storm events along Pope, Upper Putah, Lower Putah, and Knoxville-Eticuera Creeks and were recorded and the water samples analyzed for pH, alkalinity, hardness, specific conductance, turbidity, dissolved oxygen, temperature, salinity, redox potential, total suspended solids (TSS), and total particulate matter (TPM). Instantaneous mass loading of selected constituents were made using stream discharge measurements, made at the time of sample collection. Water samples were also collected during four non-storm and one storm events for analysis of unfiltered THg, MeHg, TSS, and TPM along each tributary that discharge into Lake Berryessa. A total of one hundred thirty-five streambed sediment samples were collected to determine the spatial variation of THg, organic content, and grain size distribution.
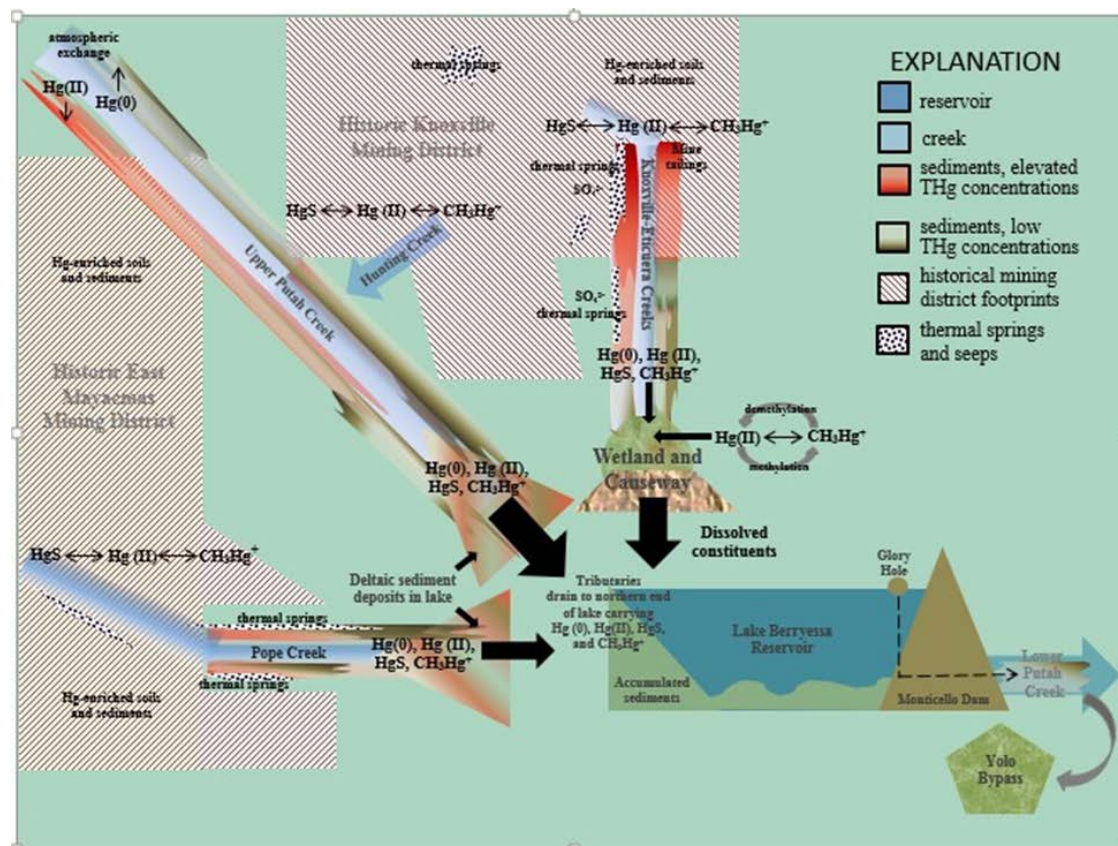

Figure 19. Cartoon depicting the tributaries contributing sediment and mercury loads to Lake Berryessa and mercury source areas in the upper watershed (Sparks, 2016).

As expected the tributary reaches that contained the highest THg in streambed sediment were near or downstream from the historical mercury mines and mercury-enriched ore deposits described above. Sparks (2016) concluded that erosion control would be the most useful remediation tool for decreasing THg and MeHg loads transported to Lake Berryessa. Figure 20 shows the mercury source areas and the mechanism for mercury loading of Lake Berryessa. The extent of the Knoxville and Mayacous mining districts are shown on the map.

Flow estimation and water quality sampling

The USGS stream gage (11453500), located below Highway 29 at monitoring station PU-1, produced the highest stage height (22.7 ft.) and discharge (32,000 cubic feet/second (cfs)) on December 11, 1937. The USGS monitoring site is generally rated as "good" with the exception estimated discharges which are rated "fair". Diversions and groundwater extraction upstream of the monitoring station can affect flow – however there is a requirement to main minimum flow in the channel for ecological purposes (Sparks, 2016). Sparks (2016) was able to obtain discharge measurements from stream gages located along Upper and Lower Putah Creeks, however, for Pope and Knoxville- Eticuera Creeks (monitoring stations PO-1 and KE-2, respectively), she used estimation techniques to determine average flow velocity and discharge using water level, cross-sectional area, wetted perimeter, hydraulic radius, energy gradient and an assumed Manning's n value. Using this technique she was able to estimate average daily discharge for Pope, Upper Putah, and Knoxville-Eticuera Creeks for water years (2012-2013 and 2013-2014). These daily discharge estimates were used in to calculate constituent loading based on data such as total particulate matter (TPM), total suspended solids (TSS), field collected turbidity, or turbidity from laboratory analysis for each tributary. Total particulate matter and turbidity (field) were collected for all samples collected at Pope, Upper Putah, Lower Putah, and Knoxville-Eticuera Creeks whereas total suspended solids and turbidity (laboratory) were collected only at the Pope, Upper Putah, and Knoxville-Eticuera Creeks at a reduced frequency.

Sparks (2016) made estimates of mercury loading using the rLoadestR model (version 3.1.1) to determine an average THg or MeHg concentration-(daily averages). The rLoadestR model uses paired values from the solids datasets and daily average discharge values to calculate a daily load (flux). THg and/or MeHg concentrations are determined from the daily flux results. The model requires a minimum of 15 data points, hence the model could not be applied to TSS and turbidity (laboratory) datasets TPM and daily average discharge datasets were paired to calculate loads for Pope, Upper Putah, Lower Putah and Knoxville-Eticuera Creeks Data collected were found to be more representative for low flow events than high flow events (Sparks, 2016).

Data collected on the project was submitted to the California Environmental Data Exchange Network (CEDEN). Quality control and field collection method protocols described in the State Water Resources Control Board's Surface Water Ambient Monitoring Program (SWAMP SOP) were followed by Sparks for the entire 24-month study period. These protocols are described in (SWRCB, 2015).

Summary of results - Sparks, 2016 study

Figure 20- Figure 34 display the most relevant field data for the HgSM model development excerpted from Sparks (2016).

Figure 20. Photographs of field monitoring locations. (a) looking upstream of monitoring station PO-1 on Pope Creek – this river reach was used in estimation of Manning's "n" channel roughness coefficient, Feb 23, 2013; (b) between monitoring stations KE-3 and KE-2 looking downstream along Knoxville-Eticuera Creek, Dec 12, 2012; (c) looking upstream from terminal end of Pope Creek draining into Lake Berryessa, Nov 17, 2012 (Sparks, 2016).
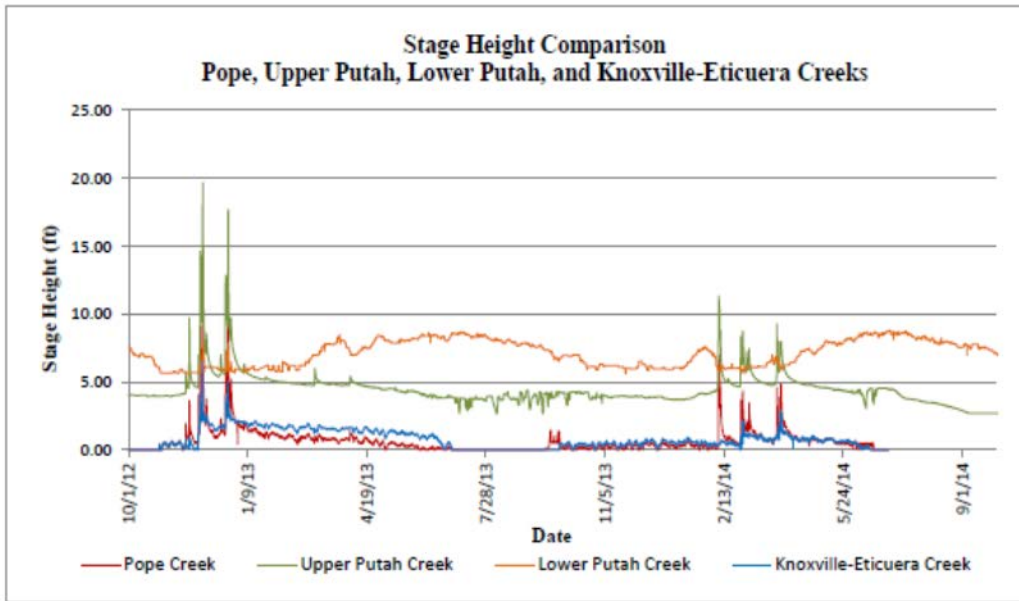
Figure 21. Stage height comparison for Pope, Upper Putah, Lower Putah and Knoxville-Eticuera Creeks - 10/1/12 – 9/30/14 (Sparks, 2016)
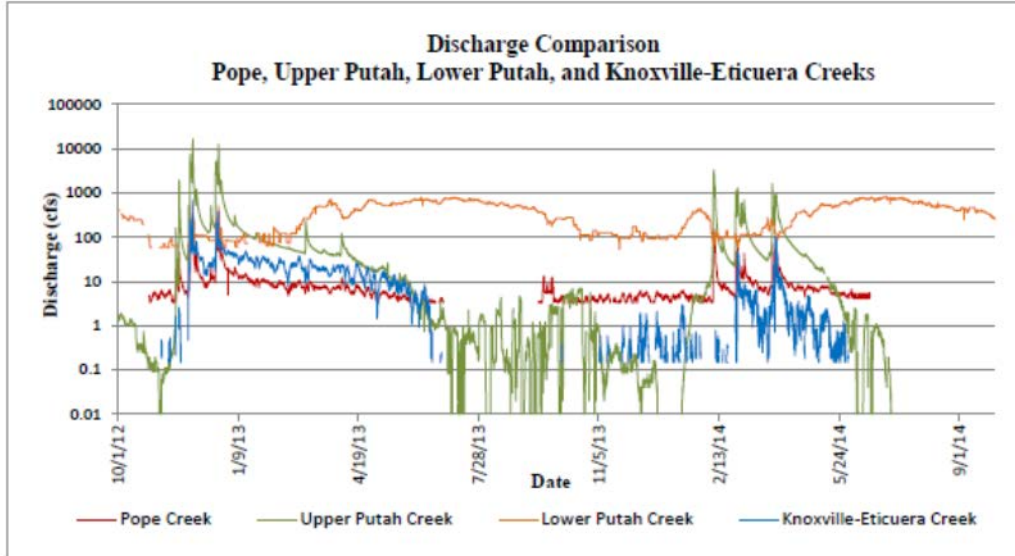

Figure 22. Stream discharge comparison for Pope, Upper Putah, Lower Putah and Knoxville-Eticuera Creeks - 10/1/12 – 9/30/14. Upper tributary streams show similar response to rainfall (Sparks, 2016).
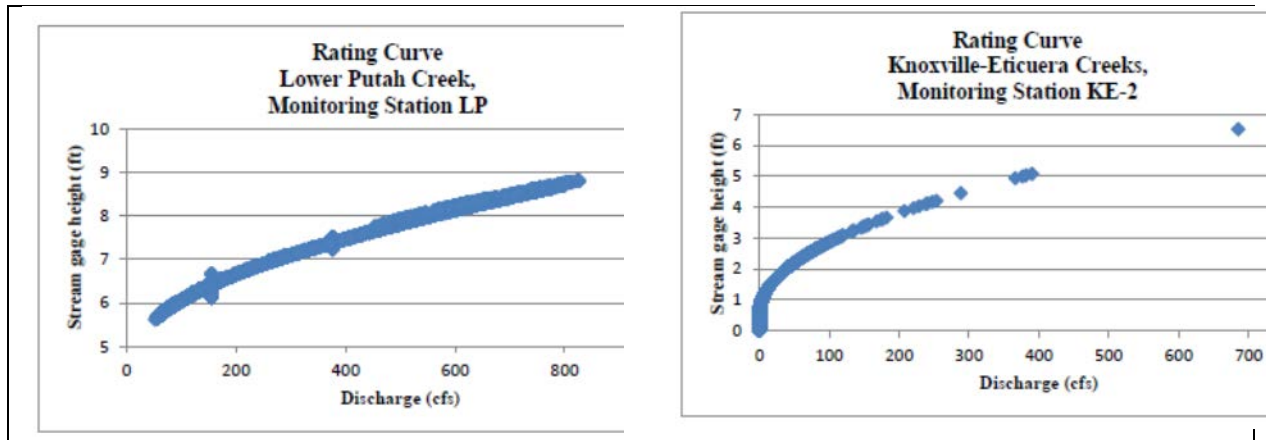
Figure 23. Stage-discharge rating curves for Lower Putah Creek and Knoxville-Eticuera Creek (Sparks, 2016).
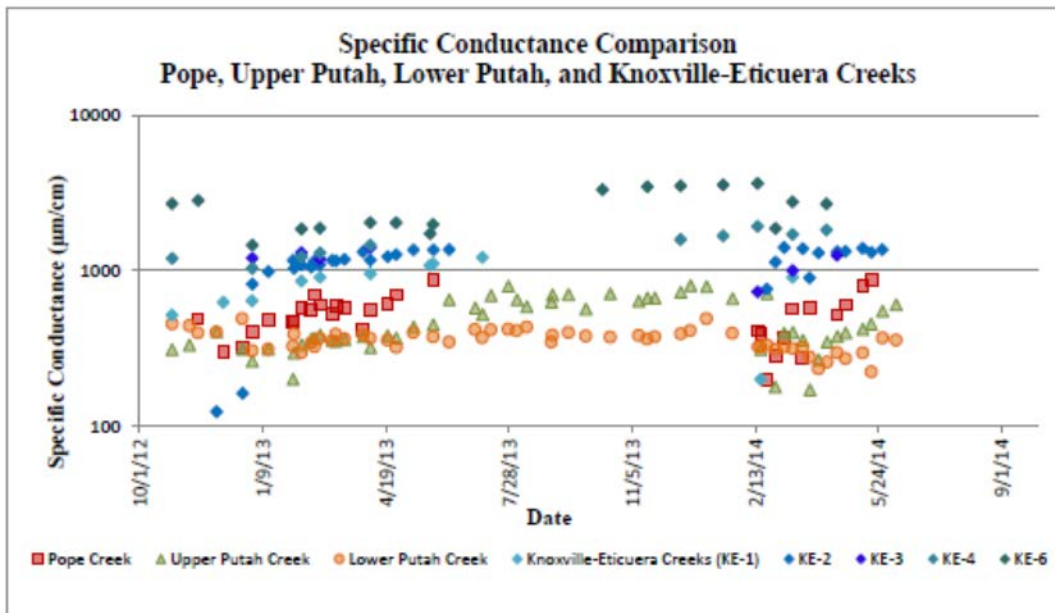

Figure 24. Comparison of specific conductance in water for Pope, Upper Putah, Lower Putah and Knoxville-Eticuera creeks - 10/1/12 – 9/30/14 (Sparks, 2016).
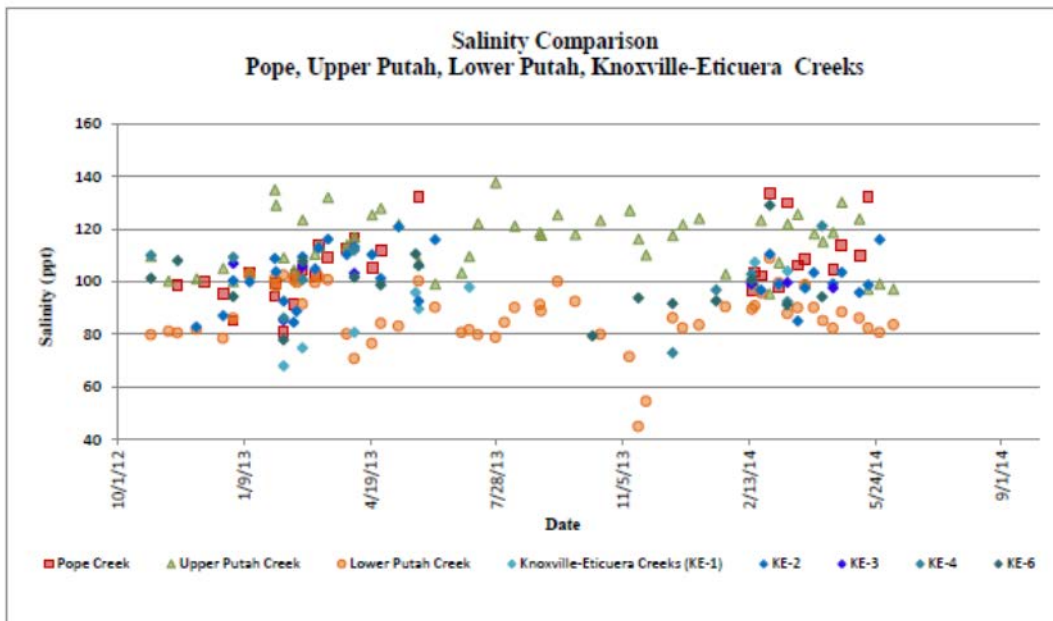
Figure 25. Comparison of turbidity in water for Pope, Upper Putah, Lower
Putah and Knoxville-Eticuera Creeks - 10/1/12 – 9/30/14 (Sparks, 2016).
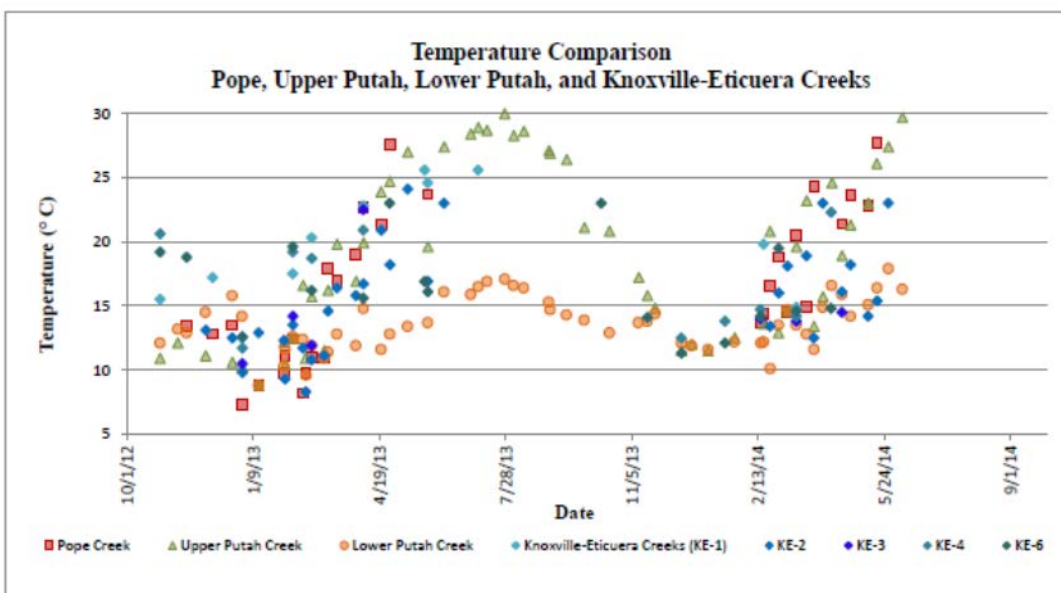

Figure 26. Comparison of water temperature for Pope, Upper Putah, Lower
Putah and Knoxville-Eticuera Creeks - 10/1/12 – 9/30/14 (Sparks, 2016).
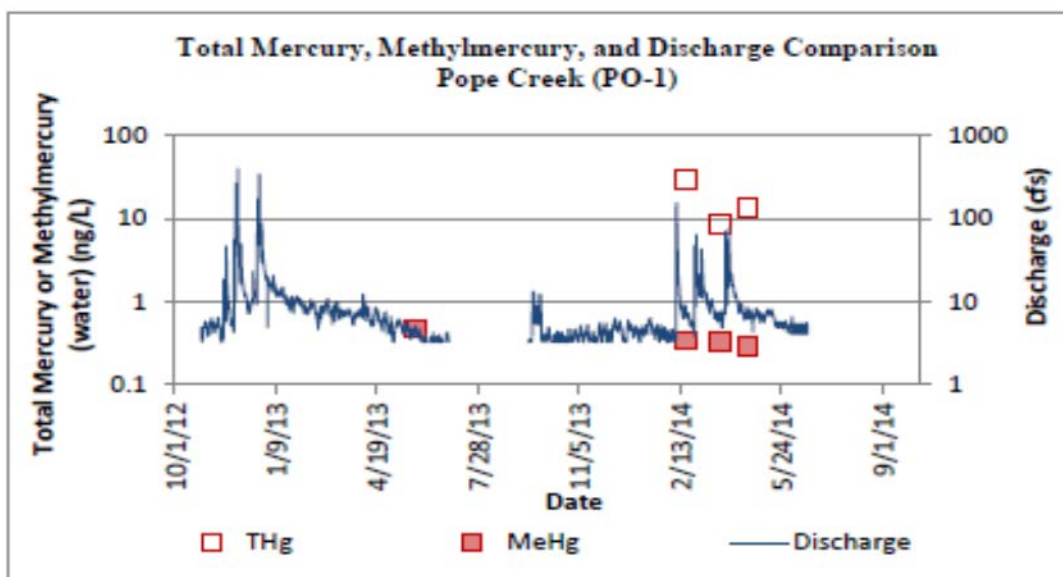
86

Figure 27. Comparison of total mercury, methylmercury and discharge in Pope, Creek - 10/1/12 – 9/30/14 (Sparks, 2016)
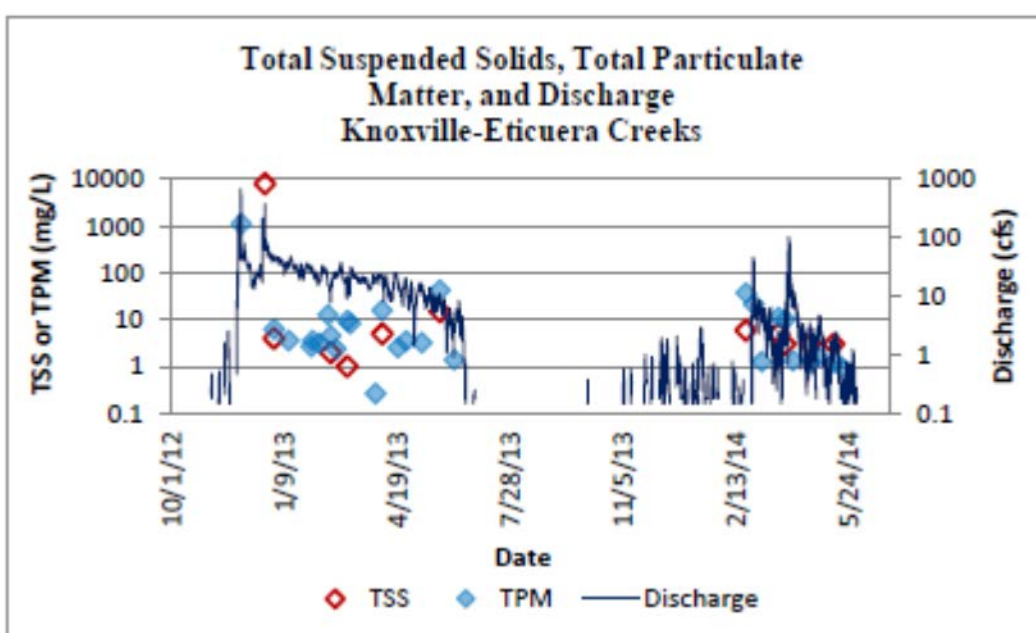

Figure 28. Comparison of total mercury, methylmercury and discharge in Knoxville-Eticuera Creek - 10/1/12 – 9/30/14 (Sparks, 2016)
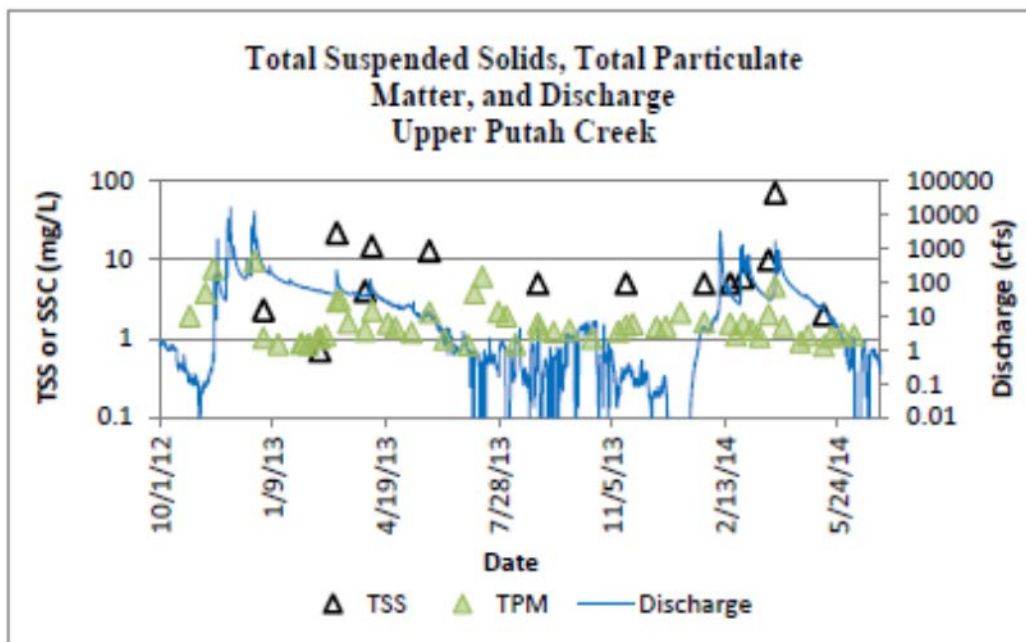
Figure 29. Comparison of total suspended solids, total particulate matter and discharge in Upper Putah Creek - 10/1/12 – 9/30/14 (Sparks, 2016).
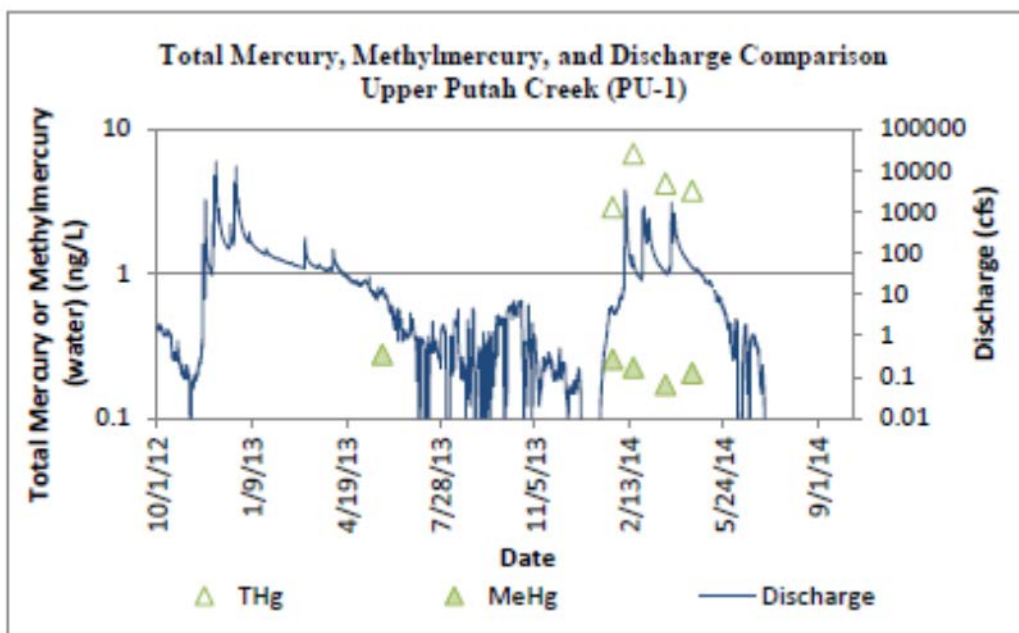
Figure 30. Comparison of total mercury, methylmercury and discharge in Upper Putah Creek - 10/1/12 – 9/30/14 (Sparks, 2016).
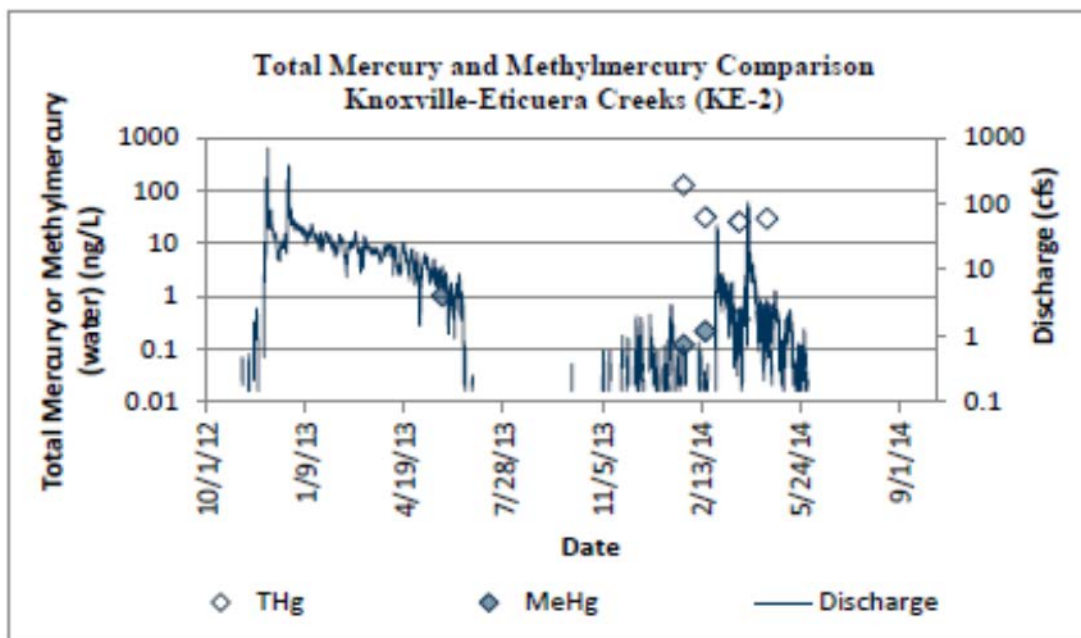
Figure 31. Comparison of total mercury, methylmercury in Knoxville-Eticuera
Creek - 10/1/12 – 9/30/14 (Sparks, 2016).

Figure 32. Comparison of total mercury and average grain size in Pope, Upper
Putah and Knoxville-Eticuera Creeks - 10/1/12 – 9/30/14 (Sparks, 2016).

Figure 33. Comparison of total mercury and average loss-on-ignition in Pope, Upper Putah and Knoxville-Eticuera Creeks - 10/1/12 – 9/30/14 (Sparks, 2016).
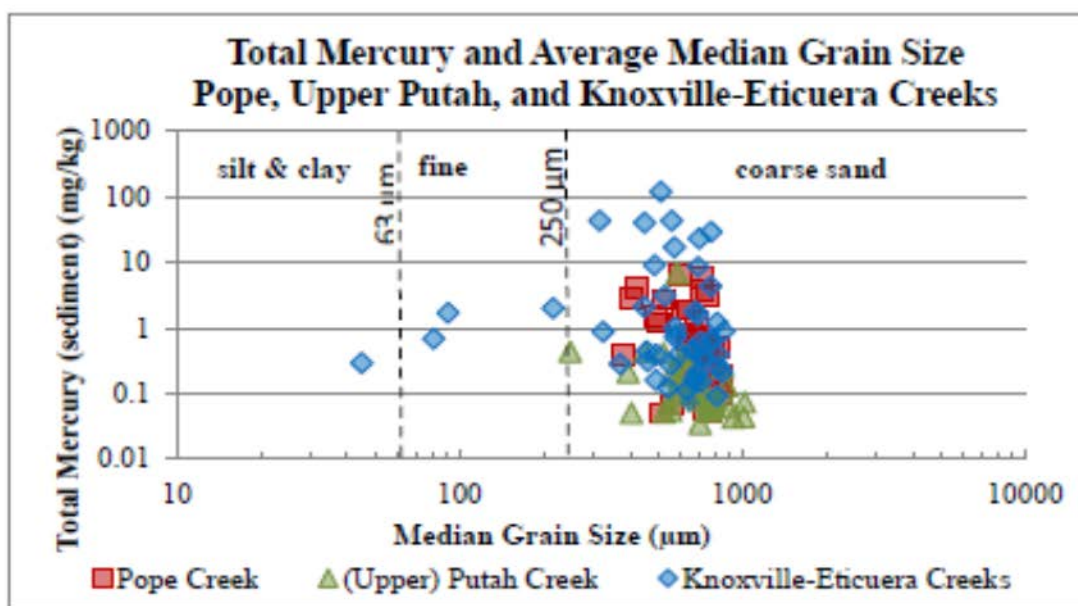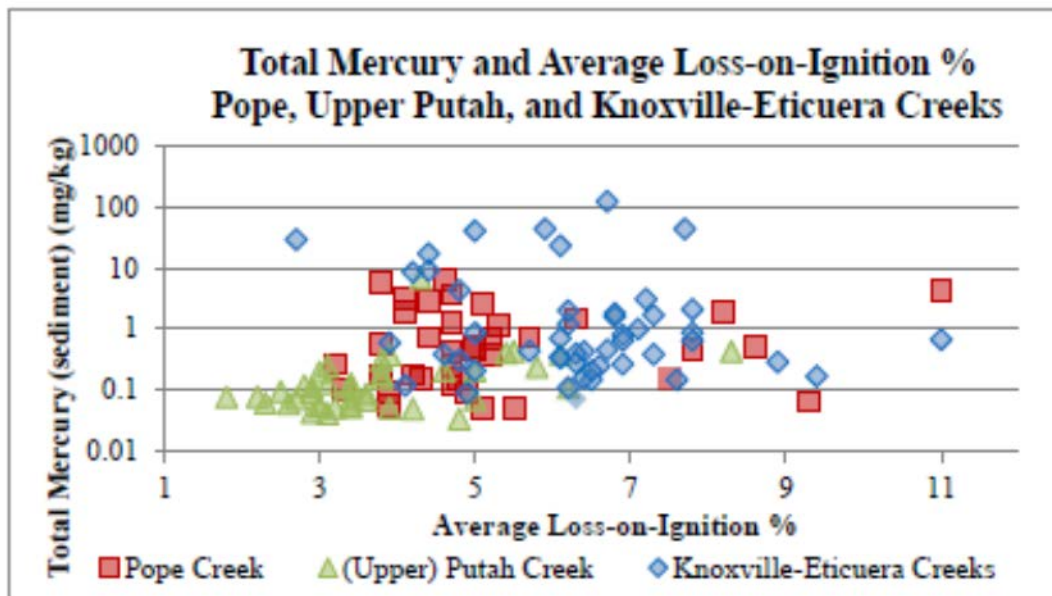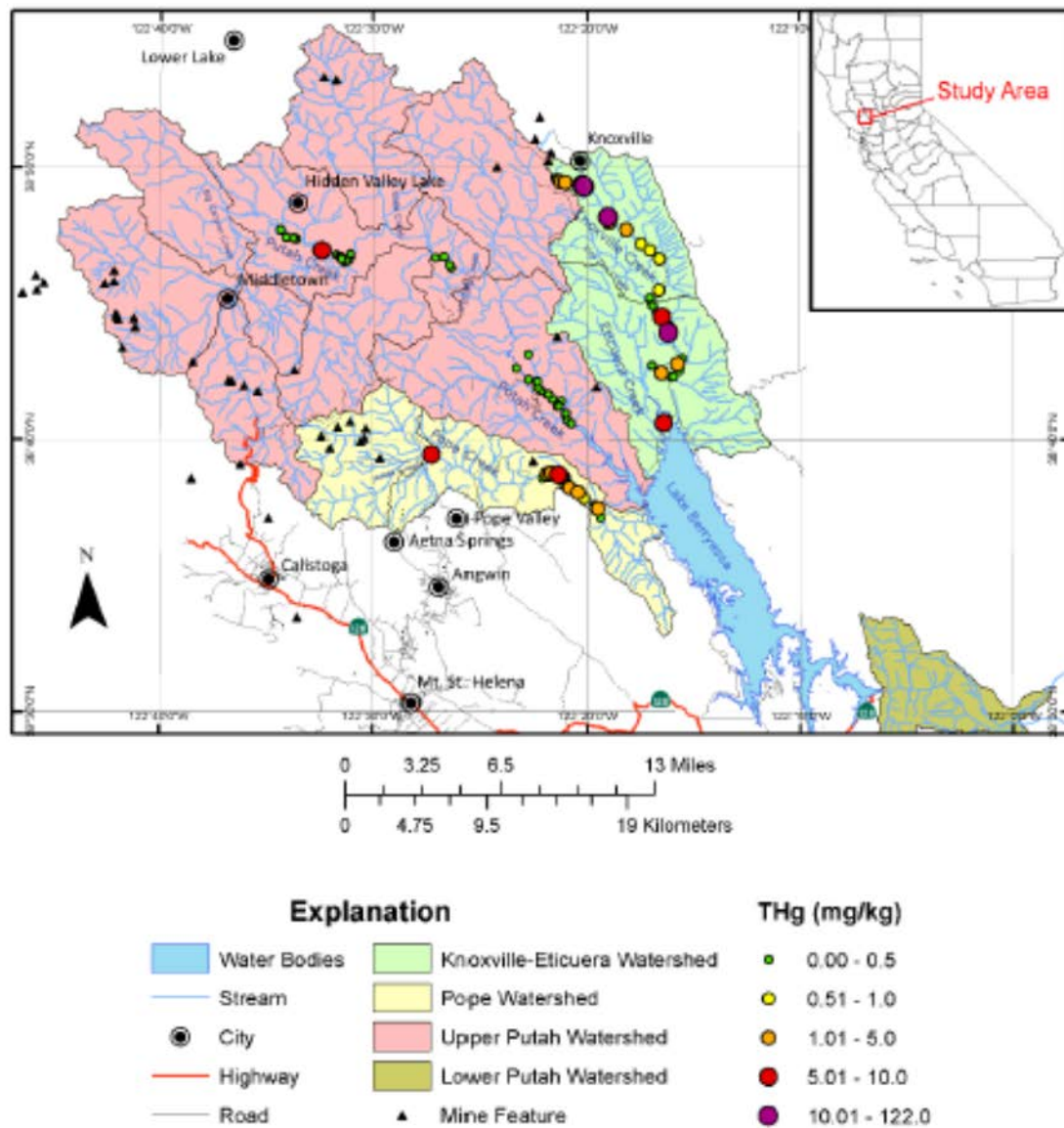
Figure 34. Comparison of total mercury and in Pope, Upper Putah and Knoxville-Eticuera watersheds showing location of the sampling sites upstream of Lake Berryessa - 10/1/12 – 9/30/14 (Sparks, 2016).

6.4.2 Summary of Key Findings - Sparks, 2016

The main objectives of the Sparks (2016) study were to develop a comprehensive baseline dataset for mercury management in the Putah Creek Watershed as the basis for long-term mercury management in Lake Berryessa. The following are key findings of the study, taken directly from Genevieve's MS thesis:

- The study produced a baseline water and sediment dataset for three tributaries draining to Lake Berryessa in the Upper Putah Creek Watershed during two relatively dry water years 2012-2013 and 2013-2014.
- Total mercury in the streams decreased upstream to downstream along each tributary.
- Methylmercury in the streams did not vary significantly by tributary.
- Methylmercury in the streams did not vary upstream to downstream, however the ratio of MeHg/THg increased from upstream to downstream along each tributary.
- Total mercury in sediments varied significantly by tributary and was highest in Knoxville-Eticuera Creeks as expected, given the location of past mining operations in the watershed.
- Total mercury in sediments decreased from upstream to downstream in Upper Putah and Knoxville-Eticuera Creeks.
- The organic content of sediments varied among the tributaries and was highest in Knoxville-Eticuera Creeks. There was a significant correlation between mercury (sediment) and organic content in Upper Putah Creek.
- The variation in THg in sediments was not adequately explained by the median grain size in each streambed.
- Water and sediment THg concentrations varied between subwatersheds and from upstream to downstream along each tributary.
- Although Upper Putah Creek had the lowest average concentrations of THg and MeHg in the water column among the three tributaries it had the highest estimated loads of THg and MeHg because of higher total discharge associated with Upper Putah Creek.

6.4.3 Implications for Mercury Resource Management – Sparks, 2016

Historic mercury mines and mercury-bearing deposits are the main sources of mercury in the three tributaries to Lake Berryessa (Sparks, 2016). The tributary with the highest THg concentrations did not have the highest loads to the reservoir. The highest THg concentrations were observed at Knoxville-Eticuera Creeks, Upper Putah Creek contributed the largest THg loads to the reservoir. The THg load from Pope Creek was the lowest of the three tributaries. Ratios of MeHg/THg were highest in Upper Putah Creek which had the lowest THg (water and sediment) concentrations of the three tributaries. Ratios were moderate for Pope Creek and lowest for Knoxville-Eticuera Creeks. The ratios may correlate

with the stream gradients; a shallow stream gradient provides greater methylation opportunities in the ponded reaches. Methylmercury generated in the tributaries eventually reaches the reservoir, concentrating to methylmercury concentrations in the reservoir and its food web that were not characterized as part of this study.

Additional mercury load and cycling studies will practical opportunities be identified to reduce MeHg exposure to humans and wildlife. With source identification and characterization, the fate and transport of mercury and methylmercury and their exposure pathways can be better understood so that so that exposure can be minimized.

These data will be of significant utility to Reclamation for the calibration and validation of the HgSM model given the differences in mercury transport observed in each tributary and the comprehensive water quality data collected simultaneously at each monitoring location. As previously mentioned, Genevieve Sparks made provision to follow SWAMP Quality Assurance and data provisioning guidelines and has supplied the database to DWR's CEDEN web portal. Ms Sparks has indicated an interest in pursuing a PhD at UC Merced extending her work in the Putah Creek watershed with a greater emphasis on mercury modeling.

6.5 Cache Creek Watershed

The Cache Creek watershed is located immediately north of the Putah Creek watershed in Lake, Colusa and Yolo Counties. Cache Creek provides the sole drainage outlet for Clear Lake, the largest natural lake entirely within California, as well as the Indian Valley Reservoir. These waterbodies are managed by the Yolo County Flood Control and Water Conservation District. Another managed feature in the Cache Creek watershed is the Cache Creek Settling Basin (CCSB), located at the mouth of Cache Creek where it flows into the Yolo Bypass, a flood conveyance that protects the City of Sacramento. The CCSB was built by the U.S. Army Corps of Engineers in 1937, with improvements in 1993, to trap sediment so that it does not accumulate in the Yolo Bypass.
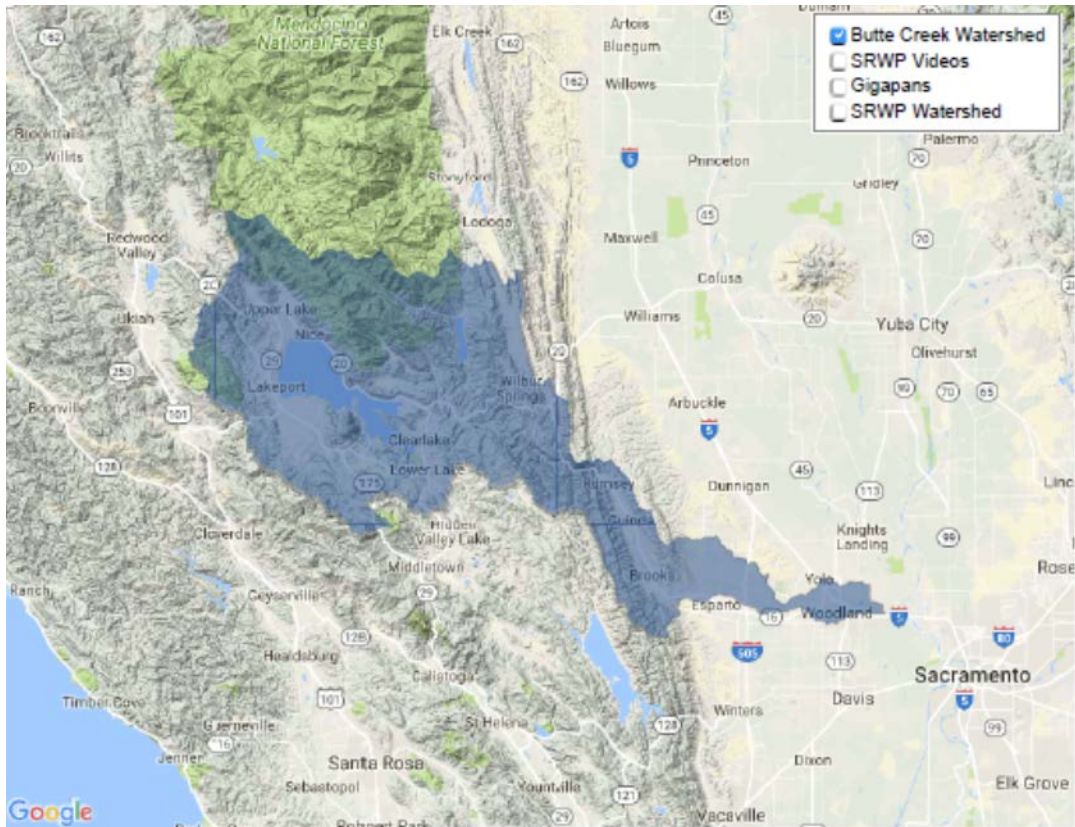
Figure 35. Map of Putah Creek (Butte Creek on map) and Cache Creek watersheds.

6.5.1 Cache Creek Watershed Data Resource

The California Regional Water Quality Control Board (RWQCB) monitored water quality, including mercury and methylmercury species, at several locations in the Cache Creek watershed during 1996-2002 as part of a Total Maximum Daily Load (TMDL) analysis (Cooke et al., 2004). All samples were analyzed for unfiltered THg, unfiltered MeHg, and suspended sediment concentration. Some samples were also analyzed for filtered THg and filtered MeHg. The RWQCB monitoring locations included Cache Creek at Rumsey, Cache Creek at Yolo, and the outflow of the Cache Creek Settling Basin (CCSB) (Figure 36).

Figure 2-1. Map of the Cache Creek watershed. The watershed area is defined as the drainage basin contributing runoff to a point at the USGS stream gaging station at Yolo. The downstream terminus at the Cache Creek Settling Basin is just beyond the extent of the map.

Figure 36. Map showing locations of stream gages in the Cache Creek watershed (from Kamman Hydrology & Engineering)

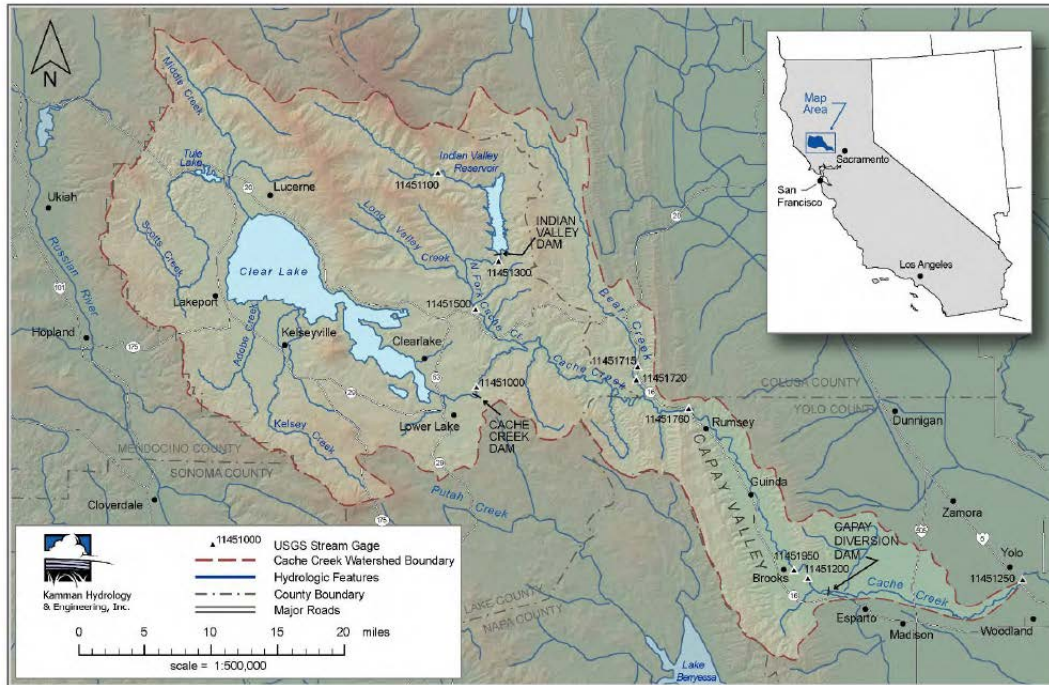The USGS monitored water quality at several sites in the Cache Creek watershed during 2000-01 as part of a study funded by CALFED focused on mercury sources and transport (Domagalski et al., 2003, 2004a, 2004b). Monitoring locations included Cache Creek at Rumsey, Cache Creek at Yolo, and several tributaries to Cache Creek: North Fork Cache Creek, Sulphur Creek, Bear Creek, and Harley Gulch (Figure 37). Forms of mercury analyzed by USGS in this period included unfiltered and filtered THg, and unfiltered and filtered MeHg. In addition, trace metals and major cations and anions were analyzed in filtered water samples, which provided information on water sources and the non-conservative nature of mercury transport (Domagalski et al., 2004b).

In Water Year 2010, in cooperation with the California Department of Water Resources (DWR), the USGS began a comprehensive study of mercury and suspended sediment transport in the lower Cache Creek watershed, an activity that is scheduled to remain ongoing through Water Year 2019. The main focus of the study is monitoring is the inflow and outflows of the CCSB and computing loads and trap efficiency of the basin for various constituents. In Water Year 2015 the USGS began water-quality monitoring at Rumsey (USGS gaging station 11451800, Cache Creek at Rumsey, CA). USGS monitoring at Rumsey continued in Water Years 2016-17, and additional monitoring is planned for Water Years 2018-19. Constituents analyzed in the ongoing mercury transport project include filtered THg, filtered MeHg, particulate THg, particulate MeHg, and particulate reactive mercury (II) (RHg(II)), a precursor to methylmercury (Alpers et al. 2008). In addition, ancillary constituents analyzed include major

Cache Creek at Rumsey, WY2015
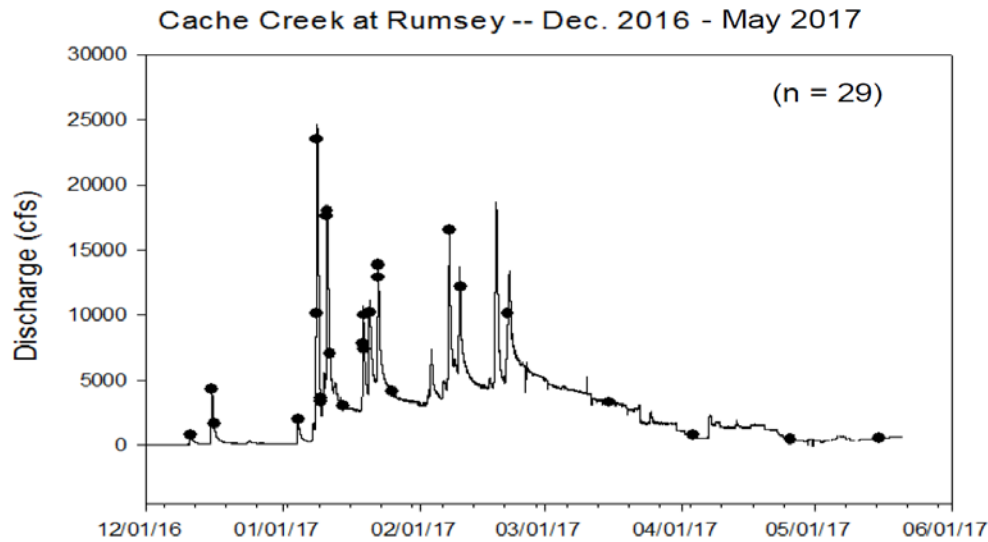
Cache Creek at Rumsey - WY 2016

96
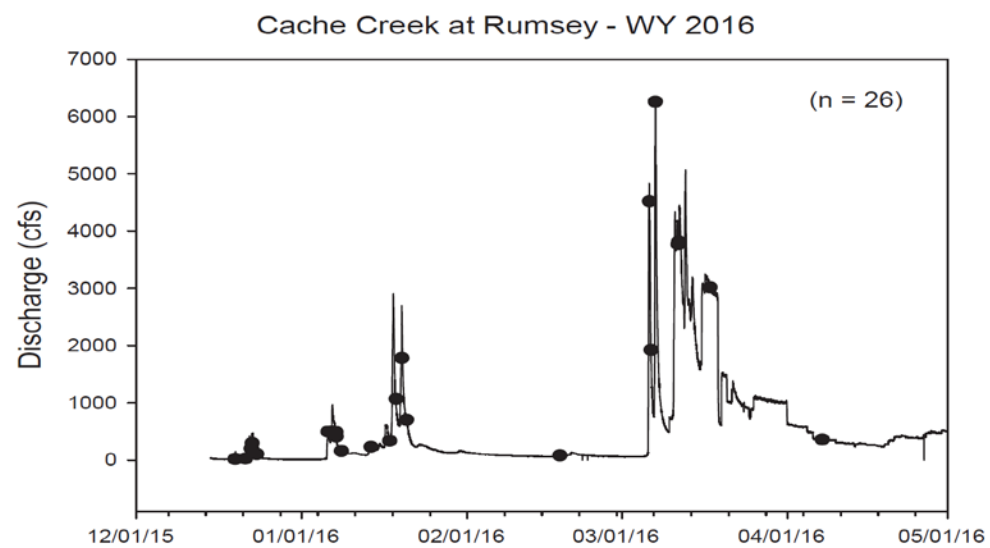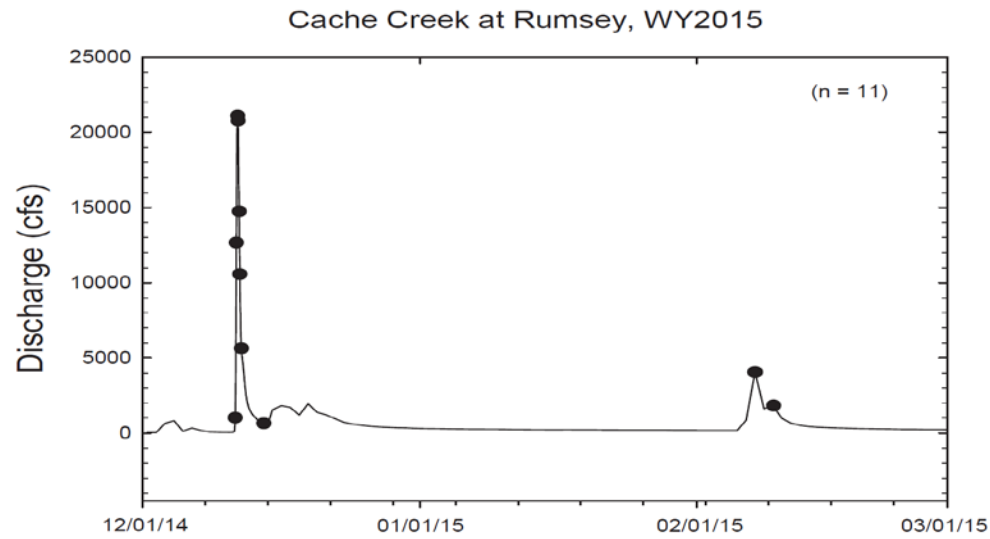
Figure 37. Time-series plots showing discharge at Cache Creek at Rumsey
gaging station (USGS station 11451800) and timing of water-quality (mercury)
samples taken by USGS during Water Years 2015-17.

anionsand alkalinity, dissolved organic carbon, carbon quality (absorption-fluorescence
spectra), and suspended sediment concentration. In addition to traditional suspended
sediment concentration with sand break (% < 0.063 mm), starting in Water Year 2015, the
detailed grain-size distribution of suspended sediment (1/4-phi intervals) was determined
using a laser-scattering analyzer (Beckman Coulter counter). The number of water samples
for which mercury data are available at sites within the Cache Creek watershed for Water
Years 2010-17 are shown in Table 10. Hydrographs for the Rumsey gage are shown in
Figure 37 along with symbols indicating the timing of USGS water-quality (mercury)
samples.

At Rumsey, the 11 water samples collected during Water Year 2015 (pre-fire) represent two
storm events including a significant runoff event in December 2014 (peak > 20,000 cfs).
During that Water Year, stream gaging at the Rumsey site was the responsibility of DWR.
On October 1, 2015 (start of Water Year 2016) the USGS took over responsibility for
operating and maintaining the gaging station at Rumsey. The USGS determined that the
Water Year 2015 discharge record at Rumsey is insufficiently accurate for detailed sediment
load calculations because of uncertainty with the rating curve. However, it should be
possible to estimate discharge values for WY2015 from the rating curve developed by USGS
during Water Year 2016.

During Water Year 2016 water-quality samples were taken at Rumsey for several small
storm events during December 2015 and January 2016, and then two larger storm events.
Because an autosampler was installed Rumsey in 2015, there is excellent

Table 12. Number of USGS water-quality (mercury) samples at sites in the Cache Creek watershed, Water Years 2010-17.

	PRE-FIRE						POST-FIRE			
	Water Year									
	2010	2011	2012	2013	2014	2015	2016	2017		Totals
Rumsey	ns	ns	ns	ns	ns	11	26	29		66
Yolo	ns	ns	ns	ns	ns	ns	ns	20		20
Road 102	16	20	19	18	5	13	17	20		128
Spillway - S	6	11	0	5	0	7	7	16		52
Spillway - N	ns	ns	ns	5	0	7	6	16		34
CCSB Outlet	15	15	8	10	0	6	16	13		83
Total	37	46	27	38	5	44	72	114		383

[NOTE: the sample counts in the above table do not include samples taken by the USGS Field Offices for suspended sediment only; ns, not sampled.]

coverage of the hydrography (rising limb, peak, and falling limb) for most storm events. Typically the autosampler was programmed to take a sample for suspended sediment concentration every 4 hours. In addition to the water-quality samples listed in Table 12, approximately 125 sampling events were carried out only for suspended sediment by the USGS during Water Years 2015-17, for the purpose of computing daily sediment loads. This level of sampling effort is scheduled to continue during Water Years 2018-19.

The stream gage at Rumsey also has continuous (15-minute) data available for turbidity and water temperature during the wet seasons of Water Years 2015-17 (typically December through April of each Water Year). No continuous data other than discharge (flow) are available for the USGS stream gage on Cache Creek at Yolo (station 11452500).

6.5.2 Defining the Area for Model Development

It is advantageous to minimize the area for the development and testing of the model, to reduce the need for computation. Using gaging stations at Clear Lake, Indian Valley Reservoir, and Bear Creek as upper boundary conditions to the model area, and the gaging station at Rumsey as a lower boundary / calibration point, will reduce the modeled area to approximately 200 square kilometers. Water-quality data are available at the three upper boundary sites for four sampling events during 2000-2001 (Domagalski et al., 2003, 2004a) and some data are available for the Bear Creek site during Water Years 2015-17 (J. Rytuba, USGS, written communication, 2017).

6.5.3 Conclusions

Based on available data, the Cache Creek Watershed appears to be an excellent place to calibrate and test the mercury mobility and transport model. The Cache Creek does not have a reservoir managed by the Bureau of Reclamation, however once the HgSM model is calibrated in the Upper Putah Creek Watershed it could be further tested with data derived from Cache Creek

7. Data Synthesis Protocols

7.1 Introduction

The successful development and application of a mercury transport simulation model depends on having information about the concentrations of Hg and MeHg both as suspended particulates and in the dissolved phase. Water-quality data including concentrations of these Hg and MeHg species are rarely available at selected river and reservoir sites over a range of flow conditions for direct model calibration (Alpers, 2017). Given this dearth of data - proxy relationships for Hg and MeHg concentrations may be used for indirect calibration using watershed properties and other available geospatial data derived from proximate watersheds with like characteristics (Alpers, 2017). Proxy relationships can be derived from the published literature and from available data in the target watersheds. Proxy relationships involving inorganic Hg are typically more robust than those involving MeHg. MeHg concentrations vary temporally and spatially within watersheds and the important factors controlling MeHg variability may not be well known in all environments.

This section was derived from Alpers, 2017 – included in a companion report entitled: "Integrated modeling of mercury transformation and transport in watersheds subject to wildfire (Draft)" Wang et al., (2017).

7.1.1 Ontology of terms

DOC – Dissolved organic carbon (mg/L)
THg, – Total mercury
THg-f, – Total mercury, filtered
THg-p, – Total mercury, particulate
THg-p,v – Total mercury, particulate, volumetric (ng/L)
THg-p,g – Total mercury, particulate, gravimetric (ng/g)
MeHg – Methylmercury
MeHg-f – Methylmercury, filtered
MeHg-p – Methylmercury, particulate
MeHg-p,v – Methylmercury, particulate, volumetric (ng/L)
MeHg-p,g – Methylmercury, particulate, gravimetric (ng/g)
K_d – Distribution coefficient, equal to concentration in solid divided by concentration in liquid. (L/kg)
K_dTHg – equals 1000*[THg-p,g]/[THg-f]
K_dMeHg – equals 1000*[MeHg-p,g]/[MeHg,f]
SSC – Suspended sediment concentration (mg/L); organics removed by treatment with hydrogen peroxide
$SUVA_{254}$ – Specific Ultraviolet Absorbance at 254 mm (absorbance at 254 mm divided by DOC)
TSS – Total suspended sediment (mg/L); includes organics

7.2 Use of correlation to directly estimate mercury constituent concentrations

First-order relationships between flow and concentrations of various mercury species in particulate and dissolved form can be derived for the preliminary model based on available field data (Alpers, 2017).

7.2.1 Particulate Total Mercury

The relationship between suspended sediment concentration (SSC) (and/or total suspended sediment, TSS) and volumetric particulate total mercury concentration (THg-p,v) at a given sampling station typically shows a strong positive correlation.

The gravimetric concentration of THg on suspended particulates (THg-p,g) is commonly expressed in ng/g, dry weight). If THg-p,g can be assumed constant at a given location for a given period, then concentrations and loads of suspended sediment predicted by the model can be used to compute concentrations and loads of THg-p for that period.

Existing models such as LOADEST (Runkel et al. 2004) and GCLAS (Koltun et al., 2006) use the relationships between flow, concentration, and in some cases, day of the year (seasonality), to develop predictions of concentration so that loads can be computed.

7.2.2 Filtered Total Mercury

It is well established in the literature that filtered total mercury (THg-f) concentration in streams tends to correlate well with dissolved organic carbon (DOC) concentration (e.g., Dittman and Driscoll, 2009; Dittman et al., 2010). The correlation between THg-f and DOC could be useful in predicting THg-f if a model that predicts DOC were available. The concentration of DOC in streams may respond differently than THg-f in some environments. For example, Bushey et al. (2008) found a counter-clockwise hysteresis relationship for DOC vs. flow and clockwise hysteresis relationship for THg-F and flow. This may relate to these constituents being generated from different parts of the soil profile or different source areas. The model of Schelker et al. (2011) simulates transport of DOC and THg-f in a watershed in the Adirondack Mountains (New York) where snowmelt is responsible for about half of the annual THg load.

7.2.3 Particulate Methylmercury

The volumetric concentration of particulate methlylmercury in water (MeHg-p,v) correlates with the concentration suspended sediment (SSC or TSS) to the extent that the gravimetric concentration of particulate methylmercury on suspended particles (MeHg-p,g) is constant.

Many factors may influence methylmercury concentrations in water and suspended sediment, including climate, temperature, pH, salinity, carbon quality, oxidation-reduction potential,

forms of sulfur and iron, land use (e.g. agricultural vs. non-agricultural), and others (Alpers et al., 2008). Therefore it is difficult to pinpoint definitive explanations for the temporal and spatial variations in MeHg-p,g observed at different sites in Cache Creek.

7.2.4 Filtered Methylmercury

Relationships between fMeHg and DOC vary widely among watersheds. For example, of the 8 steam sites evaluated by the USGS NAWQA program (Brigham et al., 2009) in Oregon, Wisconsin, and Florida (Figure 12), 3 have strong positive correlations between MeHg-f and DOC ($R^2 > 0.4$, $p < 0.0001$), 1 has a weak but significant positive correlations ($0.2 < R^2 < 0.4$, $p < 0.05$) and 4 have no significant correlation ($R^2 < 0.2$, $p > 0.05$). Slopes of the regression lines also differ markedly between sites. The relationships may be tied to watershed characteristics including wetland coverage, forest cover, hillslopes, and other geospatial data that typically are available for modeling purposes.

There is also a wide variety of responses with regard to correlations between MeHg-f and discharge. For the same 8 stream sites in Figure 12, 2 have strong positive correlations ($R2 > 0.5$, $p < 0.0001$), 2 have weak positive correlations ($0.1 < R^2 < 0.4$, $p < 0.05$), 1 has a weak negative correlation ($R^2 = 0.34$, $p < 0.0001$), and 2 have no significant correlation ($R^2 < 0.2$, $p, > 0.05$).

7.3 Distribution Coefficients

A distribution coefficient (K_d) is defined as the ratio of concentration of the same constituent in a solid to that in an aqueous phase. For total mercury in water, K_{dTHg} is equal to $1000*[THg\text{-}p,g]/[THg\text{-}f]$, where [ ] indicates concentration. The units for K_d's are $1000*[ng/g]/[ng/L]$, or L/kg.

Brigham et al. (2009) showed that Kd's for THg and MeHg vary as a function of [DOC] and [SS] (Figure 16). This relationship could be used for modeling purposes. For example, if one has a prediction of THg-p,g and either DOC or SS, one could use the relationships in Figure 16 to generate a prediction for THg-f. Similarly, if one has a prediction of MeHg-p,g and either DOC or SS, one could generate a prediction for MeHg-f. The uncertainty of such predictions could be evaluated using data for the Cache Creek watershed in relation to the data in Figure 16 from OR, WI, and FL.

7.4 Scatter in Particulate Concentration Relationship with Flow

There are two main causes for scatter in the relationship between suspended sediment and flow: (1) the hysteresis effect (systematically different concentration on rising limb vs.

falling limb for the same flow), and (2) seasonal variations in suspended sediment concentration "rating curves."

7.5 Hysteresis Effects

7.5.1 General description

Three forms of hysteretic behavior have been described in the literature: clockwise, counter-clockwise, and figure-8-shaped. The convention is to plot concentration on the vertical axis and flow on the horizontal axis, so a clockwise hysteresis loop corresponds to higher concentration on the rising limb of the hydrograph compared to the falling limb, for the same discharge.

According to Seeger et al. (2004), "Clockwise loops are generated under 'normal' stormflow conditions, when the catchment is very moist and runoff generation and sediment supply is limited to areas next to the channel (i.e., sediments are removed, transported and depleted rapidly)."

Counter-clockwise loops "occur under very high moisture and high antecedent rainfall conditions;" "flood propagation occurs as a kinematic wave" and "sediment sources are incorporated all over the catchment," some with time-delay in reaching the monitoring location (Seeger et al., 2004).

7.5.2 Seasonal Rating Curves

In some watersheds, the relationship between suspended sediment (and particle-bound constituents such as THg-p,v) shifts seasonally. During summer and fall "first flush" conditions, there are relatively high suspended sediment concentrations for a given discharge compared to the main winter storms. Suspended sediment concentrations during spring (during snowmelt conditions) are often lower than the winter storms, for a given discharge. The conditions leading to the "first flush" effect, related to higher sediment availability after an extended dry season, may apply to the Cache Creek and Putah Creek watersheds. Thus, a possible second-order refinement to the model could be seasonal rating curves for sediment and particulate-bound constituents.

7.6 Variations of Mercury Concentration with Particle Size

Unpublished USGS data from Cache Creek indicate that concentrations of THg-p,g are about twice as high in suspended sediment and floodplain sediment sieved to less than 0.020 mm (fine silt and clay, < 20 micrometers) compared with coarser size fractions. The effect

of grain-size effect may influence variations of THg-p,v as a function of discharge at a given location, and between locations in the watershed.

The grain-size effect in the Coast Ranges is much less than that observed in the Sierra Nevada, where silt and clay is typically 30 to 50 times higher in concentration than sand (Alpers et al., 2006). Therefore it should be acceptable to consider the grain-size effect on variations in THg-p,g concentration to be second-order, to be a model refinement rather than a requirement of the preliminary model.

7.7 Conclusions

Some first-order processes affecting THg and MeHg transport were described that can serve as a basis for preliminary modeling efforts. In addition, some second-order processes were described that can be used to fine-tune the model after its initial development.

8. References

Ackerman, J.T., Hartman, A., Eagles-Smith, C.A., Herzog, M.P., Davis, J., Ichikawa, G., and Bonnema, A., 2015, Estimating exposure of piscivorous birds and sport fish to mercury in California lakes using prey fish monitoring – a predictive tool for managers, United States Geological Survey Open-File Report 2015-1106.

Alpers, C.N, Taylor, H.E., and Domagalski, J.L., 2001, prepared in cooperation with the Sacramento Regional County Sanitation District, California State Water Resources Control Board, United States Environmental Protection Agency, and National Marine Fisheries Service. Metals transport in the Sacramento River, California, 1996-1997, Volume 1: methods and data, United States Geological Survey Water-Resources Investigations Report 99-4286.

Alpers, C. N., Hunerlach, M. P., May, J. T., & Hothem, R. L. (2005). Mercury Contamination from Historical Gold Mining in California. Publications of the US Geological Survey, 61(October), 7.

Alpers, C.N., Eagles-Smith, C., Foe, C., Klasing, S., Marvin-DiPasquale, M.C., Slotton, D.G., and Windham-Myers, L., 2008, Mercury conceptual model. Sacramento, Calif.: Delta Regional Ecosystem Restoration Implementation Plan, 62 p. http://www.science.calwater.ca.gov/pdf/drerip/DRERIP3._mercury_conceptual_model_final_012408.pdf

Amos, H. M., Jacob, D. J., Streets, D. G., & Sunderland, E. M. (2013). Legacy impacts of all-time anthropogenic emissions on the global mercury cycle. *Global Biogeochemical Cycles*, *27*, 410-421.

ATSDR (Agency for Toxic Substances and Disease Registry), 2005. Toxicological profile for mercury. Atlanta, GA: U.S. Department of Health and Human Services, Public Health Service.

Benoit, J., C.C. Gilmour, A. Heyes, R. Mason, and C. Miller. Geochemical and biological controls over methylmercury production and degradation in aquatic systems. In *Biochemistry of Environmental Important Trace Elements*; Chai, Y., Braids, O. C., Eds.; American Chemical Society: Washington, DC, 2003; Vol. ACS Symposium Series #835, pp 262-297.

Bloom, N.S., C.J. Watras, and J.P. Hurley. 1991. Impact of acidification on the methylmercury cycle of remote seepage lakes. Water Air and Soil Pollution 56:477-491.

Boudreau, B.P., 1998. Mean mixed depth of sediments: The wherefore and the why. Limnol. Oceanogr., 43, 524–526.

Boyer, J. M., Chapra, S. C., Ruiz, C. E., and Dortch, M. S. (1994). "RECOVERY, a mathematical model to predict the temporal response of surface water to contaminated sediments," Technical Report W-94-4, U.S. Army Engineer Waterways Experiment Station, Vicksburg, MS.

Boszke, L., Głosińska, G., Siepak, J. 2002. Some Aspects of Speciation of Mercury in a Water Environment, Polish Journal of Environmental Studies, 11, 4, 285-298.

Brigham, M.E., Wentz, D.A., Aiken, G.R., and Krabbenhoft, D.P., 2009, Mercury cycling in stream ecosystems. 1. Water column chemistry and transport: Environmental Science and Technology, v. 43, no. 8, p. 2720-2725. (http://pubs.acs.org/doi/abs/10.1021/es802694n)

Bushey JT, Driscoll CT, Mitchell MJ, Selvendiran P, Motesdeoca MR, 2008, Mercury transport in response to storm events from a northern forest landscape. Hydrological Processes. http://dx.doi.org/10.1002/hyp.7091

Carroll, R. W. H., Warwick, J. J., Heim, K. J., Bonzongo, J. C., Miller, J. R., and Lyons, W. B., 2000. Simulation of mercury transport and fate in the Carson River, Nevada,‖ Ecological Modelling, vol.125, pp. 255 –278.

Callahan MA, Slimak MW, Gabel NW, May IP, Fowler CF, Freed JR, Jennings P, Durfee RL, Whitmore, FC, Maestri B, Mabey WR, Holt BR, Gould C (1979) *Water related environmental fate of 129 priority pollutants, introduction and technical background, metals and inorganics, pesticides and PCBs.* EPA 440/4-79-029a, Washington, DC, US Environmental Protection Agency, Office of Water Waste and Management, pp. 14-1–14-15 .

Chapra, S.C. 1997. *Surface Water Quality Modeling*. New York, McGraw-Hill.

Chapra, S.C., Pelletier, G.J. and Tao, H. 2008. QUAL2K: A Modeling Framework for Simulating River and Stream Water Quality, Version 2.11: Documentation and Users Manual, Civil and Environmental Engineering Dept., Tufts University, Medford, MA.

Cole, T.M., and S.A. Wells. 2011. CE-QUAL-W2: A Two-Dimensional, Laterally Averaged, Hydrodynamic and Water Quality Model. Department of Civil and Environmental Engineering, Portland State University, Portland, OR.

Costa M., Liss P. 2000. Photoreduction and evolution of mercury from seawater. Sci. Total Environ. 161, 125.

Di Toro, D.M. 2001. Sediment Flux Modeling. J. Wiley and Sons., New York, 624p.

Dittman JA, Driscoll CT, 2009. Factors influencing changes in mercury concentrations in lake water and yellow perch (Perca Xavescens) in Adirondack lakes, Biogeochemistry 93:179-196. http://dx.doi.org/10.1007/s10533-009-9289-9

Dittman JA, Shanley JB, Driscoll CT, Aiken GR, Chalmers AT, Towse JE, Selvendiran P, 2010. Mercury dynamics in relation to dissolved organic carbon concentration and quality during high flow events in three northeastern U.S. streams. Water Resources Research. http://dx.doi.org/10.1029/2009WR008351

Domagalski, J.L., 2001, Mercury and methylmercury in water and sediment of the Sacramento River Basin, California: Applied Geochemistry, v 16, p. 1677-1691. doi:10.1016/S0883-2927(01)00068-3

Domagalski, J., Majewski, M.S., Alpers, C.N., Eckley, C.S., Eagles-Smith, C.A., Schenk, L., and Wherry, S, 2016, Comparison of mercury mass loading in streams to atmospheric deposition in watersheds in Western North American: evidence for non-atmospheric mercury sources: Science of the Total Environment, http://dx.doi.org/10.1016/j.scitotenv.2016.02.112..

Domagalski, J.L., Slotton, D.G., Alpers, C.N., Suchanek, T.H., Churchill, R., Bloom, N., Ayers, S.M., and Clinkenbeard, J., 2004, Summary and synthesis of mercury studies in the Cache Creek Watershed, California 2000-01, prepared in cooperation with the California Bay-Delta Authority, United States Geological Survey Water-Resources Investigations Report 03-4335.

Dyer K. R. 1986. Coastal and Estuarine Sediment dynamics. John Wiley & Sons. Chichester. 342 p.

EPRI (Electric Power Research Institute). 2006. Enhancement of Watershed Analysis Risk Management Framework (WARMF) for Mercury Watershed Management and Total Maximum Daily Loads (TMDLs).

EPRI (Electric Power Research Institute). 2013. Dynamic Mercury Cycling Model for Windows 7/Vista/XP. D-MCM Version 4.0 User's Guide and Technical Support. EPRI, Palo Alto, CA: 2013. Software Product ID #: 3002002518.

Evers, David C. 2005. Mercury Connections: The extent and effects of mercury pollution in northeastern North America. BioDiversit y Research Institute. Gorham, Maine. 28 pages.

Fogler H.S. 2005. Elements of Chemical Reaction Engineering. Prentice Hall, USA.

Foresman, E. (2012). USEPA Completes Delta Stressor Investigation. Pulse of the Delta - Linking Science & Management Through Regional Monitoring, (673), 18 – 27. Retrieved from http://www.pmi.org/~/media/PDF/Research/2012_Pulse_of_the_profession.ashx

Gaffney J.S. and N.A. Marley. 2014. In-depth review of atmospheric mercury: sources, transformations and potential sinks. Energy and Emission Control Technologies. 2014:2. 1-21.

Gilmour, C.C. and E.A. Henry. 1991. Mercury methylation in aquatic systems affected by acid deposition. Environ. Poll. 71:131-169.

Greimann, B.P., Lai, Y.G., and Huang, J., (2008). "Two-Dimensional Total Sediment Load Model Equations," J. Hydraulic Engineering, vol.134(8), 1142-1146.

Gustin, M. S., Lindberg, S. E., & Weisberg, P. J. (2008). An update on the natural sources and sinks of atmospheric mercury. *Applied Geochemistry*, *23*(3), 482-493.

Harris, R.C. and R.A. Bodaly. 1998. Temperature, growth and dietary effects on fish mercury dynamics in two Ontario Lakes. Biogeochemistry 40: 175-187

Harris R., D. Krabbenhoft, R. Mason, M. Murray, R. Reash and T. Saltman 2007. Chapter 1 (Introduction) in "Ecosystem Responses to Mercury Contamination: Indicators of

Change". R. Harris, D. Krabbenhoft, R. Mason, M. Murray, R. Reash and T. Saltman (Eds.). SETAC.

Hobman J.L., Wilson J.R., Brown N.L. 2000. Microbial Mercury Reduction. In: Environmental Microbe-Metal In teraction. Lovley D. R. (ed.) ASM Press, Washington.

Hudson, R.J.M., S.A. Gherini, C.J. Watras, and D.B. Porcella. 1994. "Modeling the Biogeochemical Cycle of Mercury in Lakes: The Mercury Cycle Model (MCM) and its Application to the MTL Study Lakes, in Mercury Pollution: Integration and Synthesis, Waltras and Huckabee, Editors, pp. 473-523.

Hydrologic Engineering Center (HEC). 2010a. HEC-RAS: River Analysis System User's Reference Manual Version 4.1. Hydrologic Engineering Center, U.S. Corps of Engineers, Davis, California.

Hydrologic Engineering Center (HEC). 2010b. HEC-RAS: River Analysis System Hydraulic Reference Manual Version 4.1. Hydrologic Engineering Center, U.S. Army Corps of Engineers, Davis, California.

Karickhoff S. W. 1984. Pollutant sorption in aquatic systems. J. Hydraulic Engineering, ASCE 10, 707-735.

Krabbenhoft, D.P. and D.A. Rickert. 2003. Mercury Contamination of Aquatic Ecosystems. U.S. Geological Survey. 12 June 2003 http://www.friendsoftherivers.com/env_concerns/messages/95.html

Lai, Y.G., Weber, L.J., and Patel, V.C. (2003). "Non-hydrostatic three-dimensional method for hydraulic flow simulation - Part I: formulation and verification," J. Hydraul. Eng., ASCE, 129(3), 196-205.

Lai, Y.G. and T.J. Randle. (2007). *Bed Evolution and Bank Erosion Analysis of the Palo Verde Dam on the Lower Colorado River*. Technical Service Center, Bureau of Reclamation, Denver, CO.

Lai, Y.G. (2008). *SRH-2D Theory and User's Manual version 2.0,* Technical Service Center, Bureau of Reclamation, Denver, CO.

Lai, Y.G. and Greimann, B.P. (2008). "Modeling of erosion and deposition at meandering channels," World Environmental & Water Resources Congress, May 12-16, 2008, Honolulu, Hawaii.

Lai, Y.G. (2010). "Two-Dimensional Depth-Averaged Flow Modeling with an Unstructured Hybrid Mesh," *J. Hydraulic Engineering*, ASCE, 136(1), 12-23.

Lai, Y.G. and Greimann, B.P. (2010). "Predicting contraction scour with a two-dimensional depth-averaged model," *J. Hydraulic Research*, IAHR, 48(3), 383-387.

Lai, Y.G. (2011). *Prediction of Channel Morphology Upstream of Elephant Butte Reservoir on the Middle Rio Grande*. Technical Report No. SRH-2011-04. Technical Service Center, Bureau of Reclamation, Denver, CO.

Lai, Y.G., Greimann, B.P., and Wu, K. (2011). "Soft bedrock erosion modeling with a two-dimensional depth-averaged model," *J. Hydraulic Engineering*, ASCE, vol.137(8), pp.804-814.

Lin, C.-C.; Yee, N.; Barkay, T. 2012. Microbial transformations in the mercury cycle. In Environmental Chemistry and Toxicology of Mercury; John Wiley & Sons, Inc.: Hoboken, NJ, 2012; pp 155−191.

Littrell, E.E., 1993, Mercury in Western Grebes at Lake Berryessa and Clear Lake, California, California Department of Fish and Game, no. 77 v 3, p. 142-144

Leonard, B. P. 1979. "A stable and accurate convection modelling procedure based on quadratic upstream interpolation," *Computer Methods in Applied Mechanics and Engineering,* 19, 59-98.

Mason, R.P., Fitzgerald, W.F., Morel, F.M.M., 1994. The biogeochemical cycling of elemental mercury — anthropogenic influences. Geochimica et Cosmochimica Acta 58, 3191.

Mason, R. R.; Abbot, M. L.; Bodaly, R. A.; Bullock, O. R.; Driscoll, C. T.; Evers, D.; Lindberg, S. E.; Murray, M.; Swain, E. B. 2005. Monitoring the response to changing mercury deposition. Environ. Sci. Technol. 2005, 39 (1), 14A−22A.

Marvin-DiPasquale, M., M. A. Lutz, M. E. Brigham, D. P. Krabbenhoft, G. R. Aiken, W. H. Orem, and B. D. Hall. 2009. Mercury cycling in stream ecosystems. 2. Benthic methylmercury production and sediment-pore water partitioning. Environmental Science and Technology 43: 2726-2732.

Mill, T., Mabey, W.R., Bomberger, D. C., Chou, T.W., Hendrey, D.G. and Smith, J.H. 1982. Laboratory Protocols for Evaluating the Fate of Organic Chemicals in Air and Water, Report No. EPA-600/3-82-022, US Environmental Protection Agency, Environmental Research Laboratory, Athens, Georgia, 338pp.

Morel, F.M.M., Kraepiel, A.M.L., Amyot, M. 1998. The chemical cycle and bioaccumulation of mercury. Annu. Rev. Ecol. Syst. 29, 543-566.

Nriagu, J. O. 1979. The Biogeochemistry of Mercury in the Environment. Elsevier/North Holland, Biomedical Press, New York.

O'Connor, D. J., Thomann, R. V., Schnoor, J. L., and Manciani, J. L., 1983. Modeling Toxic Substances in Natural Water Systems, Manhattan College.

Pacyna, E. G., Pacyna, J. M., Sundseth, K., Munthe, J., Kindbom, K., Wilson, S., Steenhuisen, F., et al. (2010). Global emission of mercury to the atmosphere from anthropogenic sources in 2005 and projections to 2020. *Atmospheric Environment*, *44*(20), 2487-2499. Elsevier Ltd. Retrieved from http://dx.doi.org/10.1016/j.atmosenv.2009.06.009.

Parker, G., (1990). "Surface-Based Bedload Transport Relation for Gravel Rivers," J. Hydraulic Research, 28(4):417-436.

Pirrone, N., Cinnirella, S., Feng, X., Finkelman, R. B., Friedli, H. R., Leaner, J., Mason, R., et al. (2010). Global mercury emissions to the atmosphere from anthropogenic and natural sources. *Atmospheric Chemistry and Physics*,*10*(13), 5951-5964.

Pirrone N. and T. Keating. 2014. Editors. Hemisphere transport oif air poluution 2010: mercury. United Nations Publication 11.11.E8. March 14, 2014.

Puk R., Weber J.H. 1994. Determination of mercury (II), monomethylmercury cation, dimethylmercury and diethylmercury by hydride generation, cryogenic trapping and atomic absorption spectrometric detection. Analytica Chim. Acta. 292, 175.

Regnell O, Tunlid A., Ewald G, Sangfors O. 1996. Methyl mercury production in freshwater microcosms affected by dissolved oxygen levels: role of cobolamin and microbial community composition. Can. J. Fish. Aquat. Sci. 53, 1535.

Rodi, W. (1993) "Turbulence models and their application in hydraulics," 3rd Ed., IAHR Monograph, Balkema, Rotterdam, The Netherlands.

Ruiz, C.E., Aziz, N.M., and Schroeder, P.R. 2000. "RECOVERY: A contaminated sediment-water interaction model," ERDC/EL SR-D-00-1, U.S. Army Engineer Research and Development Center, Waterways Experiment Station, Vicksburg, MS.

Rytuba, J.J., 2003. Mercury mines studies, environmental impacts of mercury mines in the Coast Ranges, California, in Gray, J.E., ed., Geologic studies of mercury by the United States Geological Survey, Circular 1248, 47 p.

Schnoor, J.L. 1996. Environmental Modeling: Fate and Transport of Pollutants in Water, Air, and Soil. New York: Wiley Interscience, 682 pp.

Schink, D. R., and N. L. Guinasso. 1977. Modelling the influence of bioturbation and other processes on calcium carbonate dissolution at the sea floor. In The fate of fossil fuel C02 in the oceans, .ed. N. R. Andersen and A. Malahoff, 375-399. New York: Plenum Press.

Seeger M, Errea M-P, Begueria S, Marti C, Garcia-Ruiz JM, Arnáez, J, 2004, Catchment soil moisture and rainfall characteristics as determinant factors for discharge/suspended sediment hysteretic loops in a small headwater catchment in the Spanish Pyrenees, Journal of Hydrology 288: 299-311.

Slowey, A.J., Rytuba, J.J., Hothem, R.L., and May, J.T., 2007. Mercury at the Oat Hill Extension Mine and James Creek, Napa County, California: tailings, sediment, water, and biota: United States Geological Survey Open-File Report 2007-1132.

Sparks, G.C. 2016. Mercury and methylmercury related to historical mercury mining in three tributaries to Lake Berryessa, Upper Putah Creek watershed, California. MS Thesis, California State University, Sacramento, CA.

State Water Resources Control Board, 2010, Impaired Water Bodies, 2010 Integrated Report (Clean Water Act Section 303(d) List/305(b) Report). Last updated August 27, 2015, accessed on April 6, 2015. http://www.waterboards.ca.gov/water_issues/programs/tmdl/integrated2010.shtml

State Water Resources Control Board, 2011, Guidance compendium for watershed monitoring and assessment, Clean Water Team Citizen Monitoring Program, http://www.waterboards.ca.gov/water_issues/programs/swamp/cwt_guidance.sht ml

State Water Resources Control Board, 2016, California Environmental Data Exchange Network. Accessed on April 6, 2016. http://www.ceden.org/

State Water Resources Control Board, 2015, State wide mercury program, addressing mercury in California's waters. Last updated January 28, 2015, accessed on April 6, 2015. http://www.swrcb.ca.gov/water_issues/programs/mercury/

Stein E.D., Cohen Y, Winer AM 1996. Environmental distribution and transformation of mercury compounds. Crit Rev Environ Sci Technol 26:1–43

Skyllberg, U., 2012. Chemical speciation of mercury in soil and sediment. In Environmental Chemistry and Toxicology of Mercury, John Wiley & Sons, Inc.: Hoboken, NJ, pp 219−258.

Tetra Tech Inc. 1996. Regional Mercury Cycling Model: A Model for Mercury Cycling in Lakes (R-MCM Version 1.0b Beta), Draft User's Guide and Technical Reference. Prepared for the Electric Power Research Institute and Wisconsin Department of Natural Resources. December 1996.

Thomann, R.V. and Mueller, J.A., 1987. Principles of Surface Water Quality Modeling and Control. Harper, New York, NY, 644 pp.

Traina S.J., McAvoy D.C., Versteeg D.J. 1995. Association of LAS with dissolved organic matter. Environ Sci Technol 30:1300–1309.

Tsiros, I.X. and R.B. Ambrose. 1999."An Environmental Simulation Model for Transport and Fate of Mercury in Small Rural Catchments", Chemosphere, Vol. 39, No. 3, pp. 477-492.

Turner D.R. 1987. Speciation cycling of arsenic, cadmium, lead and mercury in natural waters. In: Lead, Mercury, Cadmium in the Environment, Huthinson T.W., Meema K.M. (eds.), Chichester.

Tyler G. 1992. Mercury in soil - distribution, speciation and biological effect. Nordic Council of Ministers. Copenhagen.

Ullrich S.M., Tanton T.W., Abdrashitova S.A. 2001. Mercury in the aquatic environment: a review of factors affecting methylation. Crit Rev Environ Sci Technol 31:241-293.

USEPA (United States Environmental Protection Agency). 1997. Mercury Study Report to Congress, Volumes I through VIII. Office of Air Quality Planning and Standards and ORD. (EPA/452/R-97-001 thru 010; December 1997).

Varekamp, J. C., & Buseck, P. R. (1986). Global mercury flux from volcanic and geothermal sources. Applied Geochemistry, 1, 65-73.

Wang, Q., D. Kim, D.D. Dionysiou, G.A. Sorial, and D. Timberlake, 2004. Sources and remediation for mercury contamination in aquatic systems—a literature review. Environmental Pollution, vol. 131, pp.323-336.

Wang, J.,C.N. Alpers, Y. Lai, N.W.T. Quinn, J.Weigand and J. Sholtes. 2017. Integrated modeling of mercury transformation and transport in watersheds subject to wildfire. US Bureau of Reclamation, Research and Development Office, Denver CO.

Wentz, D., Brigham, M., Chasar, L., Lutz, M., & Krabbenhoft, D. (2014). Mercury in the Nation's Streams - Levels , Trends , and Implications Circular 1395. Whitman, W.G., (1923), Preliminary experimental confirmation of the two-film theory, Chem. Metall. Eng. 29, 146–148.

Windham-Myers, L. (2014). Methylmercury cycling in wetlands managed for rice agriculture and wildlife: Implications for methylmercury production, transport, and bioaccumulation. *Science of the Total Environment*, *484*(1), 219–220. http://doi.org/10.1016/j.scitotenv.2014.01.046

Windham-Myers, L., Fleck, J. a., Ackerman, J. T., Marvin-DiPasquale, M., Stricker, C. a., Heim, W. a., … Alpers, C. N. (2014). Mercury cycling in agricultural and managed wetlands: A synthesis of methylmercury production, hydrologic export, and bioaccumulation from an integrated field study. *Science of the Total Environment*, *484*(1), 221–231. http://doi.org/10.1016/j.scitotenv.2014.01.033.

Windham-Myers, L., & Jabusch, T. (2012). Yolo Bypass Findings could help Wetland Managers reduce the Methylmercury Problem. Pulse of the Delta - Linking Science & Management Through Regional Monitoring, (673). Retrieved from http://www.pmi.org/~/media/PDF/Research/2012_Pulse_of_the_profession.ashx

Winterwerp, J. C. and van Kersteren, W. G. M., 2004. Dev. in Sedimentology 56.

Wool, T. A., Ambrose, R. B., Martin, J. L., and Comer, E. A., 2006. Water quality analysis simulation program (WASP) version 6.0 draft: user's manual. available from: http://www.epa.gov/athens/wwqtsc/html/wasp.html.

Wyels, W., 1987. Regional mercury assessment: Central Valley Regional Water Quality Control Board.

Zhang, Z., Johnson, B.E. 2015a. Aquatic Nutrient Simulation Modules (NSMs) Developed for Hydrologic and Hydraulic Models. ERDC/EL TR-15-X, U.S. Army Engineer Research and Development Center, Vicksburg, MS.

Zhang, Z., Johnson, B.E. 2015b. Aquatic Contaminant and Mercury Simulation Modules Developed for Hydrologic and Hydraulic Models. ERDC/EL TR-15-X, U.S. Army Engineer Research and Development Center, Vicksburg, MS.

Zillioux,E. J. Porcella, D. B., and Benoit, J. M., 1993. Mercury cycling and effects in freshwater wetland ecosystems,‖ Environmental Toxicology and Chemistry, vol. 12, pp.2245–2264.